1949

Magnetohydrodynamic waves and instabilities in the solar atmosphere

Thesis for the Degree of Doctor of Philosophy (PhD)

Noémi Kinga Zsámberger
Supervisor: Prof. Róbert Erdélyi

UNIVERSITY OF DEBRECEN
Doctoral Council of Natural Sciences and Information Technology
Doctoral School of Physics
Debrecen, 2024

Hereby I declare that I prepared this thesis within the Doctoral Council of Natural Sciences and Information Technology, Doctoral School of Physics, University of Debrecen in order to obtain a PhD Degree in Natural Sciences at Debrecen University. The results published in the thesis are not reported in any other PhD theses.
2024.07.18

Zsámberger Noémi Kinga

……
doctoral candidate

Hereby I confirm that Noémi Kinga Zsámberger candidate conducted her studies with my supervision within the Physical Methods in Interdisciplinary Research Doctoral Program of the Doctoral School of Physics between 2017. and 2024. The independent studies and research work of the candidate significantly contributed to the results published in the thesis. I also declare that the results published in the thesis are not reported in any other theses. I support the acceptance of the thesis.

2024.07.18
.

……
supervisor

Magnetohydrodynamic waves and instabilities in the solar atmosphere

Dissertation submitted in partial fulfilment of the requirements for the **doctoral** (PhD) degree in physics

Written by Noémi Kinga Zsámberger certified physicist

Prepared in the framework of the Doctoral School of Physics of the University of Debrecen Physical Methods in Interdisciplinary Researches programme

Dissertation advisor: Prof. Róbert Erdélyi

The official opponents of the dissertation:

Dr. .....…… .....

Dr. .....… .....

The evaluation committee:

Chairperson: Dr. ……. …….

Members: Dr. ……. …….

Dr. ……. …….

Dr. ……. …….

Dr. ……. …….

The date of the dissertation defense …… .....

Abstract

The solar atmosphere is a highly structured, complex and coupled plasma system permeated by ubiquitous magnetic fields and subject to a variety of flows. All these factors contribute to the formation of numerous waveguide structures, which, in turn, are capable of supporting magnetohydrodynamic (MHD) waves. This thesis was prepared with the aim of studying these waves and their instabilities using a family of multi-layered Cartesian waveguide models applicable to solar atmospheric features, with the further goal of providing the theoretical requirements for diagnostic tools that may be utilised in so-called solar magneto-seismological studies. In particular, we investigate the effects resulting from including different sources of asymmetry into the classical model of a magnetic slab on the stability of and the waves supported by the system.

First, we consider a static magnetic slab, which is filled with uniform, inviscid, ideal plasma and embedded in an asymmetric, non-magnetic environment that supports asymmetric flows as well. The dispersion relation of magneto-acoustic waves in this system is derived, leading to a description of quasi-kink and quasi-sausage eigenmodes guided by the system and the thresholds of asymmetry parameters required to subject these oscillations to the Kelvin-Helmholtz instability.

Then, we proceed to extend steady slab models in a different manner, by building a model comprised of a magnetic slab containing a steady flow, and embedding it in an asymmetric magnetic environment. The dispersion relation as well as its approximate solutions are derived, and the KHI-threshold is investigated for a few chosen sets of equilibrium parameters.

Next, we focus on further generalising steady slab models to configurations that are magnetised all throughout, allowing for magnetic and plasma asymmetries as well, and which contain two or three different background flows in their separate layers. The dispersion relations for both cases are obtained, and the continued refinement of solar applications of steady slab models is demonstrated through the example of magnetic bright points.

Finally, we incorporate a triangular flow profile in the central region of a symmetric slab system which is subject to a kink oscillation. The equation governing wave dispersion is derived and examined in further analytical detail in several limiting cases. The study is complemented with results from an initial numerical analysis showing the dependence of the instability range on the choice of density, magnetic, and slab width parameters.

Acknowledgements

I would like to express how grateful I am to all the fantastic people who have made this research possible. I would like to convey my thanks especially to my Supervisor, who has opened my eyes to the fascinating field of solar physics research and has provided continuous support in exploring its various facets for several years now.

I appreciate the support from researchers of the Hungarian Solar Physics Foundation, the University of Debrecen, and SP^{2}RC at the University of Sheffield. I also offer my gratitude to the organisers and participants of the UGRI scheme at the University of Sheffield, allowing me to work together with excellent undergraduate students at Department of Mathematics and Statistics. I am further grateful to Mihai Berbulescu for the PyTES root finding codes and to Balázs Asztalos for their further development, making the preparation of numerous numerical results presented throughout the following Chapters possible.

Thank you to every co-author I have had the fortune to work with, as well as every PhD student making our meetings, in person or online, a lively and understanding environment. Last but not least, I want to give my deepest thanks to my close friends and family for the wonderful people they are and the amazing things they have done.

Publications

Parts of this Thesis are based on the following publications:

- Allcock, M., Shukhobodskaia, D., Zsámberger, N. K. and Erdélyi, R. (2019): Magnetohydrodynamic waves in multi-layered asymmetric waveguides: solar magnetoseismology theory and application. *Frontiers in Astronomy and Space Sciences*, Volume 6, 48.

- Zsámberger, N. K., Sánchez Montoya, Carmen M., and Erdélyi, R. (2022): Magnetohydrodynamic waves in an asymmetric magnetic slab with different external flows *The Astrophysical Journal, Volume 937, 23.*

- Zsámberger, N. K.,Tong, Yihui, Asztalos, Balázs, and Erdélyi, R. (2022): MHD wave propagation and the Kelvin-Helmholtz instability in an asymmetric magnetic slab system *The Astrophysical Journal, Volume 935, 41.*

- Zsámberger, N. K., and Erdélyi, R. (2024): On instabilities in dynamic magnetic slabs driven by kink waves [in preparation]

List of additional publications that are not parts of this thesis[1]:

- Zsámberger, N. K., Allcock, M. and Erdélyi, R. (2018): Magneto-acoustic Waves in a Magnetic Slab Embedded in an Asymmetric Magnetic Environment: The Effects of Asymmetry. *The Astrophysical Journal*, Volume 853, 136.

- Zsámberger, N. K. and Erdélyi, R. (2020): Koronafűtés és mágneses hullámok: Miért forró a Nap légköre? *Fizikai Szemle*, Vol. 70/3. pp. 80-89.

- Oxley, W., Zsámberger, N. K. and Erdélyi, R. (2020): Standing MHD Waves in a Magnetic Slab Embedded in an Asymmetric Plasma Environment: Slow Surface Waves *The Astrophysical Journal*, Volume 890, 109.

- Oxley, W., Zsámberger, N. K. and Erdélyi, R. (2020): Standing MHD Waves in a Magnetic Slab Embedded in an Asymmetric Magnetic Plasma Environment: Surface Waves *The Astrophysical Journal*, Volume 898, 19.

- Zsámberger, N. K. and Erdélyi, R. (2020): Magnetoacoustic Waves in a Magnetic Slab Embedded in an Asymmetric Magnetic Environment. II. Thin and Wide Slabs, Hot and Cold Plasmas. *The Astrophysical Journal*, Volume 894, 123.

- Zsámberger, N. K. and Erdélyi, R. (2021): Magnetoacoustic Waves in a Magnetic Slab Embedded in an Asymmetric Magnetic Environment. III. Applications to the Solar Atmosphere. *The Astrophysical Journal*, Volume 906, 122.

[1]The publications listed here are not included in the main results listed in the current thesis for two related reasons: as (1) they detail the specifics of MHD wave propagation in static slab systems, as opposed to ones containing bulk background flows, (2) they were included in a separate PhD thesis submitted at The University of Sheffield (Zsamberger (2022)).

Contents

List of Figures

List of accompanying materials

Animated Figures for Chapter 2

- SM1: The phase speeds of supported waves as a function of the slab width (kx_0) at changing values of M_{A2} and fixed $M_{A1} = -0.2$. Available as panel (a) in the animated version of Figure 4 of (Zsámberger et al., 2022a).
- SM2: The phase speeds of supported waves as a function of the slab width (kx_0) at changing values of M_{A2} and fixed $M_{A1} = -0.1$. Available as panel (b) in the animated version of Figure 4 of (Zsámberger et al., 2022a).
- SM3: The phase speeds of supported waves as a function of the slab width (kx_0) at changing values of M_{A2} and fixed $M_{A1} = 0.1$. Available as panel (c) in the animated version of Figure 4 of (Zsámberger et al., 2022a).
- SM4: The phase speeds of supported waves as a function of M_{A2} at changing values of the slab width (kx_0) and fixed $M_{A1} = -0.2$. Available as panel (a) in the animated version of Figure 5 of (Zsámberger et al., 2022a).
- SM5: The phase speeds of supported waves as a function of M_{A2} at changing values of the slab width (kx_0) and fixed $M_{A1} = -0.1$. Available as panel (b) in the animated version of Figure 5 of (Zsámberger et al., 2022a).
- SM6: The phase speeds of supported waves as a function of M_{A2} at changing values of the slab width (kx_0) and fixed $M_{A1} = 0.1$. Available as panel (c) in the animated version of Figure 5 of (Zsámberger et al., 2022a).
- SM7: The phase speeds of supported waves as a function of M_{A2} at changing values of the slab width (kx_0) and fixed $M_{A1} = 0.2$. Available as panel (d) in the animated version of Figure 5 of (Zsámberger et al., 2022a).
- SM9: Phase speeds of waves in a symmetric slab as a function of the slab width (kx_0), at changing values of symmetric flows $M_{A1} = M_{A2}$. Available as panel (a) in the animated version of Figure 7 of (Zsámberger et al., 2022a).
- SM10: Phase speeds of waves in a symmetric slab as a function of $M_{A1} = M_{A2}$ at changing values of the slab width (kx_0). Available as panel (b) in the animated version of Figure 7 of (Zsámberger et al., 2022a).
- SM11: Phase speeds of waves in a symmetric slab as a function of the slab width (kx_0), at changing values of M_{A2} and fixed $M_{A1} = -0.1$. Available as panel (c) in the animated version of Figure 7 of (Zsámberger et al., 2022a).

- SM12: Phase speeds of waves in a symmetric slab as a function of M_{A2} at changing values of the slab width (kx_0) and fixed $M_{A1} = -0.1$. Available as panel (d) in the animated version of Figure 7 of (Zsámberger et al., 2022a).
- SM13: Phase speeds of waves in an asymmetric slab as a function of the slab width (kx_0), at changing values of $M_{A1} = M_{A2}$. Available as panel (e) in the animated version of Figure 7 of (Zsámberger et al., 2022a).
- SM14: Phase speeds of waves in an asymmetric slab as a function of $M_{A1} = M_{A2}$ at changing values of the slab width (kx_0). Available as panel (f) in the animated version of Figure 7 of (Zsámberger et al., 2022a).

These Figures are part of the paper by (Zsámberger et al., 2022a) and are available at the publisher's website (`https://iopscience.iop.org/article/10.3847/1538-4357/ac8427`).

Chapter 1.
Introduction

Abstract

This Introduction provides an overview of the physical theories and conclusions of solar physics research which the methods and results of this thesis on magnetohydrodynamic (MHD) wave propagation and instabilities in waveguides within the solar atmosphere are built upon. First, a brief description of the basic structure of the Sun and in particular its stratified atmosphere is given. Next, the Chapter describes the fundamentals of magnetohydrodynamics, including a summary of the equations of ideal MHD. Finally, the Kelvin-Helmholtz instability and MHD wave propagation in uniform and structured environments is discussed, describing especially recent advances in the generalisation of the magnetic slab model.

1.1. Our Sun

The Sun is arguably the single most important celestial body from the perspective of life on Earth. Understandably, it has fascinated and motivated multitudes of people throughout history, and it has been a subject of both everyday and scientific interest for a long time. With its distance of (on average) 149.6 million kilometres from Earth, on a cosmic scale, our central star is just an arm's length away from us. Solar physics research continues to occupy a special position within astronomy, due to both the Sun's relative closeness to our planet as well as its characteristics. Namely, it is a star of type G2V in the prime of its long main-sequence life, and thus it counts as an "average" star, which makes it possible to look at it as a "laboratory" of plasma- and stellar physics, where we can test any theoretical conclusions we arrive to within these fields using incomparably more detailed observations than what our measurements of distant stars would allow. In the following Sections, we discuss the internal structure of the Sun, as well as the layers of its atmosphere, based mainly on the overviews provided by Golub and Pasachoff (2009) and Priest (2014). Figure 1.1a serves as a visual accompaniment to this description, showing an artistic rendering of the global layers of the solar interior and atmosphere.

The Sun is by far both the largest and most massive object in Earth's vicinity, containing over 99% of the total mass of the solar system. Beyond its gravitational pull, its

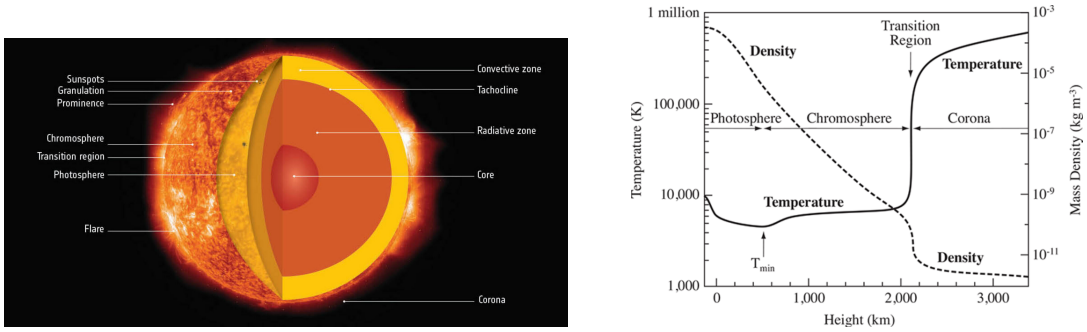

(a) (b)

Figure 1.1: (a)The structure of the solar interior and atmosphere. Source: ESA (2019). (b) Temperature and density variation with height in the solar atmosphere according to the VAL model. Source:Avrett and Loeser (2008).

importance also stems from serving as the dominant energy source for most of the various other celestial bodies found in the heliosphere. This energy is produced in the *core* of the Sun, where temperatures reach approximately 15 million K and the particle density is of a magnitude of 10^{32} m^{-1}. Under these circumstances, the matter constituting our star is in a plasma state. Moreover, the particles possess enough energy to counter the repulsive electromagnetic force between identical charges. This makes the nuclear fusion of four hydrogen nuclei possible and leads to the creation of a helium nucleus. There is, however, a small fraction of the original particle mass which gets converted into smaller byproducts of the fusion reaction. The γ-rays and electron neutrinos thus produced carry energy outwards from the heart of our Sun towards its outer shells.

The Sun's interior is divided into further regions based on different methods of energy transfer. Of the 700 Mm solar radius ($R_\odot$), the core constituted the innermost 25%, surrounded by the *radiative zone* ($0.25R_\odot < r < 0.75R_\odot$). Here, the photons generated in the core are carried outward through a random walk process as they keep colliding, being absorbed and re-emitted, while losing part of their energy and shifting in wavelength from the gamma range towards the lower-energy visible spectrum.

A thin shear layer called the *tachocline* separates the radiative zone from the *convective zone* around it (500-700 Mm). The tachocline itself is suspected to play a crucial role in generating the global magnetic field of our star. As opposed to radiative diffusion below the tachocline, the dominant energy transfer process above this layer is convection. This is due to the presence of a high temperature gradient, which can induce convective instability, displacing blobs of plasma vertically upwards. Once it reaches the surface, the buoyant plasma proceeds to radiate its energy into the solar atmosphere. As the blob's temperature decreases, it then sinks back down and the cycle of convection can start all over again.

Above the convective zone, we find the *solar atmosphere*. In contrast to the opaque solar interior, photons can directly escape into space from the atmosphere. It is further divided up into three main layers, starting (at the lowest height) with the *photosphere*.

Relatively dense and opaque plasma fills this thin layer, which serves as the Sun's visible surface, starting from the height where the optical depth reaches unity. As the plasma rising in convective cells from below reaches this surface, it cools and starts sinking again, which manifests as a multitude of irregularly shaped convective cells called granules. In the heart of these granules, the plasma rises up from the layers beneath, making these areas look bright and warm. Colder areas of downflow appearing as dark intergranular lanes separate these seats of convective upflow from one another.

Giant cells and mesogranulation extend the structuring present in the photosphere to larger scales. A further important source of structuring is the concentration of magnetic fields. In areas of enhanced magnetic flux, such as sunspots, pores, and magnetic bright points, convection is at least partially inhibited, while pressure and temperature conditions differ from those of the general granular structure.

The upper boundary of the photosphere is the height where the solar atmospheric plasma reaches its minimum temperature. The unexpected temperature distribution of the solar atmosphere (which can also be observed in Figure 1.1b) with its minimum of around 4500 K at the top of the photosphere and with its swift climb back up to a few million K in the corona constitutes a puzzling question for astronomers. This so-called solar atmospheric heating question still remains one of the main motivations for the continued study of the solar atmosphere.

Moving radially further out, the next shell in the solar atmosphere is the *chromosphere* (0.5-2.5 Mm above the surface). This region is one of complex structuring, with the most notable element being a "forest" of short-lived and thin jets of plasma called spicules. An additional structural change can be observed in this layer: as the chromospheric plasma becomes more rarefied with height, the highly concentrated radial magnetic fields of the photosphere can spread out in this higher atmospheric region, forming a magnetic canopy parallel to the solar surface.

Overall, the temperature in the chromosphere keeps slowly rising and the density keeps gradually decreasing. Then at approximately 2 Mm height, both parameters show a sudden jump. This thin layer, where the temperature abruptly increases by as much as two orders of magnitude, is the *transition region*, binding the chromosphere together with the searing hot and highly rarefied plasma of the *solar corona*. At its greatest extent, the outer part of the corona expands in a continuous stream of particles, transitioning into the *solar wind*.

The coronal plasma is dominated by the presence of magnetic fields, giving rise to structuring on a large scale consisting of helmet-shaped streamers (regions of closed magnetic field lines near intermediate solar latitudes) and coronal holes (areas of open magnetic field lines, particularly in the vicinity of the poles). Furthermore, the corona is rich in arcs of ionised plasma following strands of bent magnetic field lines, forming the so-called coronal loops - a solar atmospheric structure especially significant in magnetic seismology.

A commonly used description of the temperature and density distribution throughout the solar atmosphere is provided by the VAL (Vernazza-Avrett-Loeset) model (Avrett and

Loeser, 2008). According to this description, the density keeps decreasing throughout the entire atmosphere, with a sharp drop at transition region heights interrupting its otherwise gentler slope. The temperature, however, first keeps falling until we reach the top of the photosphere, and then - counter-intuitively, since we are still moving away from the energy-producing core) - starts increasing again. Moreover, it jumps by as much as two orders of magnitude in the narrow transition region, to a few million K in the corona. In order maintain these high temperatures in the outer atmosphere and balance out radiative losses, as well as accelerate the particles of the solar wind, an alternate means of energy transport must exist. Various mechanisms have been suggested as solutions to this elusive atmospheric heating problem, however, the full solution to the question likely involves a combination of multiple different processes which may operate on various scales. These mechanisms can be hydrodynamic in character (e.g. acoustic or pulsation waves), or of a magnetic nature (reconnection and waves). Among other sources, e.g. Erdélyi and Nelson (2016) provides a summary of these contributing factors.

1.2. The Mathematical Description of Plasma Behaviour

Throughout the complex environment of the solar atmosphere, the matter is in a plasma state. The collective behaviour of such a collection of particles is described by kinetic plasma theory by applying statistical mechanics. The current Section gives a brief description of the process of obtaining the equations of magnetohydrodynamics (MHD) from the broader approach of kinetic theory and the necessary assumptions that need to be made along the way, following mainly the derivation detailed in Goedbloed and Poedts (2004) and Priest (2014). Finally, a summary of the ideal MHD equations is provided, which will be utilised throughout the rest of this thesis to derive dispersion relations for our Cartesian waveguide models.

1.2.1. Moments of the Boltzmann Equation

Consider a plasma consisting of electrons and one kind of ions, where the total number of particles is constant, and the mixture fulfils the condition of approximate charge neutrality over distances exceeding the so-called Debye length ($\lambda_D = \sqrt{\frac{\epsilon_0 k_B T}{nq}}$, where $k_B \approx 1.38\times$ J K^{-1} is Boltzmann's constant, n is the particle density, q is the charge of a particle, $\epsilon_0 = \frac{1}{\mu_0 c^2} \approx 8.85 \times 10^{-12}$F s^{-1} is the permittivity of free space, $\mu_0 = 4\pi \times 10^7$N A^{-2} is the permeability of free space, and $c = 299792458$ m s^{-1} is the speed of light). A large collection of charged particles can be considered a charge-neutral plasma if $\frac{4\pi n \lambda_D^3}{3} \gg 1$, meaning that the number density of particles is very large in a sphere with radius $r = \lambda_D$.

The statistical description provides information about such a plasma using distribution functions $f_\alpha(\mathbf{r}, \mathbf{v}, t)$ for the electrons and ions ($\alpha = e, i$), defined as the density of the representative points of particles of type α in a six-dimensional phase space formed by position

(x, y, z) and velocity (v_x, v_y, v_z) coordinates. The motion of the collection of representative points in phase space is described by the total time derivative of the distribution function, which will be affected by interactions and collisions between the particles, as expressed by the Boltzmann equation:

$$\frac{\partial f_\alpha}{\partial t} + \mathbf{v} \cdot \frac{\partial f_\alpha}{\partial \mathbf{r}} + \frac{q_\alpha}{m_\alpha}(\mathbf{E} + \mathbf{v} \times \mathbf{B}) \cdot \frac{\partial f_\alpha}{\partial \mathbf{v}} = C_\alpha. \tag{1.1}$$

Here, we used the notation $\mathbf{v} \cdot \frac{\partial}{\partial \mathbf{r}} = v_x \frac{\partial}{\partial x} + v_y \frac{\partial}{\partial y} + v_z \frac{\partial}{\partial z}$ (and a similar notation for the $\frac{\partial}{\partial \mathbf{v}}$ term). The electric and magnetic fields include both the external and the averaged internal fields generated from long-range particle interactions, and C_α represents the rate of change of the distribution function stemming from short-range particle interactions (collisions).

The Boltzmann equation can be incorporated into a closed system of equations by combining it with Maxwell's equations:

$$\nabla \cdot \mathbf{E} = \frac{\rho*}{\epsilon_0}, \qquad \text{Gauss' law} \tag{1.2}$$

$$\nabla \cdot \mathbf{B} = 0, \qquad \text{Gauss' magnetic law} \tag{1.3}$$

$$\nabla \times \mathbf{E} = -\frac{\partial \mathbf{B}}{\partial t}, \qquad \text{Maxwell-Faraday equation} \tag{1.4}$$

$$\nabla \times \mathbf{B} = \mu_0 \mathbf{j} + \frac{1}{c^2}\frac{\partial \mathbf{E}}{\partial t}. \qquad \text{Ampére's law} \tag{1.5}$$

Briefly, these define the sources of the electric field, the non-existence of magnetic monopoles, the spatially varying electric field generated by a temporally changing magnetic field, and the magnetic fields generated by a change in the electric field or an electric current ($\mathbf{j}$). To complete the set of equations, the source terms for the charge and current densities need to be connected to the distribution functions:

$$n_\alpha(\mathbf{r}, t) = \int f_\alpha(\mathbf{r}, \mathbf{v}, t) d^3v, \qquad \rho*(\mathbf{r}, t) = \sum q_\alpha n_\alpha,$$

$$\langle \mathbf{v}_\alpha \rangle = \mathbf{u}_\alpha(\mathbf{r}, t) = \frac{1}{n_\alpha(\mathbf{r}, t)} \int \mathbf{v} f_\alpha(\mathbf{r}, \mathbf{v}, t) d^3v, \qquad \mathbf{j}(\mathbf{r}, t) = \sum q_\alpha n_\alpha \mathbf{u}_\alpha. \tag{1.6}$$

In order to obtain macroscopic equations from the set of microscopic ones, we expand in a finite number of moments of the Boltzmann equation. First, by integrating over velocity space, we get the zeroth moment of Equation (1.1), which is the continuity equation for particles of species α:

$$\frac{\partial n_\alpha}{\partial t} + \nabla \cdot (n_\alpha \mathbf{u}_\alpha) = 0. \tag{1.7}$$

The first moment of the Boltzmann equation, or the momentum equation, is obtained by multiplying with $m_\alpha \mathbf{v}$ and integrating over the velocities:

$$\frac{\partial}{\partial t}(n_\alpha m_\alpha \mathbf{u}_\alpha) + \nabla \cdot (n_\alpha m_\alpha \langle (\mathbf{vv}\rangle_\alpha) - q_\alpha n_\alpha (\mathbf{E} + \mathbf{u}_\alpha \times \mathbf{B}) = \int C_{\alpha\beta} m_\alpha \mathbf{v} d^3v, \tag{1.8}$$

where $C_{\alpha\beta}$ is the contribution of collisions between particles α and β to the collision term C_α.

Lastly, the second scalar moment of Equation (1.1), the energy equation, can be obtained by multiplying with $\frac{1}{2}m_\alpha v^2$ and integrating over velocity space:

$$\frac{\partial}{\partial t}(n_\alpha \frac{1}{2} m_\alpha \langle v^2 \rangle_\alpha + \nabla \cdot (n_\alpha \frac{1}{2} m_\alpha \langle v^2 \rangle_\alpha) - q_\alpha n_\alpha \mathbf{E} \cdot \mathbf{u}_\alpha = \int C_{\alpha\beta} \frac{1}{2} m_\alpha v^2 d^3 v. \tag{1.9}$$

Rather than taking further moments of the Boltzmann equation, we close this set of equations by defining thermal quantities in terms of random particle velocities $\tilde{\mathbf{v}_\alpha} = \mathbf{v} - \mathbf{u}_\alpha$ (with $\langle \tilde{\mathbf{v}_\alpha} \rangle = 0$). These are the:

temperature	$T_\alpha(\mathbf{r}, t) = \frac{m_\alpha}{3k_B} \tilde{\mathbf{v}_\alpha},$
stress tensor	$\mathbf{P}_\alpha(\mathbf{r}, t) = n_\alpha m_\alpha \langle \tilde{\mathbf{v}_\alpha} \tilde{\mathbf{v}_\alpha} \rangle = p_\alpha \mathbf{I} + \pi_\alpha,$ with $p_\alpha = n_\alpha k_B T_\alpha,$
heat flow	$\mathbf{h}_\alpha(\mathbf{r}, t) = \frac{1}{2} n_\alpha m_\alpha \langle \tilde{v_\alpha}^2 \tilde{\mathbf{v}_\alpha} \rangle,$
momentum transfer	$\mathbf{R}_\alpha(\mathbf{r}, t) = m_\alpha \int C_{\alpha\beta} \tilde{\mathbf{v}_\alpha} d^3 v,$
heat transfer	$\mathbf{Q}_\alpha(\mathbf{r}, t) = \frac{1}{2} m_\alpha \int C_{\alpha\beta} \tilde{v_\alpha}^2 d^3 v,$

where $\mathbf{I}$ is the unit tensor, and so π_α contains the off-diagonal terms of the pressure tensor ($\mathbf{P}$). Finally, the results of transport theory are utilised to explore the relationship between these thermal quantities and the gradients of macroscopic quantities involving transport coefficients (e.g. viscosity, heat conductivity, resistivity).

1.2.2. From the Kinetic to the MHD Description of Plasmas

The next major step in moving from the distribution functions of kinetic theory, which can evolve in short length and time scales, towards a macroscopic description of the plasma, is to assume that the ions and electrons undergo frequent collisions, leading to a two-fluid description of the magnetised plasma valid on timescales much longer than the collisional relaxation times of ions and electrons: $\tau_H \gg \tau_i \gg \tau_e$. Next, we assume that the plasma consists only of electrons with charge $q_e = -e$ and one kind of ion ($q_i = Ze$), utilise the thermal quantities and transport coefficients mentioned above, and neglect most of the dissipative terms (namely, viscosity and heat flow: $pi_{e,i} \to 0$, $\mathbf{h}_{e,i} \to 0$). However, the small terms due to momentum transfer and heat generation associated with resistivity are kept ($\mathbf{R}_e = -\mathbf{R}_i \approx e n_e \eta \mathbf{j}$). With these intermediate assumptions, we may write the set of resistive two-fluid equations as

$$\frac{\partial n_\alpha}{\partial t} + \nabla \cdot (n_\alpha \mathbf{u}_\alpha) = 0, \tag{1.10}$$

$$n_\alpha m_\alpha \left(\frac{\partial \mathbf{u}_\alpha}{\partial t} + \mathbf{u}_\alpha \cdot \nabla \mathbf{u}_\alpha \right) + \nabla p_\alpha - n_\alpha q_\alpha (\mathbf{E} + \mathbf{u}_\alpha \times \mathbf{B}) = \mathbf{R}_\alpha \tag{1.11}$$

$$\frac{\partial p_\alpha}{\partial t} + \mathbf{u}_\alpha \cdot \nabla p_\alpha + \gamma p_\alpha \nabla \cdot \mathbf{u}_\alpha = (\gamma - 1) Q_\alpha, \tag{1.12}$$

where Q_α is the scalar resistivity (with $Q_e + Q_i = -(\mathbf{u}_e - \mathbf{u}_i) \cdot \mathbf{R}_e \approx \eta |\mathbf{j}^2|$).

The final step towards reaching a magnetohydrodynamic description of the plasma requires us to combine the two-fluid equations by adding pairs of them (multiplied by charge and mass factors), and to define macroscopic one-fluid variables from the thus obtained combinations of two-fluid variables such as the:

total mass density	$\rho = n_e m_e + n_i m_i,$	(1.13)
charge density	$\rho* = -e(n_e - Z n_i),$	
centre of mass velocity	$\mathbf{v} = \frac{n_e m_e \mathbf{u_e} + n_i m_i \mathbf{u_i}}{\rho},$	
current density	$\mathbf{j} = -e(n_e \mathbf{u}_e - Z n_i \mathbf{u_i}),$	
pressure	$p = p_e + p_i.$	

At this point, a couple of further assumptions need to be made. First of all, it is assumed in the single fluid description that the time required to reach temperature equilibrium between electrons and ions is short compared to other characteristic times, and therefore $T_e = T_i$. The above-mentioned requirement of quasi charge-neutrality now means that $|n_e - Z n_i| \ll n_e$. In order to consider the plasma as a single conducting fluid without distinguishing its individual species, as we do in the MHD description, we must remove the dependence on the small length- and time-scale phenomena of the two-fluid equations. For this reason, it is assumed that the electrons and ions have small relative velocities ($|\mathbf{u}_i - \mathbf{u}_e| \ll v$), and that the motions in the system happen at non-relativistic speeds ($v \ll c$). We consider only the length scales much larger than the cyclotron radii of the particles involved: $\lambda_{MHD} \gg r_{cyc}$ and time scales much longer than the periods associated with the cyclotron frequencies: $\tau_{MHD} \gg \omega_{cyc}^{-1}$.

Finally, if we now combine the resulting one-fluid moment equations with the Maxwell-equations (Equations 1.2-1.5) under the constraints listed above, we obtain the set of resistive MHD equations:

$$\frac{\partial \rho}{\partial t} + \nabla \cdot (\rho \mathbf{v}) = 0 \tag{1.14}$$

$$\rho \frac{D\mathbf{v}}{Dt} = -\nabla p + \mathbf{j} \times \mathbf{B} \tag{1.15}$$

$$\frac{\partial \mathbf{B}}{\partial t} \nabla \times \mathbf{E} = 0, \tag{1.16}$$

$$\frac{\partial p}{\partial t} + \mathbf{v} \cdot \nabla p + \gamma p \nabla \cdot \mathbf{v} = (\gamma - 1) \eta |\mathbf{j}|^2, \tag{1.17}$$

where $D/Dt = \partial/\partial t + \mathbf{v} \cdot \nabla$ i the material or total derivative, $\mathbf{j} = \frac{1}{\mu_0}\nabla \times \mathbf{B}$ and $\mathbf{E}' = \mathbf{E} + \mathbf{v} \times \mathbf{B} = \eta\mathbf{j}$ as stated in Ohm's law. Substituting these into Equation (1.16), we end up with the following form of the induction equation:

$$\frac{\partial \mathbf{B}}{\partial t} = \nabla \times (\mathbf{v} \times \mathbf{B}) - \frac{1}{\mu_0}\nabla \times (\eta \nabla \times \mathbf{B}), \tag{1.18}$$

where the first term describes the generation of the magnetic field connected to plasma motions, and the second term is responsible for its dissipation. However, if the time scales considered are faster than the resistive decay of the magnetic field, the second term in Equation (1.18) will be negligibly small. In addition, many astrophysical plasmas are perfectly conducting ($\mathbf{E} + \mathbf{v} \times \mathbf{B} = \eta\mathbf{j} = 0$), allowing us to neglect the heating term related to Ohmic dissipation on the right-hand side of Equation (1.17).

With the considerations made above, we can obtain the set of ideal MHD equations as

$$\frac{\partial \rho}{\partial t} + \nabla \cdot (\rho \mathbf{v}) = 0 \tag{1.19}$$

$$\rho \frac{D\mathbf{v}}{Dt} = -\nabla p - \frac{1}{\mu}\mathbf{B} \times (\nabla \times \mathbf{B}) \tag{1.20}$$

$$\frac{\partial \mathbf{B}}{\partial t} = \nabla \times (\mathbf{v} \times \mathbf{B}) \tag{1.21}$$

$$\frac{D}{Dt}\left(\frac{p}{\rho^\gamma}\right) = 0, \tag{1.22}$$

where p, and ρ, $\mathbf{v}$, $\mathbf{B}$, are the pressure, density, velocity, magnetic field strength, respectively, and the solenoidal condition on the magnetic field has to be fulfilled ($\nabla \cdot \mathbf{B} = 0$). Equation (1.19) represents the conservation of mass, stating that the density at a point can only increase (decrease) if mass flows into (out of) its surrounding region. Equation (1.20) is the momentum equation, which is essentially Newton's equation of motion for a fluid (plasma) element, expressing its acceleration under the effects plasma pressure gradients and the Lorentz force. The latter may be broken down into two terms using Ampére's law:

$$\mathbf{F_L} = \mathbf{j} \times \mathbf{B} = \frac{1}{\mu_0}\nabla \times \mathbf{B} \times \mathbf{B} = \frac{(\mathbf{B} \cdot \nabla)\mathbf{B}}{\mu_0} - \nabla \frac{B^2}{2\mu_0}. \tag{1.23}$$

The first term in Equation (1.23) is the magnetic tension force acting as a negative stress in the direction parallel to $\mathbf{B}$. The second term is the magnetic pressure force, which results in a positive stress in the direction normal to the magnetic field.

Equation (1.21) is the induction equation for ideal MHD, coupling together the evolution of the plasma and the magnetic field through the presence of the velocity term on the right-hand side. Finally, Equation (1.22) is the form of the energy equation for adiabatic processes, where the ratio of specific heats, $\gamma = c_p/c_v$, takes the value of $5/3$, and the right-hand side of the equation becomes zero, as any energy lost is balanced out by energy gains. This system of partial differential equations will serve as the starting point for deriving

dispersion relations for magnetic slab systems throughout the remaining chapters.

1.3. The Study of Waves in the Solar Atmosphere

The solar atmosphere is structured by the presence of gravity and magnetic fields, giving rise to a wide array of waveguides and observed oscillations (De Pontieu et al., 2005; Komm et al., 2015). The following Section provides a brief introduction to the MHD description of these wave detections (following mainly Priest (2014)) and their importance within the broader field of solar physics.

1.3.1. MHD Waves

If we examine a uniform plasma environment permeated by a magnetic field, and allow the equilibrium quantities of the system to come under the effect of a time-dependent linear perturbation, which may be described as $f(\mathbf{r},t) = f_{eq} + f_I(\mathbf{r},t)$, where the parameter f can be the pressure, the density, or the components of the magnetic field strength and the velocity. For linear perturbations, we require that $f_I \ll f$. Using these perturbed quantities while neglecting second- or higher-order terms, we can linearise the idea MHD equations. The details of this process can be found in e.g. Priest (2014). If we assume that $\mathbf{v_{eq}} = 0$ and combine the linearised equations, we can obtain a generalised MHD wave equation for disturbances in a uniform magnetised plasma:

$$\frac{\partial^2 \mathbf{v_I}}{\partial t^2} = c_{eq}^2 \nabla(\nabla \cdot \mathbf{v_I}) + (\nabla \times [\nabla \times \{\mathbf{v_I} \times \mathbf{B_{eq}}\}]) \times \frac{\mathbf{B_{eq}}}{\mu_0 \rho_{eq}}. \tag{1.24}$$

Next, we look for plane wave solutions with wavenumber vector $\mathbf{k}$ and the angular frequency ω as $\mathbf{f_I}(\mathbf{r},t) = \mathbf{f_I} \exp(i[\mathbf{kr} - \omega t])$, letting us obtain (after some rearranging) the following equations:

$$\begin{aligned}(-\omega^2 + k^2 c_{eq}^2 + k^2 v_A^2)(\mathbf{k} \cdot \mathbf{v_I}) = k^3 v_A^2 \cos(\theta_B)(\hat{\mathbf{B_{eq}}} \cdot \mathbf{v_I}), \text{ and} \\ k \cos(\theta_B) c_{eq}^2 (\mathbf{k} \cdot \mathbf{v_I}) = \omega^2 (\hat{\mathbf{B_{eq}}} \cdot \mathbf{v_I}).\end{aligned} \tag{1.25}$$

with θ_B denoting the angle between the magnetic field and the propagation direction, k denoting the magnitude of the wavenumber vector, and $\hat{\mathbf{B_{eq}}}$ being the unit vector in the direction of the magnetic field. Introduced here are some characteristic speeds of the system, namely, $v_A = \left(\frac{B_{eq}^2}{\mu_0 \rho_{eq}}\right)^{0.5}$, the equilibrium Alfvén speed, and $c_{eq} = \left(\frac{\gamma p_0}{\rho_0}\right)^{0.5}$, the equilibrium sound speed. Equation (1.25) has two types of solutions: transverse Alfvén wave solutions with $\omega = \pm\omega_A = \pm k v_A \cos(\theta_B)$, and magneto-acoustic (or magnetosonic) waves, which are the solutions to the quadratic equation in ω^2 below:

$$\omega^4 - \omega^2 k^2 (c_{eq}^2 + v_A^2) + c_{eq}^2 v_A^2 k^4 \cos^2(\theta_B) = 0. \tag{1.26}$$

These magneto-acoustic waves can be further categorised as slow and fast modes propagating with:

$$\omega_{slow} = \frac{1}{2}k^2(c_{eq}^2 + v_A^2)\left(1 + \sqrt{1 - 4c_T^2\cos^2(\theta_B)}\right),$$
$$\omega_{fast} = \frac{1}{2}k^2(c_{eq}^2 + v_A^2)\left(1 + \sqrt{1 + 4c_T^2\cos^2(\theta_B)}\right), \tag{1.27}$$

respectively, where $c_T^2 = (c_{eq}^2 v_A^2)/(c_{eq}^2 + v_A^2)$ is the square of the so-called tube or cusp speed. The magnetosonic- as well as the Alfvén waves can all propagate forward along or backward opposite to the magnetic field lines.

1.3.2. Introduction to Solar Magneto-Seismology

In the previous Section, we outlined some principles of the theory magnetohydrodynamics and MHD waves. In this section, we proceed to highlight their relevance in understanding the complex plasma laboratory that is our Sun's atmosphere. In this endeavour, the new and constantly evolving field of solar magneto-seismology (SMS) provides a versatile toolkit, when it comes to understanding and measuring the properties of the multitude of possible solar waveguides. These methods of SMS are built upon the principle that the parameters of the waves supported by a guiding medium are determined by its physical and geometric properties. Some of these parameters can be obtained from direct observations (e.g. temperature, density, or geometric size). Furthermore, We are able to measure temporal and spatial wave properties (such as frequencies, periods and amplitudes). These types of measurements are often more easily accomplished than e.g. an attempt at directly determining the magnetic field strength or some transport coefficients.

As we will show, it is possible to carry out theoretical studies to obtain a mathematical relationship between these quantities (see for example the equations of wave dispersion in a magnetic slab system summarised in Section 1.5). Complementing these theoretical models with concrete observations may then allow us to solve inversion problems, although this might be a challenging task. The eventual aim is to determine unknown parameters of the solar plasma which we may not be able to obtain directly purey from observations (Arregui and Goossens (2019); Erdélyi (2006a,b); Banerjee et al. (2007); Andries et al. (2009)).

MHD waves also count among the possible mechanisms of energy transfer for solving the atmospheric heating question. Their ubiquity and importance in our physical understanding of the solar plasma environment led to a rapid development of theoretical studies on MHD waves in our star's atmosphere (De Moortel and Nakariakov, 2012) as early as the 1970s (see e.g. Rosenberg (1970); Roberts et al. (1984)).

The rapid theoretical advancements were later also joined by the improvements in the spatial and temporal resolution of detectors. The recent past and the immediate future of magneto-seismology are both bright, thanks to both refinements in theory, and to an

unprecedented spatial and temporal resolution being achieved by both ground-and space-based detectors. The detection of transversal waves in coronal loops, with the help of TRACE [Transition Region and Coronal Explorer] in 1998 has become the symbol of this scientific turning point (Aschwanden et al., 1999; Nakariakov et al., 1999; Ruderman and Erdélyi, 2009; De Moortel and Nakariakov, 2012). Since then, numerous observational studies have been published on MHD waves detected in a plethora of solar features, such as coronal plumes, arcades, flares and spicules (Aschwanden, 2005, De Moortel, 2005, Banerjee et al., 2007, de Moortel, 2009, Mathioudakis et al., 2013, Arregui, 2015). This can be tied back to both the continued advances in spatio-temporal resolution in our observations, and to the availability and variety of both space-based observatories, for example, SOHO, SDO, and STEREO, and ground-based telescopes, such as DST, and SST (Nakariakov and Verwichte, 2005; Banerjee et al., 2007; Ruderman and Erdélyi, 2009; Wang, 2011; Arregui et al., 2012b; De Moortel and Nakariakov, 2012; Mathioudakis et al., 2013). Currently, we are on the brink of a new age of observational mega-projects, with the newest generation of observing stations in the planning or early operations phases. The first one of these, the Daniel K. Inouye Solar Telescope (DKIST) has already made its first observations, and it will hopefully be joined by the planned EST (European Solar Telescope) within about a decade.

1.4. The Kelvin-Helmholtz Instability

In addition to the physical properties of waveguides, a necessary and important part of investigating MHD waves in solar structures in the presence of flows is the study of whether they become subject to the Kelvin-Helmholtz instability (KHI). Therefore, in the following, we provide a short background section on this instability and its role in a solar context.

In the presence of the Kelvin-Helmholtz instability in fluids or plasmas, the loss of stability results from the existence of shearing motions in the medium. The phenomenon was named after the first scientists to describe it: William Thomson (1st Baron Kelvin) British and Hermann von Helmholtz German physicists (Helmholtz, 1868; Thomson, 1871). The instability can occur either due to the presence of velocity shear in a single fluid, or due to a difference in velocities across an interface between two fluids. As illustrated in Figure 1.2, when this boundary (shown in panel (a)) suffers a small perturbation (panel (b)), then some of the velocity streamlines are compressed, which results in a faster flow and a decrease in pressure. In other areas, the streamlines expand, the flow becomes slower, and the pressure increases. Overall, this generates a pressure gradient which works towards making the original perturbation grow larger (panel (c)). Eventually, the perturbation steepens, enters the nonlinear regime, and rolls up into a vortex (shown in panel (d) of Figure 1.2).

The KHI is known both in hydrodynamics (HD) and magnetohydrodynamics (MHD). In the purely HD case, if surface tension is absent, a boundary between two layers of

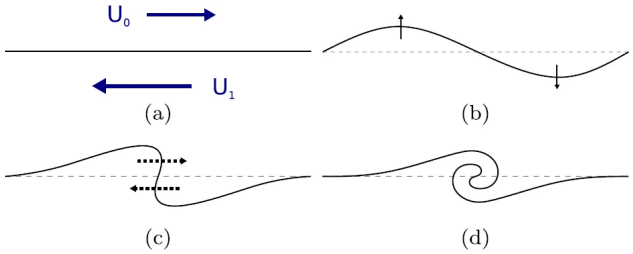

Figure 1.2: The evolution of the KHI at an interface with oppositely directed background flows Source: Barbulescu and Erdélyi (2018).

inviscid, immiscible fluids which are in relative motion, will always be subject to the KHI. If surface tension is not negligible, then, up to a critical flow speed, the boundary between the two fluids may be stabilised.

In MHD, the presence of a magnetic field can markedly change this stability threshold. Chandrasekhar (1961) analysed the linear phase of the KHI in two basic equilibrium configurations. First, at a tangential interface between two regions of different flow speed (U_0 and U_1), density (ρ_0 and ρ_1) and magnetic field strength (B_0 and B_1), he found that the instability sets in when $\frac{B_0^2+B_1^2}{\mu\rho_0\rho_1}(\rho_0+\rho_1) \leq (U_0-U_1)^2$, if the flows and the magnetic fields are all parallel to the interface. Here, the perturbations perpendicular to the interface stretch the magnetic field lines and thus cause a restoring force to appear. This process is essentially analogous to the HD case, but the stabilising role of the surface tension is now played by the magnetic field. On the other hand, Chandrasekhar (1961) also found that when the magnetic field is perpendicular to the flows, the field lines are not stretched, no restoring force is generated. Therefore, the field has no such stabilising effect, and the interface can always become subject to the KHI when perpendicular perturbations occur.

Nature provides abundant examples of the Kelvin-Helmholtz instability, on Earth as well as in space. Both the atmosphere and the oceans of our planet can give rise to instances of the KHI (Mak, 2011; Smyth and Moum, 2012; Miles, 1957). It can be found in our magnetosphere (Hasegawa et al., 2004; Miura, 1984), and, leaving the solar system, even in supernova remnants (Wang and Chevalier, 2001), or in interstellar clouds (Vietri et al., 1997). Although the various magnetic fields of our star can potentially have a stabilising effect, the KHI has still been observed in a solar context, for example in the flank regions of Coronal mass ejections (CMEs) (Ofman and Thompson, 2011; Foullon et al., 2011; Möstl et al., 2013), and in some solar jets (Kuridze et al., 2016; Bogdanova et al., 2018; Zhelyazkov et al., 2018).

1.5. The Study of MHD Waves in Magnetic Slabs

The methods of solar magneto-seismology described in general terms in Section 1.3.2 require us to conduct theoretical studies of MHD waves guided by structured simple geometries. The two basic building blocks used in solar physics are magnetic flux tube and slab

models. In the current study, we only detail wave behaviour in slabs, but e.g. Priest (2014) or Edwin and Roberts (1983) provide a summary of the basics of flux tube studies.

1.5.1. Symmetric Slabs

In a series of classical studies, Roberts (1981a) and Edwin and Roberts (1982) investigated the properties of magneto-acoustic waves first at an interface (Roberts, 1981a), then in a magnetic slab enclosed in a non-magnetic environment (Roberts, 1981b) (see panel a of Figure 1.3), and eventually in a magnetic environment (Edwin and Roberts, 1982). By

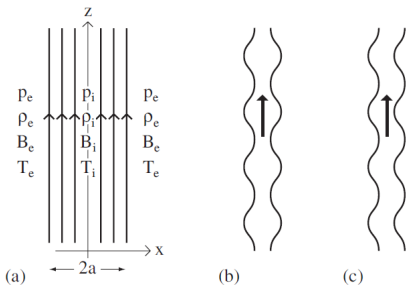

Figure 1.3: The model of a symmetric magnetic slab and its eigenmodes. Source: Priest (2014).

linearising the ideal MHD equations and looking for plane wave solutions propagating along the field, Edwin and Roberts (1982) obtained the dispersion relation of MHD waves in a symmetric magnetic slab in the following form:

$$\rho_e(v_{Ae}^2 - \omega^2)m_0 \begin{pmatrix} \tanh(m_0 x_0) \\ \coth(m_0 x_0) \end{pmatrix} + \rho_0(k^2 v_{A0^2} - \omega^2)m_e = 0, \tag{1.28}$$

where the index 0 (e) denotes a parameter inside (outside) of the slab, and m_e and m_0 contain the sound-, Alfvén-, and tube speeds of each region:

$$m_j = \left\{ \frac{\left(k^2 v_{Aj}^2 - \omega^2\right)\left(k^2 c_j^2 - \omega^2\right)}{\left(v_{Aj}^2 + c_j^2\right)\left(k^2 c_{Tj}^2 - \omega^2\right)} \right\}^{1/2}, \qquad j = 0, e. \tag{1.29}$$

The dispersion relation, Equation (1.28), in fact, represents the concise form of two equations together. The top line with the $\tanh(m_0 x_0)$ function describes sausage eigenmodes, while the bottom line with $\coth(m_0 x_0)$ represents kink modes (illustrated in panels (b) and (c) of Figure 1.3, respectively). Based on whether they are oscillating or evanescent inside the slab, both kinds of modes can also be described as body or surface waves.

1.5.2. Asymmetric Slabs

These "classical" magnetic slab models treated the environment of the slab as symmetric. However, our growing understanding and improving observations of the Sun suggest that

a generalisation of this geometry to include various sources of external asymmetry can be beneficial. The first asymmetric slab study was published by Allcock and Erdélyi (2017). It served as the asymmetric equivalent of the configuration described by Roberts (1981b), providing both an analytical and numerical study of the consequences of external density asymmetry. This model was further generalised by re-introducing external magnetic fields, thus placing the slab in an environment where all the equilibrium quantities (pressures, densities and magnetic field strengths) were allowed to be asymmetric (Zsámberger et al., 2018; Zsámberger and Erdélyi, 2020, 2021). Since magnetic fields weave through and through the interconnected solar atmosphere, it is reasonable to expect that we will encounter asymmetries in both the external densities and the magnetic fields.

To summarise the equilibrium configuration of this extended model, now the two interfaces (at $x = \pm x_0$) divide the volume up into three separate domains of magnetised plasma, characterised by

$$N(x) = \begin{cases} N_1 & x < -x_0, \\ N_0 & |x| < x_0, \\ N_2 & x_0 < x, \end{cases} \tag{1.30}$$

where N_j can denote densities, pressures, temperatures, and magnetic field strengths, while $N_j =$ constant (for $j = 0, 1, 2$). Figure 1.4 provides an illustration of the equilibrium state of this asymmetric magnetic slab system. Zsámberger et al. (2018) obtained the dispersion

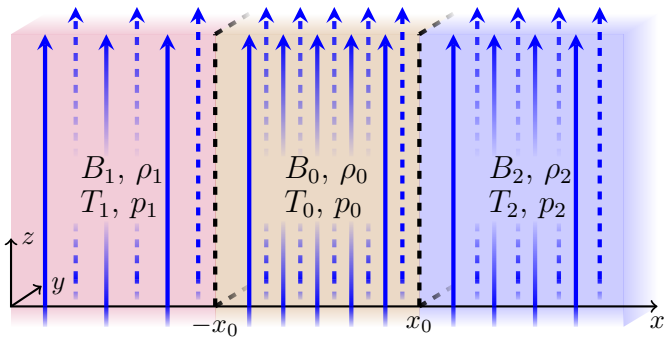

Figure 1.4: Equilibrium configuration of a magnetic slab embedded in an asymmetric magnetic environment. Adapted from Allcock et al. (2019).

relation for this fully magnetic asymmetric configuration as

$$2m_0^2\left(k^2v_{A1}^2-\omega^2\right)\left(k^2v_{A2}^2-\omega^2\right)+2\frac{\rho_0}{\rho_1}m_1\frac{\rho_0}{\rho_2}m_2\left(k^2v_{A0}^2-\omega^2\right)^2 + \rho_0m_0\left(k^2v_{A0}^2-\omega^2\right)\left[\frac{m_2}{\rho_2}\left(k^2v_{A1}^2-\omega^2\right)+\frac{m_1}{\rho_1}\left(k^2v_{A2}^2-\omega^2\right)\right]\left[\tau_0+\frac{1}{\tau_0}\right]=0, \tag{1.31}$$

where

$$m_j^2 = \frac{\left(k^2 v_{Aj}^2 - \omega^2\right)\left(k^2 c_j^2 - \omega^2\right)}{\left(v_{Aj}^2 + c_j^2\right)\left(k^2 c_{Tj}^2 - \omega^2\right)}, \qquad j = 0, 1, 2. \tag{1.32}$$

In the general case, the dispersion relation for the slab in an asymmetric environment does not decouple into two separate equations for sausage and kink modes (see Allcock and Erdélyi (2017) for the externally non-magnetic and Zsámberger et al. (2018) for the externally magnetic case). When the external asymmetry is weak, it is possible to obtain an approximation of Equation (1.31) which can then be decoupled into two separate equations, one for weakly asymmetric quasi-sausage and another for weakly asymmetric quasi-kink modes:

$$(k^2 v_{A0}^2 - \omega^2)\left[\frac{\rho_0}{\rho_1}\frac{m_1}{(k^2 v_{A1}^2 - \omega^2)} + \frac{\rho_0}{\rho_2}\frac{m_2}{(k^2 v_{A2}^2 - \omega^2)}\right] + 2m_0 \begin{pmatrix}\tanh\\ \coth\end{pmatrix}\{m_0 x_0\} = 0. \tag{1.33}$$

Although this approximation may potentially mean some limitations to the applicability of the model, it greatly increases its analytical tractability. Approximate solutions for a number of limiting cases, such as the thin- and wide-slab approximations, and the high- and low-beta limits were obtained both for strongly and weakly asymmetric magnetic slabs by Zsámberger and Erdélyi (2020). With the help of numerical results, the future applicability of the model to several solar atmospheric features (such as prominences, light bridges, or magnetic bright points) was demonstrated (Zsámberger and Erdélyi, 2021), and the SMS tools of the amplitude ratio and minimum perturbation shift methods were described by Allcock and Erdélyi (2018) and Zsámberger and Erdélyi (2022b). An extension of the new SMS toolkit for standing, instead of propagating, waves guided by asymmetric slab configurations was investigated in Oxley et al. (2020a) and Oxley et al. (2020b).

A complete generalisation of static asymmetric multi-layered Cartesian models was described by Shukhobodskaia and Erdélyi (2018) for the externally non-magnetic case, and further improved in Allcock et al. (2019) for the completely magnetic case. These last two configurations contain an infinite number of slabs, providing easily applicable models for complex solar waveguides, such as a sunspot divided into several umbral cores by light bridges or a magnetic bright point and its environment of the intergranular lane between two granules on the solar surface.

1.5.3. On the Eigenmodes of Asymmetric Slab Models

As noted above, in a symmetric slab system, the general dispersion relation decouples into two separate equations, irrespective of the presence or absence of external magnetic fields (see Roberts (1981b) and Edwin and Roberts (1982)). One of these (containing the $\tanh(m_0 x_0)$ function in the form of the dispersion relation shown in Equation (1.28)) describes the sausage modes, for which the amplitude of the velocity perturbation ($\hat{v_x}$) is described by an odd function, resulting in the anti-phase oscillation of the slab boundaries.

The solutions to the second ($\coth(m_0 x_0)$) line of the dispersion relation are the kink waves, which are described by an even $\hat{v_x}$ function, and which have the slab boundaries oscillating in phase (Roberts, 1981b).

In contrast, we reiterate that the full and exact dispersion relation of an asymmetric slab system (again, regardless of the magnitude of the external magnetic fields) does not decouple into separate equations governing sausage and kink modes in the general case. Any asymmetry introduced affects both "sausage" and "kink" type solutions, giving them some mixed properties of the symmetric sausage and kink modes. To differentiate them from their symmetric counterparts, these asymmetric eigenmodes were named by Allcock and Erdélyi (2017) quasi-sausage in the case of the in-antiphase oscillations and quasi-kink waves for the in-phase oscillations. This nomenclature was later adopted by the other asymmetric slab studies, too.

Visually, the most striking difference between the symmetric and asymmetric eigenmodes is that in the latter, the transverse velocity shows an asymmetric distribution across the slab and its environment, which manifests as different amplitudes of oscillation at the two interfaces on its boundaries. This effect is shown in Figure 1.5, in which the solid black curve displays numerical results obtained for the transverse velocity perturbation ($\hat{v_x}(x)$) as a function of the transverse spatial coordinate, x, overlaid on an illustration of an asymmetric system containing a dense and strongly magnetised slab. In this Figure, the blue arrows depict the background magnetic fields, and the brightness of the grey shading the magnitude of the background densities (with darker colours representing denser areas). Figure 1.5a shows a slow quasi-sausage surface mode, 1.5b is a slow quasi-kink surface mode, while Figure 1.5c displays a fast quasi-sausage body mode of order one, and 1.5d depicts a fast quasi-kink body mode of order one. The results were obtained using the following set of background parameters: $v_{A0} = 0.7c_0$, $v_{A1} = 0.2c_0$, $v_{A2} = 0.1c_0$, $c_1 = 2.2279c_0$, $c_2 = 1.8742c_0$, $\rho_1/\rho_0 = 0.28$, and $\rho_2/\rho_0 = 0.4$. Panels 1.5a and 1.5b show solutions in a narrow slab (with $kx_0 = 0.685$), but panels 1.5c and 1.5d display solutions from a wider slab ($kx_0 = 2.790$).

Although this is a less immediately obvious characteristic of asymmetric eigenmodes, another important difference from their symmetric counterparts is that the magnetic surface in the geometric centre of the slab remains unperturbed for symmetric sausage modes and is minimally perturbed for symmetric kink modes, this surface of zero or minimum perturbation is shifted away from the midpoint in the case of quasi-sausage and quasi-kink waves. Allcock and Erdélyi (2017); Zsámberger et al. (2018); Allcock and Erdélyi (2018) and Zsámberger and Erdélyi (2022b) explore in further detail how the density and magnetic asymmetries influence the direction and magnitude of this shift, as well as how the mixed character of the asymmetric eigenmodes may be used to develop new tools of solar magneto-seismology.

It must also be noted that both the asymmetric quasi-kink and the "pure" kink eigenmodes show in-phase oscillations, the cross-sectional width of the central slab is left un-

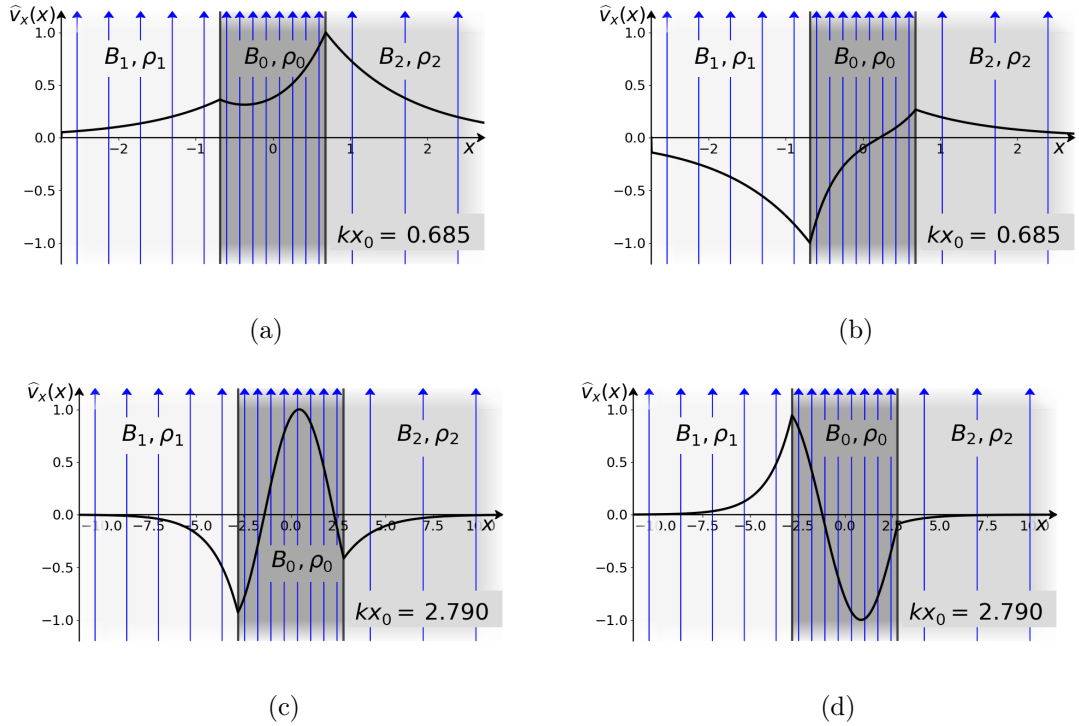

Figure 1.5: The transverse velocity perturbation amplitude of eigenmodes in an asymmetric magnetic slab. Figure adapted from Allcock et al. (2019).

changed in a symmetric system, but quasi-kink modes in an asymmetric system do not preserve the slab's area (or volume) in the same way.

As the last part of the Introduction, we provided this detailed description of asymmetric eigenmodes because, as it will be seen in later Chapters, too, asymmetric slab systems are in general characterised by the presence of quasi-sausage and quasi-kink eigenmodes instead of purely kink or sausage oscillations. Therefore, these are the types of solutions we will be referring to when presenting our results on the frequencies and the stability of waves in asymmetric steady slab systems throughout the study.

1.6. Outline of the Thesis

This dissertation is part of an effort to investigate propagating MHD waves in both symmetric and asymmetric solar waveguides, as well as the effects of steady background flows on wave properties and the instability limits of these configurations. Both analytical and numerical solutions are provided for the equations describing wave dispersion in these waveguide systems, and, where possible, instability limits are also obtained. In the Introduction, we provided a general background to MHD waves and the KHI in solar physics, as well as an overview of recent developments in the rapidly evolving field of studying asymmetric solar waveguides, focusing on static Cartesian slabs. Notably, the properties

of asymmetric eigenmodes are described, which serves both as an aid for the following Chapters and a motivation for the continued expansion of asymmetric waveguide models.

Chapter 2 deals with the details of MHD wave propagation and the Kelvin-Helmholtz instability in a magnetic slab that is embedded in an asymmetric non-magnetic environment, where the environment also contains asymmetric background flows. The dispersion relation is derived for this case, and then various approximations are utilised to provide analytical solutions to it in limiting cases relevant to the solar environment. The Chapter concludes with a numerical study, extending the investigation of the problem to a wide range of slab width and Alfvén Mach number parameters.

In Chapter 3, a different approach to generalising steady slab models is studied. Namely, the slab is placed in an asymmetric *magnetic* environment, and the focus returns to a bulk background flow contained within the slab region itself. After deriving the general dispersion relation for this case, the weak asymmetry and thin slab approximations are used to describe how the frequencies of the eigenmodes relate to the characteristic speeds, densities, slab with and flow speed parameters. Furthermore, the threshold of the Kelvin-Helmholtz instability onset and its relation to the introduced asymmetry is briefly studied. The analytical description is again complemented by presenting numerical solutions to the full dispersion relation.

Building on the models described in the previous Chapters, next, Chapter 4 deals with an example of a potential further generalisation of the slab model for asymmetric steady flows in an asymmetric magnetic environment, and a potential application of this model to magnetic bright points. After this final particular case, the most general case of the asymmetric slab system is investigated, in which all regions can be characterised by different pressures, densities, temperatures, magnetic fields, and background flow speeds.

In Chapter 5, we focus on a jet-like symmetric slab configuration containing a linear velocity profile and under the effect of a kink oscillation. The equation describing wave dispersion is derived and compared to the corresponding relation in the lack of an internal magnetic field within the jet structure. The Chapter concludes with the description of a few cases of analytical interest for the configuration and a collection of illustrative examples of numerical solutions.

Finally, in Chapters 6 and 7, the main results of this series of investigations are summarised, and future avenues of study are suggested in order to further our understanding of wave propagation and instabilities of jet-like asymmetric waveguide systems in the solar atmosphere.

Chapter 2.
Magnetohydrodynamic Waves and the Kelvin-Helmholtz Instability in a Magnetic Slab Enclosed by an Asymmetric Plasma- and Flow Environment

Abstract

In this Chapter, we focus on propagating MHD waves in steady slabs. Unlike previous asymmetric Cartesian studies, in the asymmetric slab model laid out here, the presence of bulk background flows plays an important role. After summarising previous results about magnetic slabs incorporating a steady flow, we discuss new results on placing asymmetric flows in the slab system. We derive the general dispersion relation as well as its weak asymmetry approximation. Finally, we present both an analytical and a numerical study of the dependence of the solutions to the dispersion relation on the density and flow asymmetry present in the system. The paper Zsámberger et al. (2022a) serves as the basis of this Chapter.

2.1. Chapter Introduction

The solar atmosphere is shaped by the presence of magnetic fields, which create a dynamic and inhomogeneous medium rich in waveguides that enable the propagation of a wide range of magnetohydrodynamic (MHD) waves. The wide variety of magnetic solar waveguides has inspired the continuous improvement of both theoretical models and observational methods, as we discussed in the previous Chapter. The expansion of traditionally symmetric slab models to a multi-layered asymmetric waveguide containing an infinite number of slabs has already been discussed in the Introduction. This, however, is only one possible avenue towards the generalisation of Cartesian waveguide models. In the current Chapter, we move on to the study of a new class of generalised slab models, namely, that of steady slabs. These configurations incorporate bulk background motions in at least one region within the volume, which requires us to consider new physical effects on top of the ones described in relation to static models.

A fundamental difference from static models is including a steady flow in the slab system (even a symmetric one), we create the possibility of shearing motions in the configuration, which, can under some circumstances lead to the onset of the KHI, as it was explained in Section 1.4. So, while the solutions to dispersion relations of static slabs always yielded stable results, the stability of waves guided by steady slabs must also be investigated.

A secondary effect of the presence of a bulk background flow can be a shifting of the phase- and cut-off speeds of waves guided by a specific system, even in a symmetric case (see e.g. Nakariakov and Roberts (1995)). Further important effects that may arise from the presence of background flows are beyond the scope of the current study (see e.g. negative-energy wave instabilities or resonant flow instabilities in Taroyan and Ruderman (2011) and Ryutova (2015)).

The work presented in the current Chapter focuses on introducing background flows into the kind of piece-wise uniform asymmetric slab model which was generalised for kinetic asymmetry by Allcock and Erdélyi (2017). The first step towards the extension of this model was taken by Barbulescu and Erdélyi (2018), who described the effects of adding a steady background flow into the internal slab region embedded in an asymmetric non-magnetic environment. They analysed the propagation of magneto-acoustic waves and the KHI-threshold. The authors obtained the full dispersion relation and confirmed that in the presence of internal (or, as we will see in the following, external) flows, the analysis of eigenmodes should be extended to negative phase speeds to account for the symmetry-breaking and the potential change of character between backward- and forward-propagating modes. To demonstrate the usefulness and easy applicability of their model, Barbulescu and Erdélyi (2018) also modelled a CME flank region as a steady asymmetric slab to explain the observational detection of the KHI described by Foullon et al. (2011). While an estimate of CME ejecta density could be obtained with this simple model, it was noted that the validity of this result is limited by the inability of the model to explain why the KHI was only observed on one side of the slab, and not observed between the CME core and flank regions, too. These considerations provide a concrete motivation to further develop steady slab models that e.g. include external magnetic fields everywhere (see Chapter 3), or one which is characterised by the presence of asymmetric flows, as described in the current Chapter 2.

First, in Section 2.2, the dispersion relation for a magnetic slab embedded in an asymmetric non-magnetic environment containing asymmetric flows is derived. Then, in Sections 2.3.1-2.3.1, analytical approximations are obtained for the frequencies of the eigenmodes. A further analytical study is carried out in Sections 2.3.3 - 2.3.4, throughout which we investigate the influence of small density and flow asymmetries on the frequency and the stability of supported waves. Lastly, in Section 2.4 delivers an extensive numerical investigation of solutions in this slab system.

2.2. Wave Dispersion in an Asymmetric Steady Slab System

2.2.1. The Equilibrium of a Slab in an Asymmetric Non-Magnetic Environment with Steady Flows

The configuration investigated in this Chapter is that of a slab of magnetised plasma bounded by two interfaces at $\pm x_0$, described by density, pressure and temperature ρ_0, p_0 and T_0, respectively, and permeated by a vertical magnetic field $\mathbf{B}_0 = (0, 0, B_0)$. The slab is embedded in an asymmetric environment, defined as having density, pressure and temperature ρ_1, p_1 and T_1 on the left-hand-side, and ρ_2, p_2 and T_2 on the right-hand-side. In this first step, the environment of the slab is non-magnetic. Both external regions contain time-independent flows denoted as $\mathbf{U}_1 = (0, 0, U_1)$ and $\mathbf{U}_2 = (0, 0, U_2)$, as also illustrated in Figure 2.1. Here, red arrows indicate the external flows, while blue arrows show the internal magnetic field. The equilibrium background parameters must be chosen such that the condition of total pressure balance is fulfilled: $p_1 = p_0 + \frac{B_0^2/2}{\mu} = p_2$.

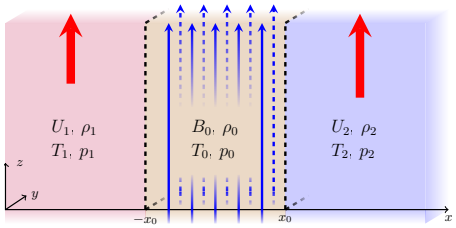

Figure 2.1: The equilibrium configuration of the magnetic slab with asymmetric external steady flows. Source: Zsámberger et al. (2022a).

In Chapter 1, we summarised the equations of ideal MHD in Equations (1.19) - (1.22). These were, however, detailing the static case; and so now we must re-state them for the case involving a bulk background flow to guarantee their validity throughout the slab system. (In the case of the central slab, this new form can be reduced back to the static form stated in the Introduction, but for the environmental regions, the background motions result in additional terms staying in our system of equations.) With these considerations in mind, the form of the MHD equations from which we will obtain the governing equation of disturbances in the slab system is the following:

$$\rho \frac{D\mathbf{v}}{Dt} = -\nabla p - \frac{1}{\mu_0}\mathbf{B} \times (\nabla \times \mathbf{B}), \tag{2.1}$$

$$\frac{\partial \rho}{\partial t} + \nabla \cdot (\rho \mathbf{v}) = 0, \tag{2.2}$$

$$\frac{D}{Dt}\left(\frac{p}{\rho^\gamma}\right) = 0, \tag{2.3}$$

$$\frac{\partial \mathbf{B}}{\partial t} = \nabla \times (\mathbf{v} \times \mathbf{B}). \tag{2.4}$$

2.2.2. The Dispersion Relation

Since we concern ourselves with magneto-acoustic waves propagating parallel to the slab boundaries and the magnetic fields, for the following investigation, we restrict ourselves to the choice of $k_y = 0$ and $v_y = 0$. This provides a simple analytical framework, but, it must be noted that it also precludes the study of e.g. y-dependent Alfvén waves.

Next, we linearise the equations about a static basic state by introducing small, time-dependent perturbations as explained in Section 1.3.

We substitute the perturbed variables into Equations (2.1) - (2.4)), and by neglecting second-order terms, obtain the linearised equations detailed below:

$$\rho_0 \frac{\partial v_x}{\partial t} = -\frac{\partial p}{\partial x} + \frac{B_0}{\mu}\left(\frac{\partial b_x}{\partial z} - \frac{\partial b_z}{\partial x}\right), \qquad \rho_0 \frac{\partial v_z}{\partial t} = -\frac{\partial p}{\partial z}, \tag{2.5}$$

$$\frac{\partial \rho}{\partial t} + \rho_0 \nabla \cdot \mathbf{v} = 0, \tag{2.6}$$

$$\frac{\partial p}{\partial t} = c_0^2 \frac{\partial \rho}{\partial t}, \tag{2.7}$$

$$\frac{\partial b_x}{\partial t} = B_0 \frac{\partial v_x}{\partial z}, \qquad \frac{\partial b_z}{\partial t} = -B_0 \frac{\partial v_x}{\partial x}. \tag{2.8}$$

We Fourier-decompose Equations (2.5)-(2.8) by assuming that the linear perturbations are of the form $f(\mathbf{r}, t) = \hat{f}(x)e^{i(kz-\omega t)}$, where, as before, ω is the angular frequency, and k is the z-component of the wavenumber vector ($\boldsymbol{\kappa} = (k_x, k_y, k_z)$). Combining the Fourier-form of the linearised MHD equations yields an ordinary differential equation for $\widehat{v_x}$ in each region of the slab system. In the slab interior, this equation takes the form of

$$\widehat{v_x}'' - m_0^2 \widehat{v_x} = 0, \tag{2.9}$$

where

$$m_0^2 = \frac{(k^2 v_{A0}^2 - \omega^2)(k^2 c_0^2 - \omega^2)}{(c_0^2 + v_{A0}^2)(k^2 c_{T0}^2 - \omega^2)}, \qquad c_{T0}^2 = \frac{c_0^2 v_{A0}^2}{c_0^2 + v_{A0}^2}. \tag{2.10}$$

Here, as before, c_0 v_{A0}, and c_{T0} denote the sound speed, Alfvén speed and tube speed associated with the central region, the slab itself. This expression is formally identical to the corresponding equation for a symmetric slab derived by (Roberts, 1981b), but it is only valid for the perturbation inside the slab.

Performing the same steps using the parameters of the external layers, where there are no magnetic fields, but there are flows present, we obtain the following ODEs:

$$\widehat{v_x}'' - m_j^2 \widehat{v_x} = 0, \tag{2.11}$$

where

$$m_j^2 = k^2 - \frac{\Omega_j^2}{c_j^2}. \tag{2.12}$$

Due to the presence of flows, these expressions, instead of the simple angular frequency,

here, the Doppler-shifted frequencies for the two sides of the slab appear, defined as $\Omega_j = \omega - kU_j$ for $j = 1, 2$.

We require that perturbations in the slab should have no effect on the plasma far away from the system, meaning we exclude leaky modes from our investigation and require that the waves be evanescent outside the slab. Mathematically, this is expressed by the condition that $m_1^2 > 0$ and $m_2^2 > 0$. However, both positive and negative values of m_0^2 are allowed, as the solutions inside the central slab can be both evanescent (surface waves) or oscillatory (body waves, with $m_0^2 < 0$).

For the trapped oscillations, using arbitrary constants A, B, C and D, the general solution of Equations 2.9 and 2.11 is of the form

$$\widehat{v}_{xj}(x) = \begin{cases} A(\cosh(m_1 x) + \sinh(m_1 x)), & x < -x_0, \\ B\cosh(m_0 x) + C\sinh(m_0 x), & |x| \leq x_0, \\ D(\cosh(m_2 x) - \sinh(m_2 x)), & x > x_0. \end{cases} \tag{2.13}$$

We match these solutions across the two interfaces at $x = \pm x_0$ by using the continuity of the Lagrangian displacement and the total pressure perturbation as boundary conditions:

$$\begin{aligned} \frac{\widehat{v}_{x1}(x=-x_0)}{\Omega_1} &= \frac{\widehat{v}_{x0}(x=-x_0)}{\omega}, & \qquad \frac{\widehat{v}_{x2}(x=x_0)}{\Omega_2} &= \frac{\widehat{v}_{x0}(x=x_0)}{\omega}, \\ \widehat{p_{T1}}_{-x_0} &= \widehat{p_{T0}}_{-x_0}, & \qquad \widehat{p_{T0}}_{x_0} &= \widehat{p_{T2}}_{x_0}, \end{aligned} \tag{2.14}$$

where the perturbation of the total pressure can be expressed as

$$\widehat{p_T}(x) = \widehat{v'}_{xj}(x) \begin{cases} \dfrac{i\rho_1\Omega_1}{m_1^2} = \frac{\Lambda_1}{m_1}, & x < -x_0 \\ \dfrac{-i\rho_0(k^2 v_{A0}^2 - \omega^2)}{m_0^2\omega} = \frac{\Lambda_0}{m_0}, & |x| \leq x_0 \\ \dfrac{i\rho_2\Omega_2}{m_2^2} = \frac{\Lambda_2}{m_2}, & x > x_0. \end{cases} \tag{2.15}$$

Using Equation (2.13) and the associated boundary conditions (2.14) and (2.15), we obtain a system of four homogeneous algebraic equations, which can be written in matrix form as

$$\begin{pmatrix} (C_1 - S_1)/\Omega_1 & -C_0/\omega & S_0/\omega & 0 \\ 0 & -C_0/\omega & -S_0/\omega & (C_2 - S_2)/\Omega_2 \\ \Lambda_1(C_1 - S_1) & \Lambda_0 S_0 & -\Lambda_0 C_0 & 0 \\ 0 & \Lambda_0 S_0 & \Lambda_0 C_0 & \Lambda_2(C_2 - S_2) \end{pmatrix} \begin{pmatrix} A \\ B \\ C \\ D \end{pmatrix} = \begin{pmatrix} 0 \\ 0 \\ 0 \\ 0 \end{pmatrix}, \tag{2.16}$$

where $S_j = \sinh(m_j x_0)$ and $C_j = \cosh(m_j x_0)$ (for $j = 0, 1, 2$). We search for non-trivial solutions of this system of equations by requiring that the determinant of the matrix on

the left-hand side should be zero, which leads us to the following equation:

$$2\left(\Lambda_0^2\omega^2+\Lambda_1\Lambda_2\Omega_1\Omega_2\right)+\Lambda_0\omega\left(\Lambda_1\Omega_1+\Lambda_2\Omega_2\right)\left(\tanh(m_0x_0)+\coth(m_0x_0)\right)=0. \quad (2.17)$$

In terms of the densities and characteristic speeds of each plasma region, this equation can be restated as

$$m_0^2\Omega_1^2\Omega_2^2+\frac{\rho_0}{\rho_1}m_1\frac{\rho_0}{\rho_2}m_2(k^2v_{A0}^2-\omega^2)^2-\frac{1}{2}m_0(k^2v_{A0}^2-\omega^2)\left(\frac{\rho_0}{\rho_1}m_1\Omega_2^2 + \frac{\rho_0}{\rho_2}m_2\Omega_1^2\right)\left(\tanh(m_0x_0)+\coth(m_0x_0)\right)=0. \quad (2.18)$$

Equation (2.18) is the full dispersion relation of magnetosonic waves propagating along the magnetic field lines in the asymmetric, externally non-magnetic slab system in the presence of asymmetric external flows. This dispersion relation remains consistent with the other asymmetric dispersion relations obtained by e.g. Allcock and Erdélyi (2017); Zsámberger et al. (2018) and Barbulescu and Erdélyi (2018), as in its most general case it remains a single equation describing both the quasi-kink and the quasi-sausage eigenmodes (described in greater detail in Section 1.5.3) together.

2.2.3. Comparison with a Symmetric Slab

As discussed in the Introduction, there is an intrinsic difference between perturbations along symmetric and asymmetric magnetic slabs. While the dispersion relation governing a symmetric slab (such as Roberts (1981b)) consists of two independent equations, corresponding to the sausage and kink eigenmodes, the dispersion relation governing an asymmetric slab is a single equation providing a coupled description of quasi-sausage and quasi-kink modes.

We can make a closer comparison between the asymmetric and the symmetric slab systems by employing the so-called weak asymmetry approximation, which requires that the densities, pressures, and flow speeds on either side of the slab should be of the same order of magnitude, so that $\lambda_2=\Lambda_2\Omega_2$ is of the same order as $\lambda_1=\Lambda_1\Omega_1$. Then we can write $\lambda_2=\lambda_1+\epsilon$ (where ϵ is a small parameter), and the following connection between these quantities may be utilised in transforming the dispersion relation:

$$1=\frac{1}{4}\frac{(\Lambda_1\Omega_1+\Lambda_2\Omega_2)^2}{\Lambda_1\Omega_1\Lambda_2\Omega_2}+\mathcal{O}(\epsilon^2)\approx\frac{1}{4}\frac{(\Lambda_1\Omega_1+\Lambda_2\Omega_2)^2}{\Lambda_1\Omega_1\Lambda_2\Omega_2}. \quad (2.19)$$

Substituting Equation (2.19) into the general dispersion relation (Equation 2.17), then multiplying by $2\Lambda_1\Omega_1\Lambda_2\Omega_2\neq0$ and factorising then yields a useful product of two terms:

$$\left[\Lambda_0\omega(\Lambda_1\Omega_1+\Lambda_2\Omega_2)+2\Lambda_1\Omega_1\Lambda_2\Omega_2\tau_0\right]\left[\Lambda_0\omega(\Lambda_1\Omega_1+\Lambda_2\Omega_2)+2\Lambda_1\Omega_1\Lambda_2\Omega_2\frac{1}{\tau_0}\right]=0. \quad (2.20)$$

Setting either factor of the expression on the left-hand-side to zero of course satisfies the equation above. It also leads to an approximate dispersion relation for sausage- and kink-type modes separately under this so-called weak asymmetry approximation, which can be summarized as

$$\Lambda_0\omega(\Lambda_1\Omega_1 + \Lambda_2\Omega_2) + 2\Lambda_1\Lambda_2\Omega_1\Omega_2\begin{pmatrix}\tanh\\ \coth\end{pmatrix}(x_0 m_0) = 0. \tag{2.21}$$

We can once again substitute Λ_j for $j = 0, 1, 2$ into this approximate dispersion relation and perform some rearranging to express it in terms of the characteristic speeds, densities, and wavenumber coefficients, leading us to the decoupled dispersion relation for waves propagating in a weakly asymmetric magnetic slab system containing asymmetric background flows:

$$(k^2 v_A^2 - \omega^2)\left(\frac{\rho_0}{\rho_1} m_1\Omega_2^2 + \frac{\rho_0}{\rho_2} m_2\Omega_1^2\right) = 2m_0\Omega_1^2\Omega_2^2\begin{pmatrix}\tanh\\ \coth\end{pmatrix}(m_0 x_0). \tag{2.22}$$

Equation (2.22) provides a form of the dispersion relation that is comparable to its symmetric counterpart in Roberts (1981b) and in fact reduces to the same equation if both background flow speeds are set to zero and the environment of the slab is turned symmetric, which seems to validate our results derived so far.

2.3. Analytical Solutions

In the following Section, we employ certain simplifications of the exact and decoupled dispersion relations (Equation 2.18 and 2.22), in order to provide tractable analytical solutions in certain limiting cases of slab width and plasma-β parameter applicable to solar atmospheric features.

2.3.1. The Effects of Slab Width

The thin-slab approximation

In this limit, the waves studied have wavelengths far greater than the width of the slab, $2x_0$, and therefore $kx_0 \ll 1$ and $m_0 x_0 \ll 1$. For quasi-sausage surface modes, this means that the $\tanh(m_o x_0) \to m_0 x_0$ in the decoupled dispersion relation, which then reduces to

$$(k^2 v_{A0}^2 - \omega^2)\left(\frac{\rho_0}{\rho_1} m_1\Omega_2^2 + \frac{\rho_0}{\rho_2} m_2\Omega_1^2\right) = 2m_0\Omega_1^2\Omega_2^2 m_0 x_0. \tag{2.23}$$

This equation may have a solution where the frequency follows $\omega^2 \to k^2 c_{T0}^2$ as $kx_0 \to 0$. This solution describes a slow quasi-sausage surface mode and can be expressed (to first

order in kx_0) as

$$\omega^2 = k^2 c_{T0}^2 \left\{ 1 - \left[2kx_0 (c_0^2 - c_{T0}^2)(c_{T0} - U_1)^2 (c_{T0} - U_2)^2 \right] \left[c_0^2 v_{A0}^2 \left(\frac{\rho_0}{\rho_1 c_1} \left\{ c_1^2 - (c_{T0} - U_1)^2 \right\}^{1/2} \{c_{T0} - U_2\}^2 + \frac{\rho_0}{\rho_2 c_2} \left\{ c_2^2 - (c_{T0} - U_2)^2 \right\}^{1/2} \{c_{T0} - U_1\}^2 \right)^{-1} \right] \right\}, \tag{2.24}$$

which will tend to $k^2 c_{T0}^2$ from below. This solution can exist when $c_1 > c_{T0} - U_1$ and $c_2 > c_{T0} - U_2$.

For quasi-kink surface modes, since $m_0 x_0 \to 0$, $\coth(m_0 x_0) \to 1/m_0 x_0$ in the decoupled dispersion relation. This, in turn, may have a solution of the form

$$\omega^2 = k^2 v_{A0}^2 - \frac{2kU_1^2 U_2^2}{x_0 \left(\frac{\rho_0}{\rho_1} \frac{(c_1^2 - U_1^2)^{1/2}}{c_1} U_2^2 + \frac{\rho_0}{\rho_2} \frac{(c_2^2 - U_2^2)^{1/2}}{c_2} U_1^2 \right)}. \tag{2.25}$$

In addition to these surface modes, body waves with $m_0^2 < 0$ can also be guided by the slab. In an attempt to emphasize the connection between the frequencies of body mode harmonics and the flow speeds in the system, we shift into a coordinate system that moves with the flow speed on one side of the slab, say U_1. This leads to the presence of the following new relative flow speeds: $U_{1,new} = 0$, $U_{0,new} = -U_1$ and $U_{2,new} = U_2 - U_1$, which contribute to the new Doppler-shifted frequencies as $\Omega_{1,new} = \omega$, $\Omega_{0,new} = \omega - kU_{0,new}$ and $\Omega_{2,new} = \omega - U_{2,new}$. Rewriting the decoupled dispersion relation for body waves and substituting in these new definitions allows us to obtain the following expression:

$$(k^2 v_{A0}^2 - \omega^2) \left(\frac{\rho_0}{\rho_1} m_1 \Omega_{2,new}^2 + \frac{\rho_0}{\rho_2} m_2 \omega^2 \right) = 2n_0 \omega^2 \Omega_{2,new}^2 \begin{pmatrix} \tan \\ -\cot \end{pmatrix} (n_0 x_0), \tag{2.26}$$

where

$$n_0^2 = -m_0^2 = -\frac{(k^2 v_{A0}^2 - \Omega_{0,new}^2)(k^2 c_0^2 - \Omega_{0,new}^2)}{(c_0^2 + v_{A0}^2)(k^2 c_{T0}^2 - \Omega_{0,new}^2)},$$
$$m_1 = \left(\frac{k^2 c_1^2 - \omega^2}{c_1^2} \right)^{1/2}, \qquad m_2 = \left(\frac{k^2 c_i^2 - \Omega_{2,new}^2}{c_i^2} \right)^{1/2}. \tag{2.27}$$

Describing body modes requires further additional considerations, since they can have an infinite number of harmonics in the frequency bands where they can occur (see eg. Roberts (1981b)). In the case of quasi-sausage body modes, we require that the $n_0 \tan(n_0 x_0)$ term in Equation (2.26) should remain finite as $kx_0 \to 0$, meaning that $n_0 x_0$ should tend to the roots of $\tan(n_0 x_0) = 0$: $n_0 x_0 \to j\pi$ for integer values of j. Slow body mode frequencies approaching the tube speed in a thin slab can then be approximated with

$\Omega_{0,new}^2 = k^2 c_{T0}^2 (1 + \nu (kx_0)^2)$. By substituting this expression for $\Omega_{0,new}$ into the condition that $n_0 x_0 \to j\pi$, an approximate expression for the slow quasi-sausage body modes can be reached. Applying a similar process to quasi-kink body modes, we arrive at the conclusion that $n_0 x_0 \to (j - 1/2)\pi$ in a thin slab. Based on these considerations, we can describe the slow quasi-sausage and quasi-kink body modes with one single formula:

$$\omega = kU_{0,new} \pm kc_{T0} \sqrt{1 + \frac{c_{T0}^4 (kx_0)^2}{c_0^2 v_{A0}^2 \pi^2 q^2}}, \tag{2.28}$$

where $q = j$ for quasi-sausage solutions, and $q = j - 1/2$ for quasi-kink waves (where $j = 1, 2, ...$). This result demonstrates the relative insensitivity of body modes to changes in the equilibrium density ratios, similar to the case of the static asymmetric slab (Allcock and Erdélyi, 2017): to quadratic order in kx_0, these solutions to the dispersion relation do not directly depend on the external environmental parameters.

The wide-slab approximation

Now looking at the other extreme case, we consider waves with wavelengths that are much shorter than the slab width, giving us $kx_0 \gg 1$. This makes the argument of both the $\tanh(n_0 x_0)$ and $\coth(n_0 x_0)$ terms in the decoupled dispersion relation (Equation 2.22) large. This, in turn, results in the following approximate dispersion relation for both quasi-sausage and quasi-kink surface waves in a wide slab:

$$(k^2 v_{A0}^2 - \omega^2) \left(\frac{\rho_0}{\rho_1} m_1 \Omega_2^2 + \frac{\rho_0}{\rho_2} m_2 \Omega_1^2 \right) = 2 m_0 \Omega_1^2 \Omega_2^2. \tag{2.29}$$

The quasi-sausage and quasi-kink surface waves were shown to tend to different frequencies in a static wide asymmetric slab system (Allcock and Erdélyi, 2017; Zsámberger and Erdélyi, 2020). The wide-slab behaviour of the eigenmodes is similar here, with the two types of waves tending to different limiting phase speeds, the values of which will depend on the magnitude of the external asymmetries.

When it comes to body waves, slow and fast modes can be described together in a wide slab. Whether both types of waves can be present in a given configuration will be decided by the ordering of all the external and internal characteristic speeds of the system. This speed ordering also determines which value the phase speed of these body modes approaches (if they exist). In the shifted coordinate system introduced above and defining $v_{max} = \max(v_{A0}, c_0)$ and $v_{min} = \min(v_{A0}, c_0)$, slow body waves can be described as $\Omega_{0,new}^2 = k^2 v_{min}^2 (1 - \nu/(kx_0)^2)$. By a similar series of steps as we demonstrated for a thin slab, now we require that $n_0 x_0 = (j - 1/2)\pi$ for quasi-sausage modes to keep $n_0 \tan(n_0 x_0)$ non-zero and finite. At the same time, $n_0 x_0 = j\pi$ for quasi-kink modes (where $j = 1, 2, ...$). Through some algebra, we obtain the slow body mode solutions propagating in a wide slab

as

$$\omega = kU_{0,new} \pm kv_{min}\left(1 - \frac{q^2\pi^2 v_{min}^2}{[v_{max}^2 - v_{min}^2][kx_0]^2}\right)^{1/2}, \tag{2.30}$$

where $q = j - 1/2$ for quasi-sausage modes, and $q = j$ for quasi-kink modes. Fast body modes, on the other hand, are described by the following wide-slab approximation:

$$\omega = kU_{0,new} \pm kv_{max}\left(1 - \frac{q^2\pi^2 v_{max}^2}{[v_{max}^2 - v_{min}^2][kx_0]^2}\right)^{1/2}. \tag{2.31}$$

2.3.2. Effects of the Choice of Plasma-β

The limit of infinite plasma-β

The plasma-β parameter, defined as defined as $\beta = p_{mag}/p = (2/\gamma)v_A^2/c_s^2$, describes the relative magnitudes of the magnetic- and the plasma pressure gradient forces. Generally, an asymmetric slab system with high values of plasma-β all throughout the configuration may serve as a good approximation of a structure within the high-*beta* photosphere. In the most extreme but also the simplest limit of the high-β approximation, $\beta \to \infty$. In this case, the plasma motions dominate over any magnetic effects, and the Alfvén speed is negligibly small compared to the sound speed: $v_{A0} \ll c_0$. Mathematically, this allows us to make the following simplifications in our definitions:

$$\begin{aligned} n_0^2 = -m_0^2 = -\frac{k^2c_0^2 - \omega^2}{c_0^2} \qquad & \text{for } i = 0, \text{ and} \\ m_j^2 = \frac{k^2c_j^2 - \Omega_j^2}{c_j^2} \qquad & \text{for } i = 1, 2. \end{aligned} \tag{2.32}$$

In the system of the infinite-β slab placed in an asymmetric environment containing different flows, fast body modes exist as solutions to the transformed form of the decoupled dispersion relation below:

$$\begin{pmatrix} \tan \\ -\cot \end{pmatrix}(n_0x_0) = -\frac{1}{2}\left(\frac{\rho_0}{\rho_1}\frac{m_1}{n_0}\frac{\omega^2}{\Omega_1^2} + \frac{\rho_0}{\rho_2}\frac{m_2}{n_0}\frac{\omega^2}{\Omega_2^2}\right). \tag{2.33}$$

The limit of zero plasma-β

In a low-β environment, the plasma becomes magnetically dominated, and the internal sound speed can be considered negligible when compared to the Alfvén speed. In the simplest limiting case of the zero-β approximation, the wavenumber coefficients can thus

be written as

$$n_0^2 = -m_0^2 = -\frac{k^2 v_{A0}^2 - \omega^2}{v_{A0}^2} \qquad \text{for } i = 0, \text{ and}$$
$$m_j^2 = \frac{k^2 c_j^2 - \Omega_j^2}{c_j^2} \qquad \text{for } j = 1, 2. \tag{2.34}$$

In the zero-β steady slab system studied, fast body modes can exist and are described by the simplified form of the dispersion relation below:

$$\begin{pmatrix} \tan \\ -\cot \end{pmatrix}(n_0 x_0) = \frac{1}{2} \frac{\sqrt{k^2 v_{A0}^2 - \omega^2}}{v_{A0}} \left(\frac{\rho_0}{\rho_1} \frac{m_1}{\Omega_1^2} + \frac{\rho_0}{\rho_2} \frac{m_2}{\Omega_2^2} \right). \tag{2.35}$$

2.3.3. Dependence on Asymmetry Parameters

In the next Section, we focus on uncovering how exactly the different kinds of external asymmetry influence the frequencies and the stability of solutions in a weakly asymmetric slab system. To this end, we express the solutions to the dispersion relation in terms of two small parameters: the density asymmetry, defined as

$$\delta = \frac{\rho_2 - \rho_1}{\rho_1}, \tag{2.36}$$

and the flow asymmetry,

$$\varepsilon = \frac{U_2 - U_1}{U_1}. \tag{2.37}$$

We use these expressions to expand the slow surface wave solutions described in Section 2.3.1, so that we may study competing effects of the two kinds of asymmetry on the phase speed of waves, as well as on the KHI-onset threshold Since the dependence of the frequencies of eigenmodes on density asymmetry has been explored to some degree in numerical or analytical form in static slabs (Allcock and Erdélyi, 2017; Zsámberger and Erdélyi, 2020; Oxley et al., 2020a,b), we first focused only on the new, additional source of asymmetry in steady slabs, namely, the different external flow speeds. Appendix A.1 contains the detailed results, which may be useful to read first when trying to understand the follow-up steps, in which the density, magnetic field, and flow asymmetries are all considered.

2.3.4. Dependence on Density and Flow Asymmetry

In this Section, we explore how the frequencies of the eigenmodes depend on the combined effect of the flow asymmetry and the density asymmetry, as defined in Equations (2.36)-(2.37).

Quasi-sausage modes

If we substitute the small parameters ε and δ into the slow quasi-sausage surface mode solutions from Equation (2.24) and keep only first order terms in both small parameters, then we can express the dependence of the angular frequency on the two sources of asymmetry as

$$\omega^2 = k^2 c_{T0}^2 \left\{ 1 - \frac{2\left(c_0^2 - c_{T0}^2\right) k x_0}{v_{A0}^2 c_0^2} \frac{\rho_1}{\rho_0} \frac{\left(c_T - U_1\right) c_1}{4\Big(c_1^2 - \{c_T - U_1\}^2\Big)^{\frac{3}{2}}} \left(4\Big[c_1^2 - [c_T - U_1]^2\Big]^{\frac{1}{2}} [c_T - U_1] \right.\right.$$
$$\left.\left. + \Big[2c_1^2 - 5\{c_T - U_1\}^2\Big] [c_T - U_1]\, \delta - 2\Big[2c_1^2 + \{c_T - U_1\}^2\Big] U_1 \varepsilon \right) \right\}. \tag{2.38}$$

This expression shows that (assuming all terms in the relevant products are positive, which, in such a rich problem with many free parameters might not always be the case), the density and flow asymmetries can have competing effects, with one of them working to raise the frequency of the solutions, while the other one would decrease it. In order not to overestimate the validity of this conclusion, for every specific set of slab parameters, the signs of the terms multiplying both asymmetry parameters should of course be checked.

From this solution stated in Equation (2.38), a critical flow asymmetry parameter can be expressed, above which value the oscillation can become KHI-unstable (for a given set of background and density asymmetry parameters). This limit is

$$\varepsilon > \frac{4TV^3 - 4[c_T - U_1]^2 c_1 V - [c_T - U_1]^2 c_1 \Big[2c_1^2 - 5\left\{c_T - U_1\right\}^2\Big] \delta}{2\left[c_T - U_1\right] c_1 \Big[\left\{c_T - U_1\right\}^2 - 2c_1^2\Big] U_1}, \tag{2.39}$$

where

$$T = \frac{v_{A0}^2 c_0^2}{2k x_0 \left(c_0^2 - c_{T0}^2\right)} \frac{\rho_0}{\rho_1},$$
$$V = \sqrt{c_1^2 - [c_{T0} - U_1]^2}, \tag{2.40}$$

if $U_1 > 0$ and the denominator on the right-hand-side is positive.

Quasi-kink modes

Similarly, using Equation (2.25) and the asymmetry parameters for slow quasi-kink surface waves, the angular frequency of the solutions can be expressed as

$$\omega^2 = k^2 v_{A0}^2 \left\{ 1 - \frac{2U_1^2}{v_{A0}^2 k x_0} \frac{\rho_1}{\rho_0} \frac{c_1}{25\left(c_1^2 - U_1^2\right)^{\frac{3}{2}}} \left(5\left[c_1^2 - U_1^2\right] + 2\left[2c_1^2 - 3U_1^2\right] \delta + \left[3c_1^2 + U_1^2\right] \varepsilon \right) \right\}. \tag{2.41}$$

The Kelvin-Helmholtz instability appears when the flow asymmetry is larger than a critical value of

$$\varepsilon > \frac{W - 5\left[c_1^2 - U_1^2\right]^2 - 2\left[c_1^2 - 3U_1^2\right]\delta}{\left[3c_1^2 + U_1^2\right]}, \tag{2.42}$$

where $U_1 > 0$ and

$$W = \frac{\rho_0}{\rho_1}\frac{25\left(c_1^2 - U_1^2\right)^{\frac{3}{2}} v_A^2 k x_0}{2c_1 U_1^2}. \tag{2.43}$$

Overall, this analysis has shown that when a critical value of the flow asymmetry is reached for a given (fixed) value of the density asymmetry describing the system, both the quasi-sausage and the quasi-kink waves might turn KHI-unstable. In solar physics applications, such a dangerously increased flow speed may for example be established by the formation of a pressure gradient, leading to the destabilisation of the entire waveguide.

2.4. Numerical Results

After the detailed analytical investigation of various approximations in the previous sections, in the current section, we show a collection of numerical solutions to the dispersion relation, Equation (2.18) that we obtained. Our numerical method is based on an implementation of the Newton-Rhapson method in Python, based on the piece of code used to obtain solutions in Barbulescu and Erdélyi (2018). First, all quantities are non-dimensionalised with respect to the Alfvén speed, and the following quantities are introduced: Alfvén Mach numbers $M_{Aj} = U_j/v_{A0}$ $(j = 0, 1, 2)$, dimensionless sound speeds $\bar{c}_j^2 = c_j^2/v_{A0}^2$ $(j = 0, 1, 2)$, the dimensionless tube speed $\bar{c}_{T0}^2 = c_{T0}^2/v_{A0}^2$, and phase speed $\bar{c}_{ph} = c_{ph}/v_{A0} = \omega/(kv_{A0})$. Using these quantities for the calculation, the solutions can then be easily scaled for various choices of internal magnetic field strength (Alfvén speed).

2.4.1. Solutions of the Full Dispersion Relation and the Onset of Instability

Figure 2.2 contains two dispersion diagrams displaying general solutions to Equation (2.18) obtained in the manner outlined above. It can immediately be seen from both panels of this Figure that, as expected from previous studies (Nakariakov and Roberts, 1995; Barbulescu and Erdélyi, 2018), the asymmetric background flows in the system have led to the breaking of the symmetry between forward- and backward-propagating solutions, irrespective of the relative direction of the flows. Both panels were prepared using photospheric values for the background parameters based on current estimates available in the literature: $c_0 = 11$ km/s and $v_{A0} = 12$ km/s (Keys et al., 2013), $c_1 = 8$ km/s and $c_2 = 7$ km/s (Hurlburt et al., 2002), $v_{A1} = v_{A2} = 0$ km/s (Felipe et al., 2016; Jiang et al., 2011). Estimates for the

speeds of downflows found in the vicinity of small magnetic elements of the photosphere fall between 1-10 km/s (Briand and Solanki, 1998; Socas-Navarro et al., 2004; Danilovic et al., 2010). We chose the values of equilibrium parameters such that they would fall within these expected ranges. This allows a first insight into how these different flows affect the frequencies and the stability of magnetosonic waves guided by a slab system modelling the asymmetric environment of small photospheric magnetic elements. Namely, we had set $M_{A0} = 0, M_{A1} = 0.15$, $M_{A2} = 0.65$ for panel (a) and $M_{A0} = 0, M_{A1} = -0.1$ and $M_{A2} = -0.35$ for panel (b). In both panels, green (blue) lines show the real part of the quasi-kink (quasi-sausage) mode phase speeds, and red lines display their imaginary parts. (Note that there are no trapped solutions in the hatched areas).

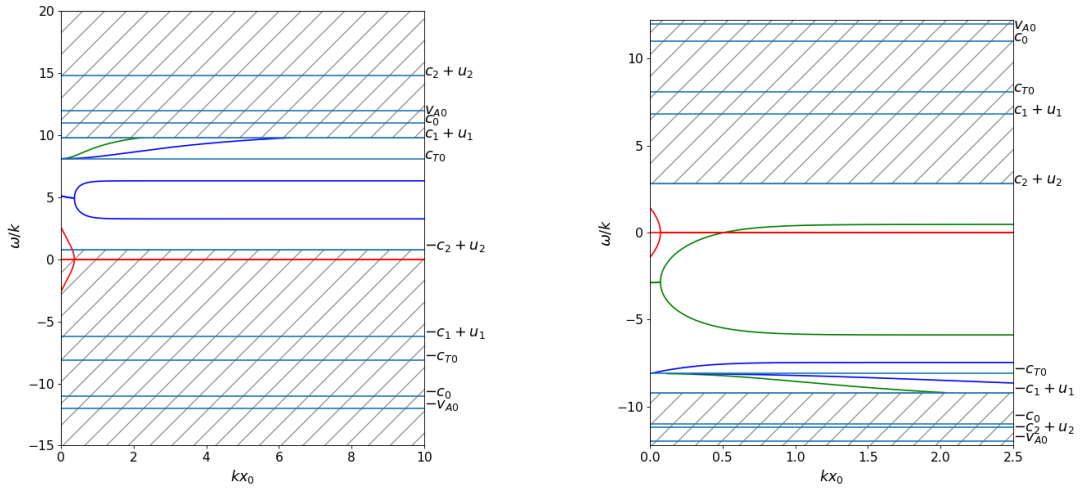

(a) (b)

Figure 2.2: Dispersion diagrams displaying the quasi-sausage and quasi-kink mode phase speeds. Source: Zsámberger et al. (2022a).

In the presence of upflows (panel a of Figure 2.2), the area between $-c_2 + U_2$ and c_{T0} guides surface waves, whereas body waves propagate with speeds between c_{T0} and $c_1 + U_1$. Note that we only plotted the first few body waves in order to keep the figure legible. The rest of the phase speed ranges could support only leaky modes, which we have excluded from the study. When it comes to the trapped waves, it can also be concluded from the non-zero imaginary parts that in a thin slab, the surface modes are subject to the KHI.

Figure 2.2b shows that instabilities can still be present in thin slabs, but all frequencies are visibly shifted in the opposite (backward-propagating) direction when the system contains downflows instead. Trapped surface waves are now propagating with phase speeds between $-c_{T0}$ and $c_2 + U_2$, whereas body modes are found to exist in a band between $-c_1 + U_1$ and $-c_{T0}$. The asymmetric steady slab system used to obtain the solutions plotted in panel (b) of Figure 2.2 is one that could be used to improve upon the modelling attempts focused on magnetic bright points in Zsámberger et al. (2018) and Zsámberger

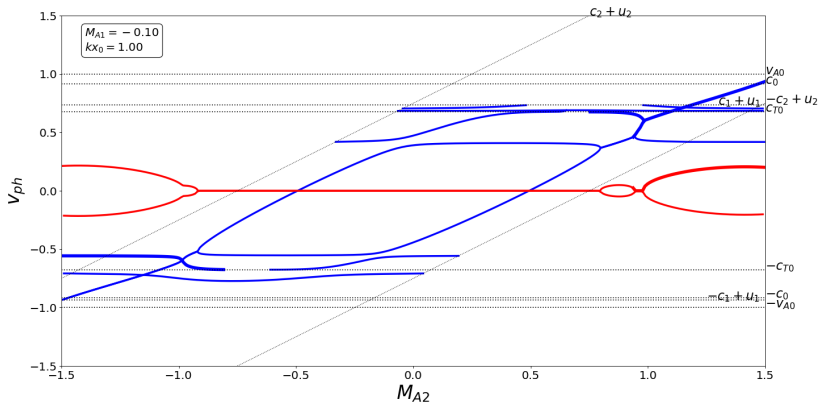

Figure 2.3: The phase speed of trapped oscillations as a function of one changing flow speed in the steady asymmetric slab system. Source: Zsámberger et al. (2022a).

and Erdélyi (2021) by including downflows of different magnitudes in the environment of the slab, corresponding to downflows expected to be found in the weakly magnetised intergranular lanes. Modelling magnetic bright points as asymmetric slab systems and the merits of each approach will be further discussed in Chapter 4.

In the next step, we make further observations about the behaviour of MHD waves in the presence of asymmetric external flows by extending the results in Figure 2.2b to a range of different flow asymmetries, as shown in Figure 2.3. We also add an extension for different magnitudes of the slab width shown in the supplementary materials SM1-SM7.

In Figure 2.3, we plotted the phase speeds of supported trapped waves for a slab system characterised by the same set of equilibrium quantities as the one from Figure 2.2b, with the exception of M_{A2}, which is left to change continuously along the x axis, changing its character from being a downflow into an upflow as we proceed from one end of the plotted range to the other. For this illustration, we fixed the slab width at an intermediate value ($kx_0 = 1$).

Let us start analysing the results shown in the diagram from the origin and describe some easily discernible patterns of the solutions. The first one of these takes the shape of a "central oval". Both the slow quasi-kink and quasi-sausage modes are present in this region of stability. (Following the convention established in our previous figures, the real (imaginary) parts of the solutions are plotted with blue (red).) In addition to this, at higher forward- ($v_{ph} > 0$) and backward-propagating ($v_{ph} < 0$) areas of the diagram, some body modes are also present. These remain stable both within and outside the range of M_{A2} covered by the "central oval".

Upon closer inspection, it can be discovered that the region we termed "central oval" is actually located towards negative Alfvén Mach number and phase speed values (at least for the current set of background parameters). The direction and magnitude of this shift in the position of the central stable region depends on both the flow speeds chosen and the

relative difference between the two speeds. This will be highlighted in further figures and supplementary materials.

Outside the "central oval", even at relatively small positive values of the right-hand-side flow, the phase speeds of the forward- and backward-propagating surface waves meet, resulting in the onset of the KHI.

The increasing flow speed to the right of the slab affects not only the instability threshold, but also the phase speeds of the waves supported by the system. This manifests as e.g. the body modes with negative phase speeds becoming leaky starting from the value of M_{A2} at which they would cross the $-c_2 + u_2$ line.

The situation is somewhat different on the negative half of the M_{A2} axis. Once $|M_{A2}|$ grows larger than a critical value, the surface modes will be KHI-unstable in this region as well. Due to the presence of the asymmetry, however, the KHI threshold for negative values of M_{A2} is not the same as for positive ones. On this side of the x axis, it is the forward-propagating body modes which become leaky even for relatively small negative M_{A2} values (starting from where they would cross the $c_2 + u_2$ line).

2.4.2. The Effects of Flow Asymmetry and Slab Width

There are two fundamental parameters whose changes need to be further explored. Firstly, the dimensionless slab width has a substantial influence over which eigenmodes can exist and which of them are stable. Figures 1 included in the Appendix and the accompanying supplementary materials SM1-SM3 plot the dependence of the phase speeds solutions on the slab width for a fixed flow on the left-hand-side but at different fixed values of M_{A2} (and therefore different magnitudes of flow asymmetry) for each panel. All diagrams were prepared using the same values for the rest of the background parameters $v_{A0} = 12\,\mathrm{km/s}$, $c_0 = 11\,\mathrm{km/s}$, $c_1 = 8\,\mathrm{km/s}$, $c_2 = 7\,\mathrm{km/s}$, normalised by the internal Alfvén speed, and $\rho_1/\rho_0 = 2.41$, $\rho_2/\rho_0 = 2.98$. These still images and series illustrate that in general, it is easier for the KHI to appear in thin slabs. Meanwhile, higher flow speeds are needed to induce the instability in wider slabs. The asymmetry between the external flows can further amplify this effect, allowing an ever wider range of wavelengths (slab widths) to become unstable as the flow asymmetry increases. The presence of asymmetry is, in fact, a key factor here. Since the flows themselves which we have chosen to plot are relatively slow (with their Alfvén Mach numbers being $-0.2 < M_{A1}, M_{A2} < 0.1$), in a symmetric configuration, they may not be strong enough to trigger an instability in the slab system for any wavelength at all (see the frames in SM1-SM3 for which $M_{A1} = M_{A2}$ in each case).

Figures 2 in the Appendix and their accompanying supplementary materials SM4-SM7 further help illustrate this effect. In these Figures and series, the phase speed is plotted as a function of the changing right-hand-side Alfvén Mach number (M_{A2}), for different fixed values of M_{A1} in each series, and a gradually changing slab width. With the gradual increase of kx_0, the "central oval" of stability also grows, meaning that an ever larger $|M_{A2}|$

is needed to bring about the KHI. The opposite is then also true: the narrower the slab becomes, the smaller the value of M_{A2} will be when the KHI appears. This connection between the slab width and the KHI-threshold was also shown in the previous section, where we derived our analytical approximate solutions to the dispersion relation.

The other parameter we explore is the sign and the magnitude of M_{A1}, the left-hand-side Alfvén Mach number. In Section 2.3, all our analytical solutions showed a dependence on the flow speed included in this quantity, and the expansions of the solutions to the dispersion relation in terms of small asymmetry parameters suggested a mathematical connection with the flow asymmetry as well. Once again, Figures 1 and 2, along with the corresponding supplementary materials confirm this finding. From a comparison between Figures 1 and series SM1-SM3, it can easily be seen that the magnitude of the fixed left-hand-side flow determines when the changing right-hand-side flow has a high enough speed to bring about the KHI for a given slab width, and larger flow speeds or larger asymmetry is needed to make wider slabs unstable.

If we look at the phase speeds of the supported eigenmodes as a function of M_{A2}, Figures 2 and series SM4-SM7 reveal that instead of the size of the "central region" of stability, the different values of flow speeds and their asymmetry will both shift the position of this "central oval". The shift can be spotted most easily by comparing the results for different fixed flows in Figure 2.

2.4.3. Exploring the Sources of Asymmetry

Preparing some further series of numerical solutions allows us an insight into how the inclusion of various kinds of asymmetries in the model influences the frequencies eigenmodes and modifies the instability thresholds.

Figure 3 in the Appendix displays the solutions to the dispersion relation valid for a symmetric slab with no flows present (essentially the one obtained by Roberts (1981b)), when $c_0 = 11$km/s, $v_{A0} = 12$ km/s, $c_1 = c_2 = c_e = 8$ km/s, and $\rho_1/\rho_0 = \rho_2/\rho_0 = \rho_e/\rho_0 = 2.41$. In this symmetric, static, low-β magnetic slab embedded in a non-magnetised plasma environment, there are no flows present to break the symmetry between the phase speeds of backward- and forward-propagating modes. All solutions for this configuration are stable. In both propagation directions ($\omega > 0$ and $\omega < 0$), we can see a pair of slow surface waves and a band of body waves, which will in the following become our basis of comparison while re-introducing different kinds of asymmetry and observing the effects in Figure 4 of the Appendix and its accompanying animations in the supplementary material (SM9-SM14). First, we add symmetric downflows to the static background of the symmetric slab, with the results displayed in Figures 4a and 4b. This shifted the phase speed (or frequency) limits on the existence of ch kind of trapped oscillation. In the static case, these limits coincided with the external sound speed (c_e), but this has now been modified to become the external sound speed shifted by the flow speed ($c_j + u_j$, where $j = 1, 2 = e$ due to the

symmetry). The phase speeds of the static solutions are changed as well. The flow speed included in the new solutions wasn't high enough to lead to the (dis)appearance of any additional solutions, nor to prompt the onset of the KHI for any wavelength in panel (a). This configuration is an example of the kind of steady slab system that Nakariakov and Roberts (1995) investigated.

In Figures 4a and 4b and the accompanying animations SM9 and SM10, the symmetric external flow speed is varied. In the general case of an externally non-magnetic slab system, trapped modes can be found only with $-c_e + u_e < v_{ph} < c_e + u_e$. However, as the flow speeds we add become different, the solutions get swept forward or backward against the static background by different amounts (as observable in Figure 4b or animation SM9). In Figures 4b, we find that when $-1 < M_{Ae} < 1$, the solutions remain stable, but, as this panel along with SM9 and SM10 also reveal, for higher flow speeds, various regions of instability can appear. As before, this happens first in thinner slabs, then, as the flow speeds are increased, potentially at all slab widths.

In Figures 4c and 4d, we start incorporating asymmetry into the system. While all other background parameters are kept symmetric, an external flow asymmetry is introduced. This results in a change of the limiting external sound speed modified with the flow speed when comparing the two environmental regions around the slab. The added flow asymmetry, as well as the higher upflow speed on the right-hand side results in visible changes in Figure 4c compared to Figure 4a: we can no longer see backward-propagating body modes among the trapped waves guided by this configuration. Additionally, for the flow asymmetry chosen in this panel, the KHI reappears when the slab is thin.

Since a flow asymmetry is now present in the waveguide, some properties observed in a fully (density and flow) asymmetric system start to appear again in Figure 4d. Because this plot was prepared using a small value of the dimensionless slab width, there is quite a wide range of KHI-unstable solutions on the diagram. For a small M_{A2} ($M_{A2} \approx -0.5$), the surface modes become unstable. When M_{A2} describes an upflow, however, the KHI can set in at a visibly smaller flow speed (corresponding to $M_{A2} \approx 0.3$), If we compare these instability thresholds, it becomes clear that the asymmetry in external Alfvén Mach numbers is $|M_{A1} - M_{A2}| \approx 0.4$ in both cases. Therefore, if the flows in our asymmetric system are oppositely directed, then a smaller flow speed for both the up- and the downflows will be enough to turn some of the solutions KHI-unstable.

Widening the slab counters this effect of flow asymmetry somewhat, as the supplementary animations to Figures 4c and 4d (SM11 and SM12, respectively) show.

Finally, we also incorporate asymmetry into the slab system following a different avenue: first we construct a static asymmetric slab model (see Allcock and Erdélyi (2017)), where $c_1 \neq c_2$ and $\rho_1 \neq \rho_2$, and then we add symmetric external flows to the system. Our Figures 4e and 4f depict the trapped solutions found in this case, accompanied by animations in SM13 and SM14. In SM13, each frame has its own fixed value of symmetric flows ($M_{A1} = M_{A2} = M_{Ae}$), for which it shows the phase speeds of trapped oscillations as a

function of the slab width. Meanwhile, in SM14, every frame shows the phase speeds of solutions as a function of M_{A2} (which is equal to M_{A1} due to the symmetry we set up) for a fixed value of the dimensionless slab width, with the latter changing frame by frame.

Depending on what the fixed value of the flow speed is, as before, different modes are allowed to propagate as they get shifted forward or backward across trapped and leaky domains by the effects of the flows. Overall, Figure 4f shows that the slab remains stable when $-1 < M_{Ae} < 1$ for a thin slab, but SM14 shows that these threshold values can become different with each new fixed slab width value.

If we now add asymmetric external flows to the static asymmetric background, we return to the original configuraiton discussed throughout this Chapter.

2.5. Conclusion

In this Chapter, we constructed and analysed a mathematical model of an isolated magnetic slab in an asymmetric environment containing asymmetric external flows. This serves as a further generalisation of the asymmetric magnetic slab model, which was initially described by Allcock and Erdélyi (2017) for the stationary and by Barbulescu and Erdélyi (2018) for the steady case.

After providing a brief summary of previous results, we detailed the process of deriving the equation governing wave dispersion in this asymmetric steady slab system from the ideal MHD equations. While in general, the dispersion relation does not decouple into separate equations governing sausage and kink-type modes, we showed that by introducing the weak asymmetry approximation, it is possible to obtain a decoupled dispersion relation for the problem. Using this equation, we found approximate solutions for the angular frequencies of the quasi-sausage and quasi-kink eigenmodes in thin and wide slabs, as well as in hot and cold plasmas. With the overall behaviour of surface and body mode solutions thus established, we proceeded to investigate the dependence of the angular frequency of surface modes on the two sources of asymmetry in the model: the differences in external densities and in external flow speeds. These findings were then complemented with a series of numerical results, which also allowed us to find solutions to a wider range of background parameters than what would be allowed by the weak asymmetry approximation.

Notably, we found that in every case, the presence of bulk background flows broke the symmetry between the phase speeds of forward- and backward propagating modes. The choice of external flow speeds and flow asymmetry proved to have a significant effect on the phase speed of eigenmodes, changing both the types and frequencies of modes supported as trapped oscillations compared to the static problem, as well as the sets of equilibrium parameters for which they remained stable. Both the density and flow asymmetry have a strong (first-order) influence on the angular frequencies of surface waves, and these effects can even compete against one another.

A major part of our analysis was establishing the limiting asymmetry parameters and

slab widths for which the Kelvin-Helmholtz instability can set in. Through an extensive numerical analysis, we found that, irrespective of the flow asymmetry, a general tendency is that thinner slabs tend to be unstable for a wider range right-hand-side flow speeds (flow asymmetries). An aspect of the existence and stability of waves in various asymmetric configurations we touched upon, but one which could merit further study in the future, was a connection between the slab width, the flow asymmetry, *and* the density asymmetry present in the system. While we used a photosphere-like distribution of background parameters as a starting point for most of our numerical results and we did introduce some changes into these parameters as we explored the different sources of asymmetry, the current study could also be expanded to encompass wholly different characteristic speed orderings to begin with (potentially representative of other features of the solar atmosphere).

As mentioned, a significant part of our numerical investigation was focused around characteristic speed values that correspond to the information we have on the photosphere - more specifically, on the circumstances in the intergranular lanes and in magnetic bright points, as these small concentrations of intense magnetic field are an excellent candidate for applying the asymmetric slab model. The KHI has already been observed on a larger scale, in the flank region of a CME by Foullon et al. (2011), and it is our sincere hope that new, high-resolution observations might soon be able to detect it in small-scale phenomena such as the bright points and their immediate environment, providing further opportunities for the study of the propagation and stability of MHD waves in the solar atmosphere.

Chapter 3.
Magnetohydrodynamic Wave Propagation and the Kelvin-Helmholtz Instability in a Magnetic Slab Enclosed in an Asymmetric Magnetic Environment

Abstract

In this Chapter, we study the magneto-acoustic waves guided by a magnetic slab enclosed in an asymmetric magnetic environment, in which the slab itself is under the effect of a steady flow, further extending the scope and potential applications of asymmetric slab models. We derive the general dispersion relation governing the propagation of MHD waves in the system and provide analytical as well as numerical solutions to it in the case of weak asymmetry. Additionally, where possible, we identify the limiting flow speeds required for the onset of the Kelvin-Helmholtz instability. The paper Zsámberger et al. (2022b) serves as the basis of this Chapter.

3.1. Chapter Introduction

Next to the further-reaching issue of solar atmospheric heating, another main motivation behind studying MHD wave propagation in flux tube and slab waveguides is to develop and refine tools for solar magneto-seismology and diagnose the plasma environment of our star's atmospheric features (Nakariakov and Verwichte, 2005; Andries et al., 2009; Ruderman and Erdélyi, 2009; Morton et al., 2012; Nakariakov and Ofman, 2001; Erdélyi and Taroyan, 2008). Since magnetic fields are ubiquitous in the dynamic solar atmosphere, they can establish a multitude of waveguides, and theoretical models available for diagnostic purposes should reflect this diversity. Enhancing the models, specifically asymmetric slab models in our case, allows them to become applicable to a more varied set of solar atmospheric features, including global structures, plumes (DeForest and Gurman, 1998), prominences (Arregui et al., 2012a), coronal loops (Banerjee et al., 2007; de Moortel, 2009), all the way down to fine-scale small features like x-ray and EUV bright points (Golub et al., 1974), spicules (Zaqarashvili and Erdélyi, 2009; Tsiropoula et al., 2012), or magnetic pores (Keys et al., 2018). In the current Chapter, we demonstrate a different possibility of

generalising steady asymmetric slab models compared to Chapter 2. Whereas before, we introduced flow asymmetry into the system of a magnetic slab embedded in an asymmetric non-magnetic environment, what we now focus on is the inclusion of an asymmetric magnetic field around a central flow. A static precursor of this model was analysed in a recent series of studies, which explored the effects of both density and magnetic asymmetry in the absence of any flows in the system, for propagating (Zsámberger et al., 2018; Zsámberger and Erdélyi, 2020, 2021, 2022a) and standing modes (Oxley et al., 2020a,b) alike and generalised to a multi-layered case by Allcock et al. (2019). Now we combine this approach with the building block of a central flow in an asymmetric (externally non-magnetic) slab system described by Barbulescu and Erdélyi (2018), and study the effects of both the flow and the magnetic asymmetry on wave propagation and instabilities in the slab model. From a practical point of view, this new addition to Cartesian models helps extend its applicability to jets in the magnetically structured solar atmosphere, such as the chromospheric spicules (discussed in more detail in Chapter 5), or macrospicules as their larger-scale equivalents (Beckers, 1972; de Pontieu et al., 2007; Pike and Mason, 1998), as well as X-ray and EUV jets observed e.g. by the YOHKOH telescope (Shibata et al., 1992).

Motivated by the plethora of potential solar applications, here we study the Kelvin-Helmholtz instability of the propagating MHD waves guided by an asymmetric magnetic slab subject to a steady flow in its central region. First, in Section 3.2 we derive a full dispersion relation for magnetosonic waves propagating along the field lines in the slab. Then, in Section 3.4, we investigate the case of weak asymmetry in further analytical detail, obtaining a decoupled dispersion relation and several approximate solutions in frequently used limits such as a thin slab or a low-β regime. Where possible, we also use these approximations to provide analytical limits for the flow speed required for the onset of the KHI. Finally, in Section 3.5, a collection of numerical solutions to the full and the approximate dispersion relations is presented and compared. These results help us demonstrate how the flow speed and the slab width can affect the phase speeds and the stability of waves in this slab system. We also investigate how closely our approximations can be aligned with the full dispersion relation, before we present our conclusions in Section 3.6.

3.2. Wave Dispersion in a Steady Slab Placed in an Asymmetric Magnetic Environment

3.3. The Equilibrium Configuration

The model we consider here is that of a three-dimensional asymmetric magnetic slab waveguide, filled with ideal, inviscid plasma and permeated by an equilibrium magnetic field in the z-direction all throughout. As before, the waveguide is divided into three layers by

two plane interfaces placed at $x = \pm x_0$. The equilibrium parameters can be summarised as follows:

$$N(x) = \begin{cases} N_1 & x < -x_0, \\ N_0 & |x| < x_0, \\ N_2 & x_0 < x, \end{cases} \tag{3.1}$$

where $N_j =$ constant (for $j = 0, 1, 2$), and N_j denotes any of the following physical quantities: densities, ρ, pressures, p, temperatures, T, and vertical magnetic field strengths, $\mathbf{B} = (0, 0, B)$. Parameters indexed $j = 0$ denote quantities inside the slab, while $j = 1$ and $j = 2$ stand for parameters in the left- and right-hand-side environmental regions, respectively. In addition to the background quantities above, the central region is also subject to a steady flow in the vertical direction: $\mathbf{V}_0 = (0, 0, V_0)$. This equilibrium configuration is illustrated in Figure 3.1, with blue arrows representing the magnetic fields and the red arrow showing the presence of a steady flow inside the slab.

When setting up the equilibrium, we require that the condition of total pressure balance is fulfilled by the equilibrium quantities:$p_1 + \frac{B_1^2}{2\mu} = p_0 + \frac{B_0^2/2}{\mu} = p_2 + \frac{B_2^2}{2\mu}$, so that the magnetic and plasma pressures in each region can counteract one another and ensure the stability of the system.

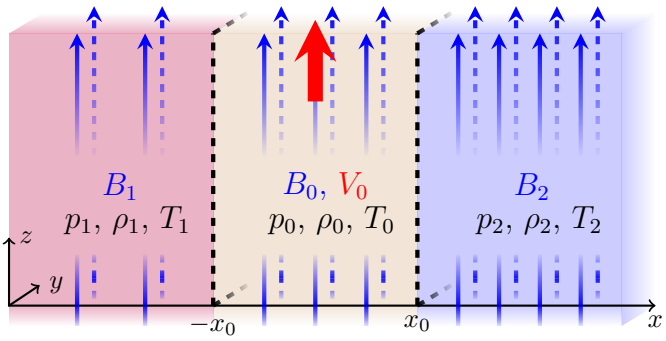

Figure 3.1: Illustration of the equilibrium configuration for the magnetic slab including a steady flow, surrounded by an asymmetric magnetic environment. Adapted from Zsámberger et al. (2022b).

3.3.1. Derivation of the Dispersion Relation

The interactions of the plasma and the magnetic fields in the system are governed by the ideal MHD equations. Therefore, we can use a similar derivation process to the one detailed in Chapter 2.

Starting from the same form of the ideal MHD equations in the presence of bulk background flows detailed in Equations (2.1)-(2.4), we introduce linear perturbations to the system by adding small, time-dependent perturbations to the equilibrium quantities. By substituting the perturbed variables into the idea MHd equations and neglecting second-

(or higher-) order terms, we obtain a set of linearised MHD equations. Similarly to the process followed in the previous Chapter, we assume that the disturbances are independent of the y-direction ($k_y = 0$ and $v_y = 0$), look for plane-wave solutions propagating parallel to the slab boundaries by assuming that the perturbed variables can be written in the form of $\left(\mathbf{v}, \mathbf{b}, \rho', p'\right)(\mathbf{x}, t) = \left(\widehat{\mathbf{v}}, \widehat{\mathbf{b}}, \widehat{\rho'}, \widehat{p'}\right)(x)\, e^{i(kz-\omega t)}$.

Substituting the plane wave solutions defined above into the set of linearised ideal MHD equations, we are once again able to derive a single ODE for each region in the slab system:

$$\widehat{v_x}'' - m_j^2 \widehat{v}_x = 0, \tag{3.2}$$

where

$$m_0^2 = \frac{(k^2 v_{A0}^2 - \Omega^2)(k^2 c_0^2 - \Omega^2)}{(c_0^2 + v_{A0}^2)(k^2 c_{T0}^2 - \Omega^2)}, \quad \text{and} \quad m_j^2 = \frac{(k^2 v_{Aj}^2 - \omega^2)(k^2 c_j^2 - \omega^2)}{(c_j^2 + v_{Aj}^2)(k^2 c_{Tj}^2 - \omega^2)} \quad \text{for } j = 1, 2. \tag{3.3}$$

Here, $\Omega = \omega - kV_0$ denotes the Doppler-shifted frequency of waves in the central region, which appears here as only this region contains a bulk background flow. Setting the external magnetic fields to zero, Equation (3.2) becomes identical to Equation (4) in Barbulescu and Erdélyi (2018) for a magnetic slab in an asymmetric non-magnetic environment, confirming that our results so far are in agreement with the conclusions of previous studies.

The general solution of Equation (3.2) is a linear combination of the hyperbolic functions in each region, combined with arbitrary real constants A, B, C and D:

$$\widehat{v_x}(x) = \begin{cases} A(\cosh m_1 x + \sinh m_1 x), & \text{for } x < -d, \\ B\cosh m_0 x + C \sinh m_0 x, & \text{for } |x| \leqslant d, \\ D(\cosh m_2 x - \sinh m_2 x), & \text{for } x > d, \end{cases} \tag{3.4}$$

As we are still interested only in trapped modes of oscillation guided by the slab, we require that $\widehat{v_x} \to 0$ as $x \to \pm\infty$. As a reminder, for the wavenumber coefficients, this means that m_1^2 and m_2^2 must both be positive, while the sign of the internal parameter m_0^2 will decide whether a solution is a body (negative sign) or surface mode (positive sign).

Next, we match these solutions across the two interfaces by applying four boundary conditions in total. Namely, we require that the Lagrangian displacement and the total pressure perturbations have to stay continuous at $x = \pm x_0$:

$$\frac{\widehat{v}_{x1}(x=-x_0)}{\omega} = \frac{\widehat{v}_{x0}(x=-x_0)}{\Omega}, \qquad \frac{\widehat{v}_{x0}(x=x_0)}{\Omega} = \frac{\widehat{v}_{x2}(x=x_0)}{\omega}, \tag{3.5}$$

$$\widehat{p}_{T1}(x=-x_0) = \widehat{p}_{T0}(x=-x_0), \qquad \widehat{p}_{T0}(x=x_0) = \widehat{p}_{T2}(x=x_0)/, \tag{3.6}$$

where the total pessure perturbation is calculated as $p_T = p' + \dfrac{B_j \hat{\mathbf{z}} \cdot \mathbf{b}}{\mu}$ (for $j = 0, 1, 2$) .

The four boundary conditions lead to a homogeneous system of equations, which can

be expressed in matrix form as

$$\begin{pmatrix} (C_1 - S_1)/\omega & -C_0/\Omega & S_0/\Omega & 0 \\ 0 & C_0/\Omega & S_0/\Omega & (S_2 - C_2)/\omega \\ \Lambda_1(C_1 - S_1) & \Lambda_0 S_0 & -\Lambda_0 C_0 & 0 \\ 0 & \Lambda_0 S_0 & \Lambda_0 C_0 & -\Lambda_2(S_2 - C_2) \end{pmatrix} \begin{pmatrix} A \\ B \\ C \\ D \end{pmatrix} = \begin{pmatrix} 0 \\ 0 \\ 0 \\ 0 \end{pmatrix}.$$

Here, as before, we use the notation $C_j = \cosh m_j x_0$ and $S_j = \sinh m_j x_0$, for $j = 0, 1, 2$. The Λ coefficients are now defined as

$$\Lambda_j = \begin{cases} \frac{i\rho_1(k^2 v_{A1}^2 - \omega^2)}{m_1 \omega}, & \text{for } j = 1, \\ \frac{i\rho_0(k^2 v_{A0}^2 - \Omega^2)}{m_0 \Omega}, & \text{for } j = 0, \\ \frac{i\rho_2(k^2 v_{A2}^2 - \omega^2)}{m_2 \omega}, & \text{for } j = 2. \end{cases} \tag{3.7}$$

We find non-trivial solutions to this problem if the determinant of the coefficient matrix is zero, and therefore,

$$2\left(\Lambda_0^2 \Omega^2 + \Lambda_1 \Lambda_2 \omega^2\right) + \Lambda_0 \Omega \left(\Lambda_1 \omega + \Lambda_2 \omega\right) \left(\tau_0 + \frac{1}{\tau_0}\right) = 0, \tag{3.8}$$

where $\tau_0 = \tanh(m_0 x_0)$. We can expand this expression to explicitly contain the characteristic speeds of the system, and thus obtain the following form of the full dispersion relation for magnetosonic waves in a magnetic slab subject to a background flow and embedded in an asymmetric magnetic environment:

$$\begin{aligned} &2\frac{\rho_0}{\rho_1} m_1 \frac{\rho_0}{\rho_2} m_2 (k^2 v_{A0}^2 - \Omega^2)^2 + 2m_0^2 (k^2 v_{A1}^2 - \omega^2)(k^2 v_{A2}^2 - \omega^2) + \rho_0 m_0 \\ &(k^2 v_{A0}^2 - \Omega^2) \left[\frac{m_2}{\rho_2}(k^2 v_{A1}^2 - \omega^2) + \frac{m_1}{\rho_1}(k^2 v_{A2}^2 - \omega^2)\right] \left[\tau_0 + \frac{1}{\tau_0}\right] = 0. \end{aligned} \tag{3.9}$$

To further confirm that our results are in harmony with the existing literature, we note that by removing the steady flow, hence, reducing Ω to ω, we can recover the dispersion relation studied by Zsámberger et al. (2018) directly from Equation (3.9). Additionally, if the flow is kept but the magnetic fields outside the slab are reduced to zero instead, we recover Equation (11) of Barbulescu and Erdélyi (2018) for the steady slab in a non-magnetic environment. Finally, if we remove both the steady flow and the external magnetic fields, the dispersion relation (Equation 20) of Allcock and Erdélyi (2017) can also be obtained.

3.4. Approximations

The full dispersion relation (Equation 3.9) is a transcendental equation, preventing us from finding exact solutions analytically. In order to further our understanding of the complex

relationship that this equation describes between the MHD waves and the system guiding them, and to make analytical progress, in this Section, we derive analytical approximations of Equation (3.9) with applications relevant to solar physics. Furthermore, since surface mods have been shown to be more sensitive to various sources of asymmetries introduced into the magnetic slab system (Zsámberger et al., 2018; Allcock and Erdélyi, 2017) than their body mode counterparts, when deriving analytical expressions to approximate the surface mode solutions of the dispersion relation, we also study the flow speed threshold above which the surface modes we find will become unstable in an asymmetric slab.

3.4.1. Weak Asysmmetry

The full dispersion relation (Equation 3.9) for the general case of the steady magnetic slab enclosed by an asymmetric magnetic environment is a single equation determining the behaviour of all eigenmodes in the system. However, like in the previous slab system studied, it is possible to derive a decoupled dispersion relation for the problem, which, similarly to symmetric slab dispersion relations, contains a separate equation both for sausage- and for kink-type modes.

In order to do this, we require that the asymmetry should be weak, and so $\Lambda_1 \approx \Lambda_2$. Then utilising a similar expression and transformations as we did in Section 2.3, the dispersion relation (3.9) can be factorised as

$$\left[\Lambda_0\Omega\left(\Lambda_1+\Lambda_2\right)+2\Lambda_1\Lambda_2\omega\tau_0\right]\left[\Lambda_0\Omega\left(\Lambda_1+\Lambda_2\right)+2\Lambda_1\Lambda_2\omega\frac{1}{\tau_0}\right]=0 \tag{3.10}$$

By expressing this relation in terms of the densities and characteristic speeds representative of the slab system, we arrive at the weakly asymmetric or approximate dispersion relation:

$$(k^2v_{A0}^2-\Omega^2)\left(\frac{\rho_0}{\rho_1}\frac{m_1}{(k^2v_{A1}^2-\omega^2)}+\frac{\rho_0}{\rho_2}\frac{m_2}{(k^2v_{A2}^2-\omega^2)}\right)+2m_0\left\{\begin{array}{c}\tanh\\ \coth\end{array}\right\}(m_0x_0)=0. \tag{3.11}$$

As was the goal, Equation (3.11), much like dispersion relations of symmetric slab systems, consists of two simpler independent equations. One of these describes only quasi-sausage modes (the $\tanh(m_0x_0)$ line), while the other governs the dispersion of quasi-kink waves only (the $\coth(m_0x_0)$ version). This expression is also analogous to the decoupled dispersion relation (20) derived by Zsámberger et al. (2018) for the static case, and the latter can be obtained from our dispersion relation by removing the central flow from the slab while enforcing the requirements of weak asymmetry. Going one step further, if all sources of asymmetry are removed from the environment, then Equation (3.11) reduces to the "classical", symmetric and static version of the dispersion relation (Edwin and Roberts,

1982):

$$\frac{\rho_0}{\rho_e}\frac{(k^2v_{A0}^2-\omega^2)}{(k^2v_{Ae}^2-\omega^2)}m_e+m_0\left\{\begin{array}{c}\tanh\\ \coth\end{array}\right\}(m_0x_0)=0.$$

3.4.2. The Thin-Slab Approximation

When the waves propagate in a slab that is much thinner than the wavelength of the oscillations *i.e.* $kx_0 \ll 1$, it is possible to obtain analytical expressions for the frequencies of several types of eigenmodes. This limit can be applied to various solar phenomena as a first approximation, such as magnetic bright points (Liu et al., 2018) or light bridges and light walls in sunspots (Yuan et al., 2014; Yang et al., 2016, 2017).

Surface waves

The quasi-sausage surface modes propagating in this slab system are described by the $\tanh(m_0x_0)$ version of Equation (3.11), where now $m_0^2 > 0$ is required. In the limit of a slender slab, since $m_0x_0 \ll 1$, we can approximate the hyperbolic tangent function with the first term of its series: $\tanh m_0x_0 \approx m_0x_0$, and the dispersion relation simplifies to

$$(k^2v_{A0}^2-\Omega^2)\left(\frac{\rho_0}{\rho_1}\frac{m_1}{(k^2v_{A1}^2-\omega^2)}+\frac{\rho_0}{\rho_2}\frac{m_2}{(k^2v_{A2}^2-\omega^2)}\right)+2m_0^2d=0. \tag{3.12}$$

In a thin slab, the slow quasi-sausage surface mode propagates with a phase speed close to the internal tube speed modified by the flow speed. Searching for this type of solution yields the following expression for the frequency of the waves:

$$\Omega^2=(\omega-kV_0)^2=k^2c_{T0}^2\left[1+\frac{2kx_0(c_0^2-c_{T0}^2)}{\rho_0v_{A0}^2c_0^2R_v}\right], \tag{3.13}$$

where

$$R_v=\frac{\left(c_1^2-(c_{T0}+V_0)^2\right)^{\frac{1}{2}}}{\rho_1(v_{A1}^2+c_1^2)^{\frac{1}{2}}\left(v_{A1}^2-(c_{T0}+V_0)^2\right)^{\frac{1}{2}}\left(c_{T1}^2-(c_{T0}+V_0)^2\right)^{\frac{1}{2}}}$$
$$+\frac{\left(c_2^2-(c_{T0}+V_0)^2\right)^{\frac{1}{2}}}{\rho_2(v_{A2}^2+c_2^2)^{\frac{1}{2}}\left(v_{A2}^2-(c_{T0}+V_0)^2\right)^{\frac{1}{2}}\left(c_{T2}^2-(c_{T0}+V_0)^2\right)^{\frac{1}{2}}}.$$

This mode can exist when either $c_{T1} > c_{T0}+V_0$ and $c_{T2} > c_{T0}+V_0$, or $\min(c_1, v_{A1}) < c_{T0}+V_0 < \max(c_1, v_{A1})$ and $\min(c_2, v_{A2}) < c_{T0}+V_0 < \max(c_2, v_{A2})$. Different speed orderings will fulfil different inequalities of the possibilities listed above, resulting in the slow quasi-sausage surface mode approaching $\Omega^2 = k^2c_{T0}^2$ either from above or from below as $kx_0 \to 0$.

Although the weak asymmetry approximation was not studied by Barbulescu and Erdé-

lyi (2018) for their configuration, e can still observe qualitative similarities between their results and ours. Both slab systems possess quasi-sausage eigenmodes whose Doppler-shifted phase speeds approach to the internal tube speed. Also in both cases, the flow speed plays a role in shaping the correction term that scales with the dimensionless slab width. This correction term is more complex in the currently studied slab system, since it also depends on the external magnetic fields (through the external Alfvén and tube speeds). As stated before, the waves will be KHI-unstable in this system if $\mathfrak{Im}(\omega) > 0$. For the slow quasi-sausage surface waves, this means that

$$1 + \frac{2kx_0(c_0^2 - c_{T0}^2)}{v_{A0}^2 c_0^2 R_v} < 0.$$

The coefficient R_v here is a long expression which contains all the external characteristic speeds. Therefore, it can take both real (positive or negative) and imaginary values, with all of these cases encompassing several possible combinations of the characteristic speeds. Furthermore, R_v also contains the flow speed in several of its terms. Due to this somewhat unwieldy form of R_v, in order to express the critical flow speed threshold beyond which the waves become KHI-unstable, a cubic inequality in V_0^2 would have to be solved and numerous different cases would have to be examined for all possible different speed orderings. To make an exhaustive list of these cases requires a lengthy undertaking, which went beyond the scope of this general overview of the steady magnetic slab enclosed in an asymmetric magnetic environment.

A fast quasi-sausage surface mode only exists as a trapped solution in a thin slab when the external sound speeds are identical, *i.e.* $c_1 \approx c_2 \approx c_e$. Then we can look for a solution to the quasi-sausage dispersion relation which behaves like $\omega^2 \approx k^2 c_e^2$ in a thin slab, and find that the frequency of such a wave can be expressed as

$$\omega^2 = k^2 c_e^2 \left[1 + \frac{4k^2 x_0^2 c_e^2 (c_0^2 - (c_e - V_0)^2)^2}{\rho_0^2 (v_{A0}^2 + c_0^2)^2 (c_{T0}^2 - (c_e - V_0)^2)^2 R_v^2} \right], \tag{3.14}$$

where

$$R_v = \frac{1}{\rho_1 (v_{A1}^2 - c_e^2)^{\frac{1}{2}}} + \frac{1}{\rho_2 (v_{A2}^2 - c_e^2)^{\frac{1}{2}}},$$

for $c_e < \min(v_{A1}, v_{A2})$. This wave tends to the (for the moment, symmetric) external sound speed from above when longer wavelengths or thinner slabs are considered ($kx_0 \to 0$). If the sound speeds become even weakly asymmetric, the fast quasi-sausage surface mode solution will show a cut-off at the lower of the two external sound speeds.

The fast quasi-sausage surface mode frequency in the thin slab approximation (Equation 3.14) can be rewritten as

$$\omega = k c_e \left[1 - \frac{4k^2 x_0^2 c_e^2 (c_0^2 - (c_e - V_0)^2)^2}{(v_{A0}^2 + c_0^2)^2 (c_{T0}^2 - (c_e - V_0)^2)^2 R_v^2} \right]^{\frac{1}{2}},$$

where

$$R_v^2 = \rho_0^2 \left[\frac{1}{\rho_1 (c_e^2 - v_{A1}^2)^{\frac{1}{2}}} + \frac{1}{\rho_2 (c_e^2 - v_{A2}^2)^{\frac{1}{2}}} \right]^2 ,$$

and $\max(v_{A1}^2, v_{A2}^2) < c_e^2$, so that R_v^2 is positive, and R_v can remain a positive real number.

The imaginary part of the angular frequency will be greater than zero, and so the waves will become unstable, if

$$\frac{4k^2 x_0^2 c_e^2 (c_0^2 - (c_e - V_0)^2)^2}{(v_{A0}^2 + c_0^2)^2 (c_{T0}^2 - (c_e - V_0)^2)^2 R_v^2} > 1.$$

When both $(c_e - V_0)^2 c_0^2$ and $(c_e - V_0)^2 c_{T0}^2$, we can rearrange the inequality to arrive at the condition

$$A c_{T0}^2 - c_0^2 < (A-1)(c_e - V_0)^2, \tag{3.15}$$

where

$$A = \frac{(c_0^2 + v_{A0}^2) R_v}{2 k x_0 c_e}.$$

Supposing that $A - 1 > 0$, the results will be valid for $k x_0 > (c_0^2 + v_{A0}^2) R_v / (2 c_e)$ only.

In the case of speed ordering when the common external sound speed is smaller than the internal flow speed ($c_e - V_0 < 0$), then the threshold for the onset of the KHI can be found as

$$V_0 > c_e + \left(\frac{A c_{T0}^2 - c_0^2}{A - 1} \right)^{1/2} . \tag{3.16}$$

When the flow speed is lower than this critical value, even though all the other conditions set out in this derivation are fulfilled, then the magnetic fields in the system will still suppress the instability.

We now proceed to describe quasi-kink surface modes which can be guided by the asymmetric steady slab under various circumstances. In order to do this, we first take the thin-slab approximation of the quasi-kink mode decoupled dispersion relation. Since in a slender slab, the argument of the hyperbolic functions ($m_0 x_0$) is small, we can make the following approximation: $\coth m_0 x_0 \approx 1/m_0 x_0$. Then, the relevant line of Equation (3.11) simplifies to

$$d(k^2 v_{A0}^2 - \Omega^2) \left(\frac{\rho_0}{\rho_1} \frac{m_1}{(k^2 v_{A1}^2 - \omega^2)} + \frac{\rho_0}{\rho_2} \frac{m_2}{(k^2 v_{A2}^2 - \omega^2)} \right) + 2 = 0. \tag{3.17}$$

Compared to previously studied slab systems, new cut-off frequencies also appear for the quasi-kink modes. This is due to the appearance of leaky parameter regimes in a thin slab when the external Alfvén or tube speeds are asymmetric. In the case of a static slab,

the figures in Zsámberger and Erdélyi (2020, 2021) provide several examples of this.

To completely avoid leaky modes, we proceed to set the external Alfvén speeds to the same value: $v_{A1} = v_{A2} = v_{Ae}$. We can now look for the asymmetric, Doppler-shifted equivalents of the modes set out by Edwin and Roberts (1982). When v_{Ae}/v_{A0} is not of the order of the dimensionless slab width, kx_0, a solution with $\omega^2 \approx k^2 v_{Ae}^2$ may exist with an angular frequency of

$$\omega^2 = k^2 v_{Ae}^2 \left[1 - \frac{k^2 x_0^2 \rho_0^2 R_v^2}{4} \left(\frac{v_{A0}^2}{v_{Ae}^2} - \left(1 - \frac{V_0}{v_{Ae}} \right)^2 \right)^2 \right], \tag{3.18}$$

where

$$R_v = \frac{1}{\rho_1} \left(1 - \frac{c_1^2}{v_{Ae}^2} \right)^{\frac{1}{2}} + \frac{1}{\rho_2} \left(1 - \frac{c_2^2}{v_{Ae}^2} \right)^{\frac{1}{2}}.$$

In this case, $v_{Ae}^2 > max(c_1^2, >$, and the solution approaches the external Alfvén speed from below. If the waveguide is static and the flow speed is set to zero, this mode reduces to the one described by Equation (18a) of Edwin and Roberts (1982).

In the presence of the central flow, this quasi-kink wave will become KHI-unstable when

$$1 - \frac{k^2 x_0^2 R_v^2}{4} \left(\frac{v_{A0}^2}{v_{Ae}^2} - \left(1 - \frac{V_0}{v_{Ae}} \right)^2 \right)^2 < 0,$$

where $\max(c_1^2, c_1^2) < v_{Ae}^2$ so that $R_v^2 > 0$. If here, the terms fulfil that $v_{A0}^2 << (v_{Ae} - V_0)^2$ and $v_{Ae} > V_0$, then the KHI-threshold is

$$V_0 > v_{Ae} \left(1 + \left[\frac{v_{A0}^2}{v_{A2}^2} + \frac{2}{k x_0 R_v} \right] \right)^{\frac{1}{2}}. \tag{3.19}$$

We can find another quasi-kink mode solution if the external tube speeds are identical ($c_{T1} = c_{T2} = c_{Te}$). In a thin slab, the frequency of this solution tends to $\omega^2 \to k^2 c_{Te}^2$, and it can be described as

$$\omega^2 = k^2 c_{Te}^2 \left[1 - \left(\frac{\rho_0}{\rho_1} + \frac{\rho_0}{\rho_1} \right)^2 \frac{k^2 x_0^2 \left(c_e^2 - c_{Te}^2 \right) \left(v_{A0}^2 - (c_{Te} - V_0)^2 \right)^2}{4\, c_{Te}^2 v_{Ae}^4} \right]. \tag{3.20}$$

In a static slab, this wave solution corresponds to the one described by Equation (18b) of Edwin and Roberts (1982).

This mode becomes unstable when

$$1 < \left[\frac{\rho_0}{\rho_e} \right]^2 x_0^2 k^2 \left[v_{A0}^2 - \{ c_{Te} - V_0 \}^2 \right]^2 \frac{[c_e^2 - c_{Te}^2]}{c_{Te}^2 v_{Ae}^4}. \tag{3.21}$$

If the characteristic speeds and the flow speed are ordered such that $v_{A0}^2 < (c_{Te} - V_0)^2$ and

$c_{Te} < V_0$, then the KHI-threshold is at

$$V_0 > c_{Te} + \left(v_{A0}^2 + \frac{c_{Te} v_{Ae}^2}{\left[c_e^2 - c_{Te}^2\right]^{1/2}} \frac{\rho_e}{\rho_0} \right)^{1/2} . \tag{3.22}$$

Finally, for a different ordering of characteristic speeds, when $v_{Ae} \ll v_{A0}$, another type of quasi-kink surface mode solution can be found in a slender slab. Here, we have once again made the external Alfvén speeds symmetric, so that leaky regimes can completely be avoided without further requirements. Then, this quasi-kink solution behaves like

$$\omega^2 = k^2 v_{Ae}^2 \left[1 + \frac{k x_0}{2} \left\{ \frac{\rho_0}{\rho_1} + \frac{\rho_0}{\rho_2} \right\} \left\{ \frac{v_{A0}^2}{v_{Ae}^2} - \left(1 - \frac{V_0}{v_{Ae}} \right)^2 \right\} \right] . \tag{3.23}$$

In the symmetric slab without any bulk background motions, this expression corresponds to Equation (19) of Edwin and Roberts (1982), for a kink mode that tends to the external Alfvén speed from above.

This mode becomes unstable when

$$1 > -\frac{kd}{2} \left[\frac{\rho_0}{\rho_1} + \frac{\rho_0}{\rho_2} \right] \left[\frac{v_{A0}^2}{v_{Ae}^2} - \left\{ 1 - \frac{V_0}{v_{Ae}} \right\}^2 \right] . \tag{3.24}$$

Then the KHI-threshold is a function of Alfvén speeds and density ratios:

$$V_0 > v_{Ae} \left(1 + \left[\frac{v_{A0}^2}{v_{Ae}^2} + \frac{2}{k x_0 \left\{ \frac{\rho_0}{\rho_1} + \frac{\rho_0}{\rho_2} \right\}} \right] \right) . \tag{3.25}$$

As it can be seen from this discussion of surface modes and their instabilities, the problem of a steady asymmetric magnetic slab system is one that is very rich and allows for choosing the characteristic speeds in each region in numerous different ways. It must be noted that while in some cases, at higher phase speeds, multiple modes can be KHI-unstable even when the system is subject to the same background flow, the most important goal is to identify the lowest KHI threshold out of these. Namely, this one already marks the boundary between stable and KHI-unstable slab parameters, and any speeds higher than this value will also cause the instability to appear.

Body waves

Let us now move on to body waves in a steady magnetic slab placed in an asymmetric magnetic environment. Mathematically, when $m_0^2 < 0$, the decoupled dispersion relation (Equation 3.11) can be transformed into an equation that contains only trigonometric

functions:

$$(k^2v_{A0}^2-\Omega^2)\left(\frac{\rho_0}{\rho_1}\frac{m_1}{(k^2v_{A1}^2-\omega^2)}+\frac{\rho_0}{\rho_2}\frac{m_2}{(k^2v_{A2}^2-\omega^2)}\right)+2q_0\left\{\begin{matrix}-\tan\\ \cot\end{matrix}\right\}(q_0x_0)=0, \quad (3.26)$$

where $q_0^2=-m_0^2>0.$. Both fast and slow body modes can have infinitely many harmonics in the frequency bands they can exist in as trapped oscillations. In order to identify all of these harmonics, we seek solutions which ensure that the last term in the body mode dispersion relation remains finite (see eg. Roberts (1981b) for a more detailed description and application of the method).

For slow body modes, we search for solutions in the form of $\Omega^2=k^2c_{T0}^2(1+\eta(kx_0)^2)$ (for some $\eta>0$ to be determined). For quasi-sausage (quasi-kink) modes, our condition is that $q_0\tan(q_0x_0)$ ($q_0\cot(q_0x_0)$) must be bounded, and therefore q_0x_0 has to converge to the roots of $\tan(q_0x_0)=0$ ($\cot(q_0x_0)=0$). This, in turn, means that $q_0x_0=n\pi$ with $n\in\mathbb{Z}$ for quasi-sausage modes, and $q_0x_0=\left(n-\frac{1}{2}\right)\pi$ for quasi-kink modes. After substituting in q_0^2 and rearranging the expression, we can determine the value of η. This, in turn will give us a description of the quasi-sausage (top) and quasi-kink (bottom) body waves as

$$\Omega^2=k^2c_{T0}^2\left\{\begin{matrix}\left[1+\frac{(v_{A0}^2-c_{T0}^2)(c_0^2-c_{T0}^2)k^2x_0^2}{(v_{A0}^2+c_0^2)c_{T0}^2n^2\pi^2}\right],\\ \left[1+\frac{(v_{A0}^2-c_{T0}^2)(c_0^2-c_{T0}^2)k^2x_0^2}{(v_{A0}^2+c_0^2)c_{T0}^2(n-\frac{1}{2})^2\pi^2}\right].\end{matrix}\right. \quad (3.27)$$

3.4.3. Zero-β Approximation

When the plasma behaviour is dominated by the effects of the magnetic fields that permeate it, in the extreme case, the analytically favourable zero-β approximation can be used. In this Section, we will consider the plasma to be cold in all three layers *i.e.* $\beta_j=\frac{2\mu p_j}{\mathbf{B}_j^2}\to 0$, for $j=0,1,2$. Then, the sound speeds are negligible compared to the Alfvén speeds, which can be true e.g. under solar coronal conditions.

In this limit, the wavenumber parameters can be simplified to give

$$m_0^2\approx\frac{(k^2v_{A0}^2-\Omega^2)}{v_{A0}^2},\ q_0^2\approx\frac{(\Omega^2-k^2v_{A0}^2)}{v_{A0}^2},\ m_j^2\approx\frac{(k^2v_{Aj}^2-\omega^2)}{v_{Aj}^2},$$

for $j=1,2$. Slow body waves are no longer present in the system, leaving us only with the fast body modes, similarly to the symmetric case investigated by Edwin and Roberts (1982). We substitute the simplified zero-β parameters into the body mode dispersion relation (Equation 3.26), and utilise the condition of equilibrium total pressure balance ($p_1+B_1^2/2\mu=p_0+B_0^2/2\mu=p_2+B_2^2/2\mu$) to express the density ratios of the different regions in the model by a fraction containing the characteristic speeds for any two regions $i=0,1,2$ and $j=0,1,2$. Moreover, because in the zero-β approximation, the sound speeds

are negligible, the density ratio can be reduced to a ratio of Alfvén speeds:

$$\frac{\rho_i}{\rho_j} = \frac{c_j^2 + \frac{1}{2}\gamma v_{Aj}^2}{c_i^2 + \frac{1}{2}\gamma v_{Ai}^2} \approx \frac{v_{Aj}^2}{v_{Ai}^2}. \tag{3.28}$$

The zero-β dispersion relation (Equation 3.26) then takes the following concise form:

$$\frac{1}{2}\left(\frac{q_0}{m_1} + \frac{q_0}{m_2}\right) + \begin{Bmatrix} \tan \\ -\cot \end{Bmatrix}(q_0 x_0) = 0.$$

The only solutions of interest in our study are the ones which fall within the frequency range $kv_{A0}^2 < \omega^2 < k^2 v_{Am}^2$ and behave as $\Omega^2 = k^2 v_{Am}^2 \frac{\rho_m}{\rho_0}\left[1 + \frac{\nu}{k^2 x_0^2}\right]$ in a thin slab. Here, the value of the coefficient ν can be determined through a process similar to the one we employed for general thin-slab body modes in Section 3.4.2, by ensuring that the terms with the trigonometric functions remain bounded. Furthermore, the notation $v_{Am} = min(v_{A1}, v_{A2})$ stands for the smaller of the external Alfvén speeds, which we use to avoid leaky regimes. With these considerations, we find the quasi-sausage (top) and quasi-kink (bottom) mode solutions of the fast body waves in a zero-β slab system to be

$$\Omega^2 = k^2 v_{A0}^2 \begin{cases} \left[1 + \dfrac{j^2\pi^2}{k^2 x_0^2}\right], \\ \left[1 + \dfrac{(j - \frac{1}{2})^2\pi^2}{k^2 x_0^2}\right], \end{cases}$$

where $j = 1, 2, 3 \cdots$. Both of these equations contain an explicit dependence on the internal slab parameters. The external quantities only appear indirectly, through the pressure balance condition stated in Equation (3.28).

3.5. Numerical Results

In the following Section, numerical solutions are presented to the dispersion relation in several illustrative slab systems, allowing us to explore the similarities and differences between weakly and strongly asymmetric models, as well as to check how closely the weak asymmetry approximation follows the exact results as the slab is subjected to flows of various speed. The complex roots of the dispersion relation were obtained using a Python module built around the Newton-Rhapson method, adapted from the version used in Barbulescu and Erdélyi (2018) and Zsámberger et al. (2022a). Further improvements to the code were made by Balázs Asztalos, who is a co-author in the paper that the current Section is based on, namely Zsámberger et al. (2022b). For clarity, he prepared the final form of the figures included in the paper and referenced in this Section after several iterations and extensive consultations on mode identification, speed orderings, regions of

interest and the interpretation of results among the co-authors.

Similarly to Section 2.4, the dispersion relation was solved in a non-dimensionalised form derived by normalising its terms with respect to the internal Alfvén speed and introducing the Alfvén Mach number, $M_{A0} = V_0/v_{A0}$ to describe the flow speed relative to this characteristic background speed in the central region of the slab. The Figures presented here were prepared using $v_{A0} = 1$, therefore no new notation is included in them for the non-dimensionalised quantities.

3.5.1. Solutions in Weakly and Strongly Asymmetric Slab Systems

First, in Figure 3.2, we present solutions to the full dispersion relation, where the phase speed of the modes is plotted as a function of the internal Alfvén Mach number for a fixed value of the slab width (corresponding in this case to a thin slab, $kd = 0.1$), where the environment of the slab is only weakly asymmetric. As before, the real part of the phase speeds are plotted in blue, while the two branches of the imaginary part (symmetric to the $\omega/kv_{A0} = 0$ line) are shown in red in each figure.

In both panels of Figure 3.2, we investigate trapped waves exclusively, and any solutions, including unstable ones, have been removed if their phase speed would have fallen in one of the leaky domains, indicated by grey hatching in the figures (where $m_1^2 < 0$ or $m_2^2 < 0$).

Figure 3.2a shows solutions propagating in a symmetric steady slab system, characterised by the equilibrium parameters $c_0 = 0.8v_{A0}$, $c_1 = c_2 = 1.51v_{A0}$, $v_{A1} = v_{A2} = 0.9v_{A0}$, and $\rho_1/\rho_0 = \rho_2/\rho_0 = 0.5$. As opposed to this, Figure 3.2b shows how the introduction of plasma and magnetic asymmetry into the steady slab system changes the behaviour of these modes when $c_0 = 0.8v_{A0}$, $c_1 = 1.51v_{A0}$, $c_2 = 1.33v_{A0}$, $v_{A1} = 0.9v_{A0}$, $v_{A2} = 0.9v_{A0}$, $\rho_1/\rho_0 = 0.5$, and $\rho_2/\rho_0 = 0.6$.

In both the symmetric and the asymmetric cases, the slow quasi-kink modes with their phase speed falling close to the external tube speeds (as both panels have been prepared using a small value of the slab width), will be strongly affected by the flow. Propagating with phase speeds between $-c_{T2}$ and c_{T2}, they are stable modes up to quite high flow speeds, but at around $M_{A0} = 2.5$, the forward- and backward-propagating modes are shifted strongly enough by the flow to meet at the same phase speed value, which leads to the onset of the KHI (see the parabola-shaped red curve on the right-hand-side parts of the two diagrams). For all values of the Alfvén Mach number higher than this threshold value that we investigated while preparing these figures, both the symmetric and the asymmetric steady slab systems remain unstable.

In panel (a) of Figure 3.2, an additional unstable region appears, with the instability first occurring at around $M_{A0} = 2$. This instability is tied to sausage modes propagating with approximately the external sound speed ($c_e = c_1 = c_2$ for this symmetric case). A sharp cut-off can be observed in the diagram, especially when looking at the imaginary

parts of the phase speeds. This is because at high enough values of the Alfvén Mach number, the solutions would start falling within the leaky regime ($v_{ph} > c_e$). These observations could only be made in the symmetric case, because in the asymmetric slab system, the external sound speeds diverge and consequently lower the cut-off speed for the quasi-sausage modes. This results in the entire unstable region being pushed into the leaky domain (and therefore these solutions are not displayed in Figure 3.2b). Even though the slab system is only weakly asymmetric in panel (b), this small change in one of the external sound speeds already proved to be enough to illustrate one of the several new potential cut-off frequencies which can be introduced due to the presence of asymmetry and their far-reaching consequences on the stability of trapped oscillations in the model. A more in-depth investigation of the new cut-off frequencies observable in a static asymmetric magnetic slab can be found in e.g. Zsámberger and Erdélyi (2020).

Last but not least, using a high-resolution grid to solve the dispersion relation also reveals a third possible KHI-unstable flow speed regime at around $M_A = 1.5$, which, in fact, constitutes the lowest possible instability threshold both in the symmetric and the asymmetric configurations examined here. For better visibility, the details of this instability region are also shown in the inlets of the two panels in Figure 3.2.

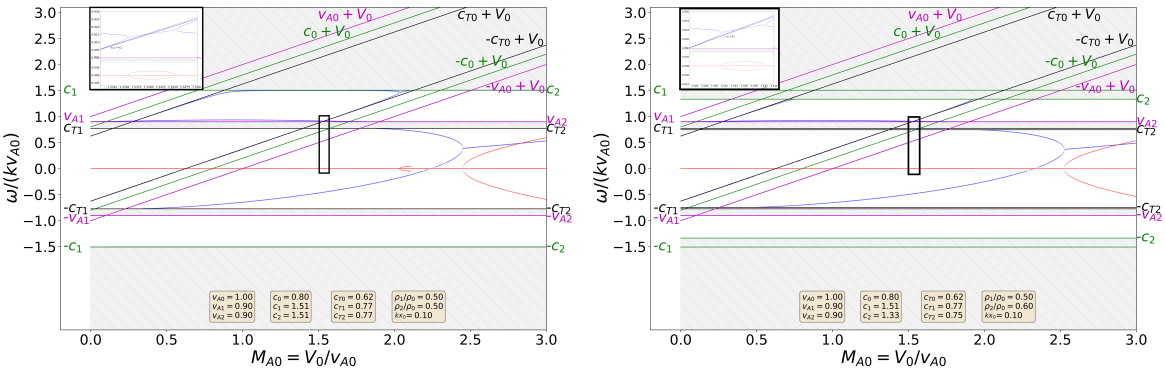

(a) (b)

Figure 3.2: Solutions of the full dispersion relation (Equation 3.9) in **(a)** a symmetric slab and in **(b)** a weakly asymmetric slab. Source: Zsámberger et al. (2022b).

As a further extension to the analytical study of the current slab system, we also conducted a numerical investigation of a strongly asymmetric steady asymmetric magnetic slab, shown in Figure 5 of the Appendix, with the following equilibrium parameters: $c_0 = 0.8v_{A0}$, $c_1 = 2.59v_{A0}$, $c_2 = 1.33v_{A0}$, $v_{A1} = 0.9v_{A0}$, $v_{A2} = 0.9v_{A0}$, $\rho_1/\rho_0 = 0.2$, and $\rho_2/\rho_0 = 0.6$.

Interestingly, looking at panel (b) of Figure 5, we find the same types of instabilities that we described in detail in Figure 3.2. Having thus found which flow speed regions are unstable in a thin slab of $kx_0 = 0.1$, we prepared panel (a) to demonstrate how the situation might change if the slab width takes a different value. It becomes immediately

obvious from Figure 5a that the slow quasi-kink modes which we identified as the cause of the instability when $M_{A0} \gtrsim 2.3$ and $kx_0 = 0.1$ are actually stable for very thin slabs. In slightly wider (but still slender) slabs, the phase speeds of the forward- and backward-propagating modes meet and the system becomes unstable for all slab widths $kx_0 \gtrsim 0.2$. Another group of stable solutions appears in this diagram, namely, that of body mode harmonics propagating with large negative and then small positive phase speeds as the slab width is increased.

Comparing Figure 3.2b and Figure 5b highlights a further consequence of the increased asymmetry: the two external sound speeds are more widely separated in Figure 5b. This results in the exclusion of a larger range of phase speeds due to the leaky character of waves propagating here. An additional notable difference between the weakly and strongly asymmetric cases is that, for our set of chosen parameters, the quasi-kink mode instability sets in at lower values of the Alfvén Mach number in the strongly asymmetric case. Both configurations implicitly contain a magnetic asymmetry as well as the explicitly stated density asymmetry, since the different density ratios require magnetic fields of different strength to be present in the external regions for the external Alfvén speeds to remain the same ($v_{Ae} = v_{A1} = v_{A2}$). The solutions found for asymmetric slab systems presented in this Section seem to indicate that due to the presence of the magnetic fields and the restoring force they generate, the KHI-threshold is still relatively high in such a slab geometry. However, it seems that the greater the asymmetry between the external regions is, the less effective the magnetic suppression of the instability may become.

As an additional step of our numerical study of the steady magnetically asymmetric slab geometry, we compared the solutions obtained by using the full and the decoupled dispersion relations to confirm that our starting point for all further analytical approximations was close to the exact solutions of the problem. In Figure 6 of the Appendix, we demonstrate that overall, both the weak asymmetry (panels a and b) and the combined weak asymmetry and thin slab (panels c and d) approximations show the same qualitative behaviour as the solutions of the full dispersion relation. Quantitatively, the difference we found between the weak asymmetry solutions of Figures 6a and 6b and the corresponding quasi-sausage and quasi-kink mode solutions of the full dispersion relation (3.2b) was of the order of 10^{-2}. Comparing the solutions between panels (a) and (c), as well as (b) and (d), the difference between thew comparing the thin-slab approximation of a weakly asymmetric configuration and the weak asymmetry approximation itself was found to be of the order of 10^{-4}. We conclude that for the specific speed ordering chosen, at least, both of these potential sources of error are orders of magnitude smaller than the characteristic speeds we used to prepare the figures.

3.6. Conclusions

In this Chapter, the effects of a steady flow on the propagation of MHD waves in a magnetic slab enclosed in an asymmetric magnetic environment were investigated. We first derived the full dispersion relation in Section 3.2, which, unlike in the case of symmetric slabs, does not decouple into two separate equations in the general case. Then in Section 3.4, an approximate (decoupled) dispersion relation was obtained for quasi-sausage and quasi-kink modes in the case when the external asymmetry in the system is weak. In this limit, it was possible to employ further approximations often used in solar physics, such as the thin slab and zero-β approximations, in order to provide analytical expressions for the angular frequencies of surface- and body-mode solutions. Where it was possible, we also found expressions for the critical internal flow speed above which the system becomes subject to the KHI, since instabilities caused by the presence of flows play a critical role in the solar atmosphere. They might contribute to the dissipation of energy and thus to maintaining the extremely high temperatures found in the corona.

We also provided numerical solutions of the phase speeds and instabilities present in symmetric, weakly asymmetric, as well as in strongly asymmetric steady slab systems. Furthermore, for a specific set of equilibrium parameters corresponding to the weak asymmetry approximation, we compared the accuracy of solving our approximate dispersion relations to solving the full, non-decoupled dispersion relation using the same numerical scheme. It must be noted that, considering all the free parameters that it possesses (characteristic speeds, densities and flow speed), the steady magnetic slab embedded in an asymmetric magnetic environment poses a very rich problem. Therefore, what we can claim with certainty is that for this particular set of background parameters, the weak asymmetry and thin slab approximations are good predictors of the phase speeds and instability limits of eigenmodes obtained from the full dispersion relation.

A worthwhile future endeavour would be to provide the solutions for an environment more closely corresponding to a feature of the solar atmosphere under the influence of a bulk background flow, and repeat the investigations into the limits of instability and the accuracy of the approximations provided. By preparing steady asymmetric Cartesian models of solar atmospheric structures and employing SMS techniques, we have the potential to diagnose the elusive properties of solar plasma. With the advent of the next generation of solar observatories, such as DKIST and EST, it is our hope that such studies can be carried out with good accuracy down to the smallest scales within the Sun's atmosphere.

Chapter 4.
Further Generalisation of Slab Models Containing Asymmetric Flows

Abstract

In this Chapter, we continue the investigation of asymmetric steady slab systems in the solar atmosphere. Combining the different methods and different sources of asymmetry introduced before, we include both asymmetric external magnetic fields (see Chapter 3) and asymmetric external flows (see Chapter 2 in the system to build a more general steady slab model. We derive the dispersion relation of the configuration, comparing it to previous results. Next, we describe a potential application of asymmetric slab geometries to modelling magnetic bright points in the solar atmosphere. Finally, to carry the extensions of this type of three-layer slab systems to completion, we build a completely asymmetric steady slab model and provide its general dispersion relation. focuses on MHD wave propagation in steady slabs. Sections of the paper Allcock et al. (2019) serve as the basis of this Chapter.

4.1. Chapter Introduction

Shaped by ubiquitous magnetic- and flow fields of variable complexity, the dynamic and finely structured solar atmosphere can give rise to numerous unique waveguide structures. Each detection of these, paired with appropriate theoretical studies, provides us with more opportunities to learn about the processes moulding the appearance of every fascinating solar atmospheric feature. Different factors, such as density differences, magnetic field concentrations, or concentrated flows, are able to influence the structures of the atmosphere and the waves that they guide, and their importance may vary in each case. Our aim in this Chapter is to provide further Cartesian models beyond the ones already presented, allowing any future studies to tailor the geometry applied in their approximation of a solar feature to the detected relative strengths of magnetic fields or flows as well as the asymmetry present in them.

The influence of steady flows on wave behaviour, specifically, has been studied in multiple geometries, encompassing both cylindrical flux tubes (see e. g. Somasundaram et al.

(1999) and Terra-Homem et al. (2003)) as well as slab systems (see e.g. Nakariakov and Roberts (1995) for a symmetric slab study and Barbulescu and Erdélyi (2018) for an asymmetric slab system).

In Section 4.2, we obtain the dispersion relation of magnetosonic waves guided by an asymmetric magnetic slab enclosed in an environment containing density, magnetic, and flow asymmetries as well. We include the high-β limit in this Section to serve as an example for potential solar applications of the model, as it corresponds to the photospheric environment of MBPs. Armed with this analytical information, we present numerical solutions for the full dispersion relation under the circumstances (equilibrium sound-, Alfvén-, and flow speeds) corresponding to magnetic bright points and their environment in the intergranular lanes, comparing the results obtained here to previous slab models of such features.

To conclude the Chapter, in Section 4.3, we continue the generalisation of asymmetric slab models, so that different plasma parameters, magnetic fields, and flow speeds are contained in all three plasma domains of the three-layer Cartesian waveguide. From the dispersion relation provided here, all other dispersion relations included in this Thesis can be derived as particular cases of this more general model.

4.2. The Slab in an Asymmetric Magnetic Environment with Steady Flows

A further interesting problem within the family of Cartesian waveguide models is a configuration where different magnetic fields permeate the entirety of the asymmetric slab system, while only the internal plasma is kept stationary (see the illustration in Figure 4.1). In the following sections, we will derive the dispersion relation for plane waves propagating in parallel to the magnetic fields of this slab system and look at illustrative examples of analytical and numerical solutions of the dispersion relation relevant to applications in solar physics.

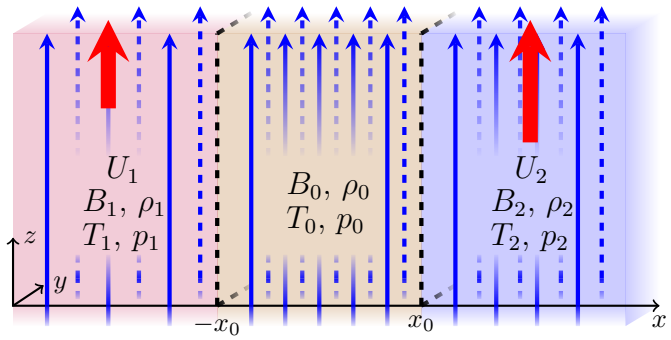

Figure 4.1: The equilibrium configuration for a magnetic slab placed in an asymmetric magnetic environment, with two different external flows in the system. Source: Allcock et al. (2019).

4.2.1. The Dispersion Relation

We derive the dispersion relation for this Cartesian model through steps formally similar to the previous two cases presented in Chapters 2 and 3. Now, however, magnetic fields permeate all three regions of plasma, and both external regions can be subject to different flows. Therefore, when going through the process of linearising the ideal MHD equations, we have to start from their form still containing bulk background flows (see Equations 2.1 - 2.4). In the central region, which is static, the equations can be simplified to the static version also presented in the Introduction (Equations 1.19) - (1.22). Due to the presence of asymmetric background flows, terms related to the two environmental regions will bring in expressions containing Doppler-shifted forms of the angular frequency of waves, while terms related to the central, static region will contain the angular frequency on its own.

As before, introduce small, time-dependent perturbations to the equilibrium parameters and obtain a linearised version of the equations of ideal MHD. We once again look for plane wave solutions that propagate in the vertical direction (parallel to the slab boundaries, magnetic fields and flows). Similarly to the two simpler cases detailed before, we can arrive at a single ordinary differential equation governing plasma motions in each region in the form of

$$\widehat{v_x}'' = m_j \widehat{v_x}, \tag{4.1}$$

for $j = 0, 1, 2$, where $\widehat{v_x}$ is the amplitude of the perturbation of the velocity in the x-direction and $'$ denotes differentiation with respect to the spatial coordinate x. In this problem, the coefficients m_j are defined as

$$m_0^2 = \frac{\left(k^2 v_{A0}^2 - \omega^2\right)\left(k^2 c_0^2 - \omega^2\right)}{\left(v_{A0}^2 + c_0^2\right)\left(k^2 c_{T0}^2 - \omega^2\right)}, \qquad m_j^2 = \frac{\left(k^2 v_{Aj}^2 - \Omega_j^2\right)\left(k^2 c_j^2 - \Omega_j^2\right)}{\left(v_{Aj}^2 + c_j^2\right)\left(k^2 c_{Tj}^2 - \Omega_j^2\right)}, \quad \text{for } j = 1, 2, \tag{4.2}$$

and $\Omega_j = \omega - kU_j$ are the Doppler-shifted frequencies for $j = 1, 2$. The solutions for the velocity perturbation amplitude are combinations of the hyperbolic trigonometric functions, which need to be matched by using the four boundary conditions resulting from the continuity of the total pressure and Lagrangian displacement perturbations. These boundary conditions can summarised in matrix form as

$$\begin{pmatrix} \frac{C_1 - S_1}{\Omega_1} & \frac{-C_0}{\omega} & \frac{S_0}{\omega} & 0 \\ 0 & \frac{C_0}{\omega} & \frac{S_0}{\omega} & -\frac{C_2 - S_2}{\Omega_2} \\ \Lambda_1(C_1 - S_1) & \Lambda_0 S_0 & -\Lambda_0 C_0 & 0 \\ 0 & \Lambda_0 S_0 & \Lambda_0 C_0 & -\Lambda_2(S_2 - C_2) \end{pmatrix} \begin{pmatrix} A \\ B \\ C \\ D \end{pmatrix} = \begin{pmatrix} 0 \\ 0 \\ 0 \\ 0 \end{pmatrix}, \tag{4.3}$$

where

$$\Lambda_0 = -\frac{i\rho_j}{\omega m_0}(k^2 v_{Aj}^2 - \omega^2), \qquad \Lambda_j = -\frac{i\rho_j}{\Omega_j m_j}(k^2 v_{Aj}^2 - \Omega_j^2) \quad \text{for } j = 1, 2, \tag{4.4}$$

and $C_j = \cosh m_j x_0$, $S_j = \sinh m_j x_0$ for $j = 0, 1, 2$. In order to find non-trivial solutions, the determinant of the coefficient matrix in Equation (4.3) must be zero, which, after substituting in the characteristic speeds and densities for the Λ_j terms and rearranging, leads us to the full dispersion relation describing the eigenmodes of oscillations in this slab system:

$$\begin{aligned}&\frac{m_0^2}{(k^2 v_{A0}^2 - \omega^2)^2} + \frac{\rho_0}{\rho_1}\frac{\rho_0}{\rho_2}\frac{m_1 m_2}{(k^2 v_{A1}^2 - \Omega_1^2)(k^2 v_{A2}^2 - \Omega_2^2)} \\ &\quad + \frac{1}{2}\frac{m_0}{(k^2 v_{A0}^2 - \omega^2)}\left(\frac{\rho_0}{\rho_1}\frac{m_1}{(k^2 v_{A1}^2 - \Omega_1^2)} + \frac{\rho_0}{\rho_2}\frac{m_2}{(k^2 v_{A2}^2 - \Omega_2^2)}\right)(\tanh m_0 x_0 + \coth m_0 x_0) = 0.\end{aligned} \tag{4.5}$$

As before, this dispersion relation still does not decouple into sausage and kink versions, and it provides one single equation that governs both quasi-sausage and quasi-kink eigenmodes in the system. However, with the further assumption of weak asymmetry, a decoupled dispersion relation can be calculated for MHD waves propagating in this asymmetric slab system as

$$(k^2 v_{A0}^2 - \omega^2)\left[\frac{\rho_0}{\rho_1}\frac{m_1}{(k^2 v_{A1}^2 - \Omega_1^2)} + \frac{\rho_0}{\rho_2}\frac{m_2}{(k^2 v_{A2}^2 - \Omega_2^2)}\right] + 2m_0\begin{pmatrix}\tanh\\ \coth\end{pmatrix}\{m_0 x_0\} = 0, \tag{4.6}$$

which will be a valid approximation when the equilibrium parameters (densities, pressures, temperatures, magnetic fields and flow speeds) in the two environmental regions are of the same order, allowing us to use $\Lambda_2\Omega_2 \approx \Lambda_1\Omega_1 + \epsilon$, where ϵ is a small quantity.

In general, we can only find exact solutions to these dispersion relations by using numerical methods. However, in some limiting cases, analytical expressions can also be given to describe the behaviour of certain modes of oscillation shown by the slab. Below, we will demonstrate this via the example of the high-β limit, which can serve as an approximation of the conditions prevalent in the solar photosphere.

4.2.2. The High-β Limit

If high-β plasma fills each region of this asymmetric Cartesian waveguide model, as it may be the case in the solar photosphere, then plasma motions dominate over magnetic effects. In the limit of infinite plasma-β, the Alfvén speeds are negligible compared to the sound speeds, and the m_j $(j = 0, 1, 2)$ coefficients in the dispersion relation are simplified considerably.

To highlight the effect of bulk background flows on the modes supported by the slab,

we can change our frame of reference and convert this asymmetric two-flow system into a waveguide model that contains one external and one internal flow. We define the new flow speeds as $U_{2,new} = 0$, $U_{0,new} = -U_{2,old}$, and $U_{1,new} = U_{1,old} - U_{2,old}$. We investigate the infinite-β limit provides us with relative ease of calculations and allows only fast body waves to be guided by the slab. These obey the following dispersion relation:

$$\frac{1}{2}\left(\frac{\rho_0}{\rho_1}\frac{m_1}{n_0}\frac{(\omega - kU_{0n})^2}{(\omega - kU_{1n})^2} + \frac{\rho_0}{\rho_2}\frac{m_2}{n_0}\frac{(\omega - kU_{0n})^2}{\omega^2}\right) = \begin{pmatrix}\tan \\ -\cot\end{pmatrix}\{n_0 x_0\}, \tag{4.7}$$

where $n_0^2 = -m_0^2$. Through a process similar to the ones we employed in Section 3.4.3, we can obtain the following analytical approximation of the frequencies of both backward- and forward-propagating fast body waves that we expect to see in this system:

$$\omega = k\left(U_{0,new} \pm c_0\left[1 + \frac{j^2\pi^2}{\{kx_0\}^2}\right]^{1/2}\right), \quad \text{for } j = 1, 2, 3..., \tag{4.8}$$

for quasi-sausage modes, and

$$\omega = k\left(U_{0,new} \pm c_0\left[1 + \frac{\left\{j - \frac{1}{2}\right\}^2\pi^2}{\{kx_1\}^2}\right]^{1/2}\right), \quad \text{for } j = 1, 2, 3..., \tag{4.9}$$

for quasi-kink modes. Both of these expressions showcase the strong, immediate effect of the flows included in the model. Numerical studies suggest that any (internal or external) flow speed can significantly change the frequency of the eigenmodes of the system, as well as the types and magnitudes of cut-off frequencies that appear. Due to the initial asymmetry present between the steady and static regions of this waveguide model, unlike in the case when the plasma environment is symmetric (Nakariakov and Roberts, 1995), the current model cannot be made symmetric or even fully externally stationary simply by changing the frame of reference. In the following section, we will illustrate the significant influence that asymmetric flows and further external parameters have on the eigenmodes of multi-layered Cartesian systems through applying such models to the magnetic bright points of the solar atmosphere.

4.2.3. Magnetic Bright Points as Asymmetric Slabs in the Photosphere

We have suggested multiple times throughout this study that magnetic bright points (MBPs) of the photosphere are excellent candidates for solar applications of asymmetric Cartesian models. These are small concentrations of strong magnetic fields (of the order of kilogauss).

We described the granular structure of the photosphere in Section 1.1, resulting from

the flows of the convective zone reaching the solar surface. In-between the granules that these convective cells form with their upflow, there are dark intergranular lanes formed from the convectional downflow. MBPs are located in these darker-looking intergranular lanes, and they show up as brighter regions because of two reasons. Firstly, the presence of concentrated magnetic fields leads to a higher magnetic pressure within MBPs, which means that a lower plasma pressure is enough to keep them in total pressure balance with their environment. This lower plasma pressure, in turn, allows observers to glance deeper into the photosphere within the area of MBPs. A second effect potentially contributing to their bright appearance is that the interior of MBPs is further heated by their environment (Rouppe van der Voort et al., 2005; Crockett et al., 2010; Keys et al., 2013).

In general solar physics studies, MBPs are often described with a cylindrical flux tube model, although their appearance can actually vary between different shapes. They are often strongly elongated, and they can even be quite irregularly shaped, especially near pores (Berger et al., 1995; Bovelet and Wiehr, 2003). This heterogeneity of MBP shapes makes it possible to approach at least some of them as magnetic slabs. And, since MBPs are wedged in-between two different neighbouring cells of the solar granulation, physical parameters on either side of a bright point may also show differences. This second fact serves as an excellent motivation to apply specifically *asymmetric* slab models when studying waves in magnetic bright points. Figure 4.2 illustrates such an MBP model, with the bright region in the centre being the magnetic slab itself, and the intergranular lane it cuts into two halves serves as the asymmetric environment. Depending on which effects are taken into account, this asymmetry can stem from density, magnetic field strength, or flow speed differences on either side of the MBP. The original sketch is based on the TiO 7058 Å observations taken by the New Vacuum Solar Telescope in Figure 11 of (Liu et al., 2018), while the completed illustration was included in Allcock et al. (2019).

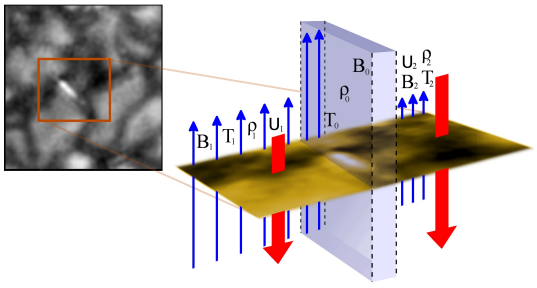

Figure 4.2: Visualisation of an elongated magnetic bright point as a non-stationary asymmetric slab. Figure adapted from Allcock et al. (2019).

Similarly to their shapes, the size distribution of MBPs has also been the subject of extensive study. Using the Swedish Vacuum Solar Telescope on La Palma, Berger et al. (1995) found that MBPs showed a lognormal size distribution, with an average of 250km (0.″35), and a modal value of 220km (0.″30). Researchers using the Dutch Open Telescope reached a comparable result (finding a dominant diameter of 220 ± 25km). They

also concluded that only in about two-thirds of cases can isolated MBPs be said to have a circular shape, while the remaining one-third of bright points are either elongated or irregular (Bovelet and Wiehr, 2003). Later, somewhat lower dominant diameter values of 160 ± 20km were established by observations made with the 1m Swedish Solar Telescope (SST) (Wiehr et al., 2004; Crockett et al., 2010). Taking into account the elongated or elliptical shapes, Sánchez Almeida et al. (2004) applied two-Gaussian fits to MBPs found in SST images. Major axis lengths of up to 350km we found, while minor axis lengths peaked at around 135km, and they mostly stayed below 200km. Solanki et al. (2010) estimated that MBPs had sizes close to the $0.''15$ spatial resolution limit of the balloon-borne SUNRISE observatory. Overall, the consensus in the existing literature point to the lower limit on the size of MBPs being at a 100-km diameter, where radiative pressure stops the convective collapse of the tube to even smaller sizes (Venkatakrishnan, 1986). Alternately, if they interact with acoustic waves, resulting in the larger flux tubes being split up into smaller parts, this lower limit may lie somewhere between 40-60km (Ryutova, 1996).

Approximating an MBP with an asymmetric magnetic slab model requires that we study one of the more elongated, less regular MBPs, and we demand that its finite major axis should be much longer than the wavelengths of the supported modes we study. If we take a large elongated MBP with a very large, 1000km length (major axis), and we prescribe that the waves should be able to complete at least 10 periods of oscillation in the slab, then the maximum wavelength we can investigate becomes $\lambda = 100$km, corresponding to a minimum required wavenumber of $k = 2\pi \cdot 10^{-1}\text{km}^{-1}$. Based on these limitations and using photospheric values of characteristic speeds, Zsámberger and Erdélyi (2021) estimated the angular frequency of waves that can be subject to investigations utilising asymmetric slab models to be around $\omega = 2\pi \cdot [0.0825, 0.1]$Hz. These are quite high-frequency oscillations, which might pose observational challenges, similarly to high-frequency acoustic waves (see e.g. Fossum and Carlsson (2004, 2005); Carlsson et al. (2007); Cuntz et al. (2007); Wedemeyer-Böhm et al. (2007)).

Identifying waves and employing SMS techniques in MBPs therefore requires images taken with extremely high spatial and temporal resolution. These should be possible to obtain with the recently completed Daniel K. Inouye Solar Telescope (DKIST), a 4-meter diameter Gregorian telescope in Haleakala, Maui, Hawaii. This is currently the largest ground-based solar observatory, and its ≤ 30 Hz frame rate and $\approx 0.''03$ spatial resolution (corresponding to 19km on the Sun) (Tritschler et al., 2015) should be sufficient to resolve oscillations within small-scale solar features such as MBPs.

Besides DKIST, once completed and operational, the European Solar Telescope (EST) will also be able to provide crucial information about MBPs. In fact, providing high-resolution and high cadence observations of MBPs is specifically laid out in the science requirements document of EST, in order to investigate the magnetic fields they incorporate, as well as their movement, and, most importantly to the topic of this study, the magnetic

coupling of the solar atmosphere at least partly through observing MHD waves guided by MBPs. In order to realise these aims, the EST goals and requirements regarding MBPs ask for observations with both the integral field unit spectrometer and the broadband imaging capability, with spatial resolutions ranging from 1" to the diffraction limit, and cadences between 1 and 10 seconds. It is hoped that these measurements will allow researchers to determine the phase relations between the Stokes-profiles, Doppler-shifts and intensity perturbations of MHD waves in MBPs, as well as confirm the presence or the lack of area perturbations during MBP oscillations, which could help identify at least "classical" symmetric sausage mode oscillations (Schlichenmaier et al., 2019).

As mentioned before, their position embedded within the dark downflow regions connecting two separate granular cells makes MBPs prime candidates for the solar applications of asymmetric magnetic slab models. This was already pointed out by Zsámberger, Allcock, and Erdélyi (2018) in the first study of a static magnetic slab model incorporating both plasma and magnetic asymmetries in the environmental regions, where it was suggested that MBPs could be studied in such a geometry while using the approximation of an incompressible plasma. Further building on this study, Zsámberger and Erdélyi (2021) presented an application of the same static asymmetric magnetic slab model in a more generalised (no longer incompressible) case. Solutions for this case, with a high-β intergranular lane enveloping the MBP, which can have any plasma-β value from low through one to high, are shown in Figure 4.3. Since there are no flows in the system yet, all the solutions are stable. Furthermore, due to the unbroken symmetry between forward- and backward-propagating waves, only the forward-propagating solutions are plotted. Solutions in panel (a) show the case when $v_{A1} = 0.205v_{A0}$, $v_{A2} = 0.3v_{A0}$, $c_0 = 1.2v_{A0}$, $c_1 = 0.7v_{A0}$, $c_2 = 0.8v_{A0}$, $\rho_1/\rho_0 = 4.329987$ and $\rho_2/\rho_0 = 3.179487$, making the MBP itself a high-*beta* slab as well. In panel (b), solutions were obtained for $v_{A1} = 0.170v_{A0}$, $v_{A2} = 0.249v_{A0}$, $c_0 = 0.913v_{A0}$, $c_1 = 0.581v_{A0}$, $c_2 = 0.663v_{A0}$, $\rho_1/\rho_0 = 4.609381$ and $\rho_2/\rho_0 = 3.384645$, meaning that the MBP itself has a plasma-*beta* value of one. Lastly, panel (c) displays solutions for a slab system where $v_{A1} = 0.0.137v_{A0}$, $v_{A2} = 0.2v_{A0}$, $c_0 = 0.733v_{A0}$, $c_1 = 0.47v_{A0}$, $c_2 = 0.53v_{A0}$, $\rho_1/\rho_0 = 5.875957$ and $\rho_2/\rho_0 = 4.314685$, so that the MBP itself is a low-*beta* slab. As the panels of Figure 4.3 show, in the static case at least, the choice of internal plasma-β in the system does not fundamentally change the types of supported solutions. In all three cases displayed, only a pair of trapped surface mode solutions were found, limited in their phase speed by the left-hand-side external sound and Alfvén speeds. The effect of changing the internal plasma-β parameter within this range of characteristic speeds resulted in changing the phase speeds/frequencies of the supported surface modes, along with the exact phase-speed-cutoff positions.

A much more dramatic difference appears if flows are introduced into the system. We presented numerical solutions to the dispersion relation of an externally non-magnetic asymmetric magnetic slab system, which had asymmetric flows in the external regions, in Section 2.4. For the sake of convenience and easy comparison, we repeat this dia-

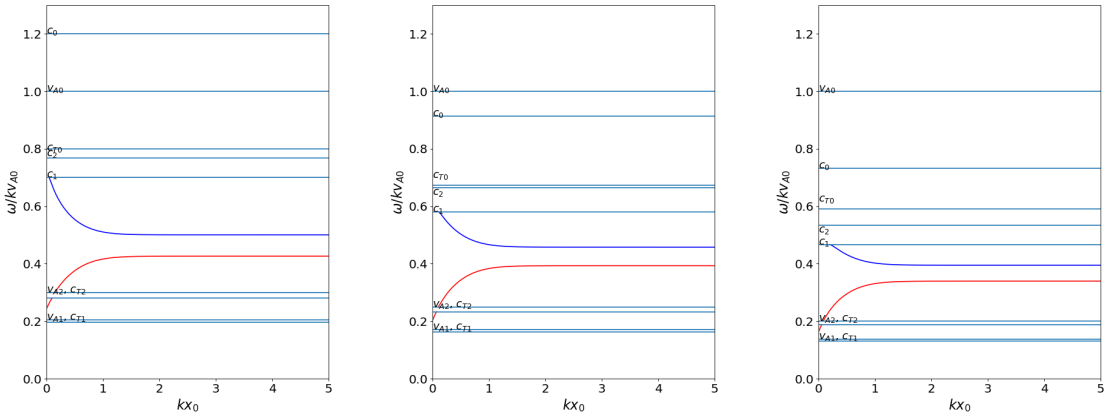

(a) (b) (c)

Figure 4.3: The phase speed of magneto-acoustic waves guided by an elongated MBP in a static, high-β asymmetric magnetic environment. Source: Zsámberger and Erdélyi (2021).

gram in Figure 4.4a, where the solutions were obtained using photospheric values for the background equilibrium parameters and a relatively weak pair of external flow speeds ($U_1 = -1.2$ km/s and $U_2 = 4.2$ km/s), within the range of estimated downflow speeds near small magnetic elements (1 km/s - 10 km/s) (Briand and Solanki, 1998; Socas-Navarro et al., 2004; Danilovic et al., 2010). This test model is an improvement upon the static application presented in the sense that it takes into account the existence of downflows of potentially different magnitudes within the intergranular lanes. Now, due to the bulk background flows introduced, instabilities can be present (indicated by the non-zero imaginary parts of solutions plotted in red). Furthermore, the phase speeds of all solutions are shifted backward by the downflows. Surface waves are now seen to propagate with phase speeds between $-c_{T0}$ and $c_2 + U_2$, and, as a new addition, body waves can also appear (see the a band between $-c_1 + U_1$ and $-c_{T0}$).

While this model already incorporates asymmetric downflows in the intergranular lanes, these environmental regions are now handled as completely non-magnetic, which may not necessarily be the case. Therefore, the expanded model described in Section 4.2 might provide a more generally applicable description of MBPs and their environment, by incorporating arbitrary asymmetric magnetic fields *and* flows both in the regions bounding the elongated slab.

We present a diagram of the phase speeds of modes supported by of magnetic slabs of various widths sandwiched between two environmental regions containing asymmetric magnetic fields and steady flows in Figure 4.4b. To obtain these solutions, we once again relied on characteristic speed information in the existing literature. As the sound speed in the photosphere is around 7 km/s (Hurlburt et al., 2002), we assumed $c_1 = 7$ km s^{-1} and $c_2 = 8$ km s^{-1}. Following Keys et al. (2013), we chose the internal sound speed as

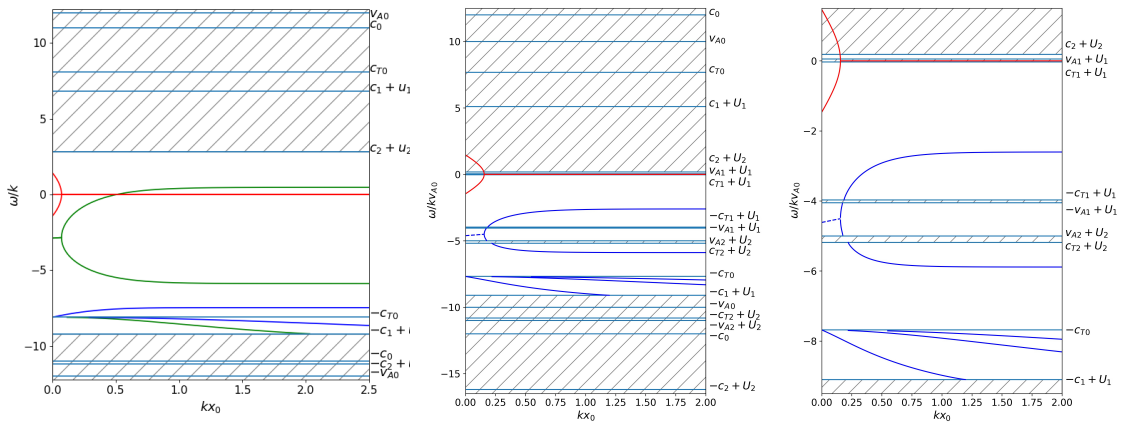

(a) (b)

Figure 4.4: (a) Dispersion diagram of an asymmetric magnetic slab system, where the environment contains asymmetric flows but not magnetic fields. Repeated from panel (b) of 2.2. (b) Solutions to the dispersion relation for an MBP and its asymmetric magnetic environment containing different downflows. The left-hand-side plot shows the full range of characteristic speeds, while the diagram on the right zooms in on the narrower region of interest at low phase speeds.

$c_0 = 12$ km s^{-1}, and the internal Alfvén speed as $v_{A0} = 10$ km s^{-1}. Since the magnetic field is significantly weaker outside an MBP than it is inside, we used external Alfvén speeds of $v_{A1} = 2.05$ km s^{-1} and $v_{A2} = 3$ km s^{-1}. We considered the equilibrium bulk flow speed inside the slab to be negligible ($U_0 = 0$ km s^{-1}), and set the other two to flow speeds within a range expected to be present as the downflows of intergranular lanes (see Briand and Solanki 1998; Socas-Navarro et al. 2004; Danilovic et al. 2010): $U_1 = -2$ km s^{-1} and $U_2 = -8$ km s^{-1}. For this choice of parameters, once again we can find both body modes and stable as well as unstable surface mode solutions. Their phase speeds are shifted compared to the previous two cases, both due to the presence of external magnetic fields and the different flow speeds. While in the static case, the characteristic speeds themselves delineate the cut-off frequencies of trapped solutions, in a steady slab, these cut-offs are shifted by the flow speeds in both the externally magnetic and non-magnetic models. However, in the externally magnetic system, there are additional forbidden regions between the Doppler-shifted Alfvén and tube speeds, in which the waves would become leaky.

Instabilities can only be found in thin slabs for the selected external flow speeds. While in Figure 4.4a, it is a very narrow range of the smallest slab width for which the speeds of the backward- and forward-propagating waves meet and the KHI sets in, in Figure 4.4b, we found instabilities up to somewhat larger slab widths (of $kx_0 \lesssim 0.25$). Only the modes subject to the Kelvin-Helmholtz instability possess a non-zero imaginary component, which corresponds to an amplitude growth factor (Barbulescu and Erdélyi, 2018). In

our hypothetical MBP, these are exclusively the surface modes ($-c_{T0} < v_{ph} < c_{T1} + U_1$), and only when they propagate in a thin slab. However, if the slab is made wider, then the oscillations can remain stable. Similarly to what we saw in Chapter 2, the instability can still exist for the relatively low, sub-Alfvénic external flow speeds we chose due to the asymmetry.

Our Figures 4.3 - 4.4b serve to demonstrate that even for a choice of similar equilibrium parameters, the inclusion or exclusion of magnetic fields and flows, as well as their asymmetry, in the environmental regions bounding the slab can make a significant difference in the types as well as phase speeds and stability of the waves that an MBP-like slab system can guide. A further interesting extension of this comparison could be based on the application of a multi-slab model such as the one described by Shukhobodskaia and Erdélyi (2018) or Allcock et al. (2019) to model not only the MBP and the intergranular lane segments that it is embedded between, but to also include information on the granular cells themselves separated by the region of the dark lane.

4.3. The General Case of a Magnetic Slab with Steady Flows

To complete the process of generalising three-layered Cartesian waveguide models of the solar atmosphere, we investigate the configuration in which asymmetric plasma parameters, flows and magnetic fields are found in all three of the plasma domains. Thus each domain contains uniform, compressible, inviscid plasma characterised by different density, ρ, pressure, p, and temperature, T values, permeated by a different vertical magnetic field, $\hat{\mathbf{B}} = B\hat{\mathbf{z}}$, and subjected to different steady flows in the vertical direction, $\hat{\mathbf{U}} = U\hat{\mathbf{z}}$, compared to any other region of plasma in the model. In summary,

$$N(x) = \begin{cases} N_1 & x < -x_0, \\ N_0 & -x_0 < x < x_0, \\ N_2 & x_0 < x, \end{cases} \tag{4.10}$$

where N_j now denotes any of the five physical scalar parameters listed above and $N_j =$ constant , for $j = 0, 1, 2$. An illustration of this slab system can be found in Figure 2.1.

Perturbations within all regions of the system are governed by the ideal steady MHD equations (see Equations 2.1 - 2.4). Similarly to the particular cases studied before, we linearise this set of PDEs and perform Fourier-analysis to find plane wave solutions that propagate along the slab (parallel to the flows and the magnetic fields). At the end of this lengthy mathematical process, the same type of ordinary differential equation is found to govern each domain:

$$\hat{v}_x'' - m_j^2 \hat{v}_x = 0, \tag{4.11}$$

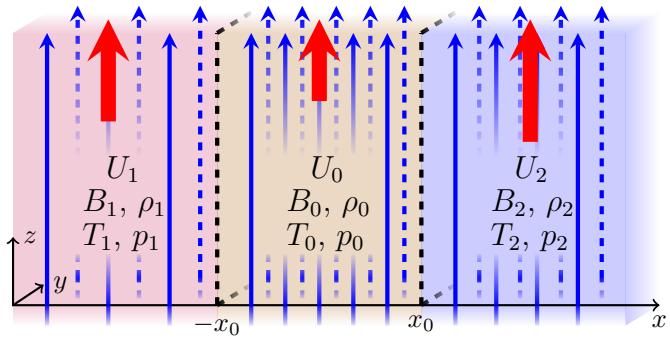

Figure 4.5: Illustration of the equilibrium configuration of a steady and magnetised slab embedded in a steady, magnetised, and asymmetric semi-infinite plasma environment. The figure has been adapted from Allcock et al. (2019).

where

$$m_j^2 = \frac{\left(k^2 v_{Aj}^2 - \Omega_j^2\right)\left(k^2 c_j^2 - \Omega_j^2\right)}{\left(v_{Aj}^2 + c_j^2\right)\left(k^2 c_{Tj}^2 - \Omega_j^2\right)}, \qquad \text{for } j = 0, 1, 2 \tag{4.12}$$

and the prime notation stands for differentiation with respect to the spatial coordinate x. Due to the presence of a steady background flow in every region, instead of the angular frequency, ω, it is exclusively the Doppler-shifted frequencies that appear in all the coefficients, defined as

$$\Omega_j = \omega - kU_j, \qquad \text{for } j = 0, 1, 2. \tag{4.13}$$

As before, we require that our solutions be evanescent far away from the slab, and we impose the continuity of the Lagrangian displacement and total pressure perturbation across both boundaries of the slab. The determinant of the matrix constructed from the coefficients in the resulting system of equations has to be zero in order to find a non-trivial solution:

$$\det \begin{pmatrix} \frac{C_1 - S_1}{\Omega_1} & \frac{-C_0}{\Omega_0} & \frac{S_0}{\Omega_0} & 0 \\ 0 & \frac{C_0}{\Omega_0} & \frac{S_0}{\Omega_0} & -\frac{C_2 - S_2}{\Omega_2} \\ \Lambda_1(C_1 - S_1) & \Lambda_0 S_0 & -\Lambda_0 C_0 & 0 \\ 0 & \Lambda_0 S_0 & \Lambda_0 C_0 & -\Lambda_2(S_2 - C_2) \end{pmatrix} = 0, \tag{4.14}$$

where

$$\Lambda_j = -\frac{i\rho_j}{\Omega_j m_j}(k^2 v_{Aj}^2 - \Omega_j^2), \qquad C_j = \cosh m_j x_0, \qquad S_j = \sinh m_j x_0 \tag{4.15}$$

for $j = 0, 1, 2$. Using these definitions, we derive the full dispersion relation for the gener-

alised steady slab as

$$\frac{m_0^2}{\rho_0^2(k^2v_{A0}^2-\Omega_0^2)^2}+\frac{m_1m_2}{\rho_1\rho_2(k^2v_{A1}^2-\Omega_1^2)(k^2v_{A2}^2-\Omega_2^2)} + \frac{1}{2}\frac{m_0}{(k^2v_{A0}^2-\Omega_0^2)}\left(\frac{m_1}{\rho_1^2(k^2v_{A1}^2-\Omega_1^2)}+\frac{m_2^2}{\rho_2^2(k^2v_{A2}^2-\Omega_2^2)}\right)(\tanh m_0x_0+\coth m_0x_0)=0. \tag{4.16}$$

Formally, this equation is analogous to Equation (1.31) governing the static asymmetric magnetic slab system. In this generalised configuration of a steady slab, however, the equations contain the Doppler-shifted frequencies instead of the "ordinary" angular frequency in every expression, including the modified m_j coefficients. For this generalised case, too, the dispersion relation is a single transcendental equation governing the behaviour of both quasi-sausage and quasi-kink modes. However, the approximation of weak asymmetry may be employed when the plasma, magnetic, and flow parameters in the two external regions are of the same magnitude, and therefore $\Omega_2\Lambda_2=\Omega_1\Lambda_1+\epsilon$, where ϵ is a small quantity. In this limit, a decoupled dispersion relation may be obtained in the following form:

$$(k^2v_{A0}^2-\Omega_0^2)\left[\frac{\rho_0}{\rho_1}\frac{m_1}{(k^2v_{A1}^2-\Omega_1^2)}+\frac{\rho_0}{\rho_2}\frac{m_2}{(k^2v_{A2}^2-\Omega_2^2)}\right]+2m_0\begin{pmatrix}\tanh\\ \coth\end{pmatrix}\{m_0x_0\}=0. \tag{4.17}$$

One must keep in mind that the dispersion relation can only be decoupled in the approximation of weak asymmetry, and not for any freely chosen degree of external asymmetries. In order to utilise this slab system for the widest possible range of applications, one should use the full dispersion relation to obtain exact quasi-kink and quasi-sausage mode solutions.

4.4. Conclusion

Finely structured, inhomogeneously distributed ubiquitous magnetic fields and bulk plasma motions of various spatial and time scales make the solar atmosphere a complex and extremely dynamic laboratory of plasma physics. In an attempt to better capture its numerous interesting features, in this Chapter, we further expanded the family of Cartesian waveguide models by incorporating equilibrium bulk flows into several regions of the asymmetric slab waveguides. After an introduction to the steady slab models in Section 4.1, we derived the dispersion relation for a magnetic slab in an asymmetric magnetic environment containing asymmetric steady flows. We performed both an analytical and a numerical investigation of solutions to the dispersion relation.

This was followed by a numerical study of the effects that incorporating or neglecting different sources of asymmetry has through the example of applying this model family to MBPs and their environment. Finally, we described the most general case of an asymmetric steady slab system consisting of three plasma layers in Section 4.3.

From our investigation of all these various steady slab models, we can conclude that an important effect of the presence of flows in any region of the model is that the angular frequencies are replaced by their Doppler-shifted counterparts for that region. The presence of even a single flow in the system visibly changes the cut-off frequencies limiting the propagation of the different eigenmodes. As noted above, further extending the model to include arbitrary flows, magnetic fields, and plasma parameters in every region of a multi-layered waveguide system offers further interesting possibilities of application in the solar atmosphere. This will grant us the opportunity to include parameters of granular regions in MBP models, as well as, in other areas of application, for example to capture the magnetic and plasma interactions within umbral cores separated by multiple light bridges in a sunspot.

Chapter 5.
On Instabilities in Dynamic Magnetic Slabs Driven by Kink Waves

Abstract

This Chapter provides a summary of initial results obtained in the course of studying symmetric magnetic slabs containing a triangular flow profile, which are under the effect of an antisymmetric (kink) oscillation. Based on hydrodynamic (Drazin, 2002) and only externally magnetic MHD-studies (Zaqarashvili et al., 2021) published in the literature, the current investigation incorporates magnetic fields in every region of the slab model. Using the limit of an incompressible plasma, the general dispersion relation is obtained for the model. Making certain further simplifying assumptions makes it possible to then express the frequencies of solutions and the conditions for their stability analytically. These results are amended with a collection of illustrative numerical solutions, which provide a first insight into a larger parametric study over a wider range of parameters. The contents of the Chapter serve as the core of a paper to be submitted shortly.

5.1. Chapter Introduction

As it has been noted in the previous Chapters, flows and jets occur on various scales and with a wide range of speeds all across the solar atmosphere. Therefore, these jet-like solar features, such as spicules, mottles, macrospicules, X-ray and UV-jets, are ideal candidates to study when trying to understand the fundamental physical processes that shape our Sun. The presence of strong enough flows in these features of its atmosphere can cause instabilities to set in, thus leading to energy dissipation, and contributing to the heating of the solar atmosphere.

These flows, along with the solar structures they permeate, may be subject to various instabilities, such as the Kelvin-Helmholtz instability discussed in the previous Chapters, which has been observed in many well-known structures within the solar atmosphere, such as prominences (Berger et al., 2010; Ryutova et al., 2010), CME flanks (Foullon et al., 2011, 2013; Ofman and Thompson, 2011), solar surges and jets (Zhelyazkov et al., 2015; Li et al., 2019). Several other types of instabilities have also been studied and observed in the

solar atmosphere, such as the Rayleigh-Taylor instability (Khomenko et al., 2014; Hillier, 2018), the resonant flow instability (Tirry et al., 1998; Taroyan and Erdélyi, 2002), or the dynamic kink instability, which might be responsible for the observed transverse motions of type II spicules, or even contribute to the destruction of these structures (Zaqarashvili, 2020).

Since the solar atmosphere is permeated by ubiquitous magnetic fields, the effect of adding magnetic fields into the purely hydrodynamic flow cases needs to be considered. Here, the orientation and topology of the magnetic field have special significance. A sufficiently strong magnetic field parallel to the axis of a flow can generally stabilise sub-Alfvénic flows (Chandrasekhar, 1961; Priest, 2014), while a transverse magnetic field seems to have no effect on the instabilities (Zaqarashvili, 2020). Since the solar magnetic fields are highly inhomogeneous and vary in strength, in some places, they might provide enough of a restoring force to stabilise flows in spicules, prominences, etc., while at other times, the instability may still occur and lead to turbulence and plasma heating.

In the current Chapter, specifically, the problem of the stability of kink-oscillating triangular jets is described and expanded with some further analytical and numerical detail. Section 5.3 provides a summary of the study of triangular jets subject to kink oscillations, both without and in the presence of magnetic fields in a slab system. As a new development, Section 5.4 proceeds to build upon this existing body of research and incorporate an additional internal magnetic field into the problem. The general dispersion relation for kink oscillations in the magnetised triangular jet is obtained and a comparison with previous studies is carried out. In Section 5.5, certain limiting cases (such as the thin-slab approximation and simple versions of the triangular profile) are described in further analytical detail, and, where these assumptions make it possible, solutions for the angular frequency and limits for the onset of instability are provided. Section 5.6 presents the results of a brief initial numerical investigation of the problem. Comparisons with the hydrodynamic case are carried out, and the influence of internal-to-external density and Alfvén speed ratios, as well as the steepness of the flow profile, on the solutions and instability limits are demonstrated. Finally, in Section 5.7, future plans to extend this exploratory study and potential applications are briefly described.

5.2. Spicules in the Solar Atmosphere

As mentioned before, the solar atmosphere is a highly complex and dynamic magnetised plasma environment, which shows elaborate structuring in various scales. This includes collimated, beam-like plasma ejections or jets, with sizes ranging from hundreds to hundreds of thousands of kilometres (Shen, 2021). A region especially rich in magnetic fine structuring and plasma flows directed along the inhomogeneously distributed field lines is the chromosphere, with its rapidly evolving jet-like elements (mottles, spicules, fibrils and dynamic fibrils, straws, rapid blue excursions) extending anywhere from the sub-arcsecond

range to several hundred arcseconds (Tsiropoula et al., 2012; Jess et al., 2015).

Chromospheric spicules are thin, elongated jet-like structures that appear as bright protrusions on the solar limb. (Tsiropoula et al., 2012). Out of the chromospheric fine structure elements, spicules have been known for the longest time, with Father Angelo Secchi of the Vatican Observatory first reporting their observation in 1877 (Secchi, 1877). The term "spicules" was then used by Roberts (Roberts, 1945), to describe 10 Mm long jets seen at the solar limb which seemed to dominate the chromosphere. Even the group behaviour shown by spicules can be traced back to early observations, with Lippincott (1957) stating that they formed so-called "porcupine" and "wheat" field patterns. Although recent high-resolution observations have broadened our knowledge about spicules and their on-disk counterparts, their exact description and modelling remains an ongoing challenge (Tsiropoula et al., 2012). For more detailed and comprehensive overviews of spicules and related structures, see e.g. Bray and Loughhead (1975); De Pontieu et al. (2007); Tsiropoula et al. (2012); Raouafi et al. (2016).

To understand the significance of spicules when it comes to the practical applications of the study of instabilities in the solar atmosphere, it must be noted that more recent observations relying on the Solar Optical Telescope aboard the Hinode satellite led to the division of spicules into two categories by De Pontieu et al. (2007). The "traditional" spicules fall into the "Type I" category, rising up from the solar limb and then falling back down. Typical flow velocities in spicules are 20-25 km/s. Their lifetimes are relatively longer ($3 - 7$ min) and they show longitudinal motions of the order of 20 km/s. "Type 2" spicules, on the other hand, are much shorter-lived features (with lifetimes of 50 – 100 s). They exhibit greater velocities (of the order of 100 km/s) and reach much higher into the atmosphere. Furthermore, although their density and temperature are similar to those of Type 1 spicules, they only show upwards motion before disappearing rapidly, which may be the case due to rapid heating. This heating might be happening due to ion-neutral collisions, the presence of the KHI, or some other instability process, such as the dynamic kink instability (De Pontieu et al., 2007; Tsiropoula et al., 2012; Zaqarashvili, 2020; Zaqarashvili et al., 2021). Therefore, studying instabilities under the physical conditions prevalent in the chromosphere, and in spicules, specifically, is an active area of research - which is also the motivation behind the following parts of the Chapter.

5.3. Triangular Jets in HD and MHD

In the previous Chapters, piece-wise constant flows in asymmetric slab configurations were investigated. Here, however, we focus on the effects of including a velocity profile in a kink-oscillating slab system, rather than on the consequences of background asymmetry. Of course, the two approaches can eventually be combined, but, based on our results so far, the full problem of transverse flow profiles in asymmetric magnetic slabs promises to be one with less analytical tractability, and a strong need for a numerical exploration over

wide parameter ranges.

A summary of some simple flows with linear transverse profiles in the purely hydrodynamic case was provided by Drazin (2002). Among these was a triangular jet (see Figure 5.1a), with its maximum velocity at the centre of the region linearly decreasing to zero. It was shown that this jet is stable to the effects of symmetric modes (also called varicose modes, corresponding to sausage modes described earlier), which are characterised by the symmetry of the streamlines about $x = 0$. However, the configuration can become unstable when long-wavelength antisymmetric (or sinuous) modes (corresponding to the kink modes) are present (Drazin, 2002).

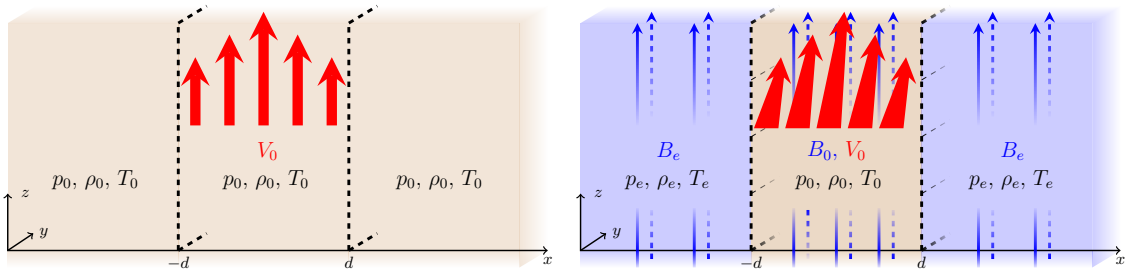

(a) (b)

Figure 5.1: (a)Illustration for the velocity profile of a triangular jet in the hydromagnetic case, based on Figure 8.5 of Drazin (2002). (b) Illustration of the problem of a triangular jet sandwiched between symmetric magnetic regions studied by Zaqarashvili et al. (2021), based on their Figure 2.

An extension of this problem was recently studied by Zaqarashvili et al. (2021), who incorporated magnetic fields into the model with the motivation to study the instabilities and lifetimes of solar spicules. He identified three main magnetic channels which may guide spicules: the upflow being contained in a magnetic flux tube, and the jet flowing between flux tubes of the same or the opposite polarity. He then modelled the case when a non-magnetic jet with a triangular profile flows between the two flux tubes, approximated by an incompressible slab-like structure of width $2d$. Figure 5.1b provides an illustration of this model.

While compressibility can in general affect the onset of instabilities, the basic properties of the instability were studied in the incompressible limit for these jets (Sen, 1964; Zaqarashvili et al., 2021). Then, with the background parameters listed above, the following dispersion relation was obtained for the jet under the effect of an antisymmetric kink

mode by Zaqarashvili et al. (2021):

$$\left(\frac{\tanh(kd)\,\rho_0}{\rho_e}+1\right)\omega^3+\left(\frac{\tanh(kd)\,(2\alpha-3)\,\rho_o}{\rho_e}+\frac{\tanh(kd)\,\alpha}{dk}-1\right)(\mathbf{k}\cdot\mathbf{V_0})\omega^2$$
$$+\left(\frac{\left(\left((-1+\alpha)\,(\alpha-3)-\frac{\alpha^2}{k^2d^2}\right)\tanh(kd)+\frac{\alpha^2}{kd}\right)\rho_0(\mathbf{k}\cdot\mathbf{V_0})^2}{\rho_e}-k_z^2v_{Ae}^2\right)\omega$$
$$+\frac{\left(\left(1-\alpha-\frac{\alpha^2}{k^2d^2}\right)\tanh(kd)+\frac{\alpha^2}{kd}\right)(-1+\alpha)\,\rho_0(\mathbf{k}\cdot\mathbf{V_0})^3}{\rho_e}$$
$$+\left(-\frac{\tanh(kd)\,\alpha}{dk}+1\right)v_{Ae}^2k_z^2(\mathbf{k}\cdot\mathbf{V_0})=0. \tag{5.1}$$

Zaqarashvili et al. (2021) also carried out a numerical investigation of this dispersion relation, finding both real (stable) and complex (unstable) solutions depending on the choice of parameters. It was established that when the magnetic field is negligible and $\alpha = 1$, the same long-wavelength kink instability is recovered that Drazin (2002) described in the hydrodynamic case. However, when magnetic fields are present, the kink instability occurs only in a certain interval of wavenumbers, the position of which depends on the chosen density ratio (ρ_0/ρ_e) and Alfvén Mach number ($M_A = V_0/v_{Ae}$, where V_0 is the maximum speed of the flow at the jet axis).

Zaqarashvili et al. (2021) explained these findings with the properties of the dynamic kink instability, which occurs when the Lorentz force generated by the surrounding magnetic field lines is not strong enough to stabilise the bent jet structure against the centripetal force. Furthermore, Zaqarashvili et al. (2021) also found that the angle of the jet with respect to the ambient magnetic field can lower the instability threshold, as only the flow-aligned component of the magnetic field can have a stabilising effect against the flow (Chandrasekhar, 1961). Finding unstable solutions and their growth rates corresponding to solar spicule parameters revealed that the growth time of the unstable modes predicted by this model can be comparable to the lifetimes of both type I (5-15 min) and type II (5-60 s) spicules, respectively, which suggests that this type of kink instability could destroy spicule structures over their observed life times (Zaqarashvili et al., 2021).

5.4. Magnetised Jets with Triangular Profiles

Further building on the model described above, this Section presents new results on kink instabilities of triangular jets modelled in a fully magnetic slab structure. This generalisation is motivated by the consideration that, although the solar magnetic field can be weaker outside concentrated magnetic flux tubes (or magnetised slabs in this approximation), it will not necessarily immediately drop to vanishing strength. This step of study makes the

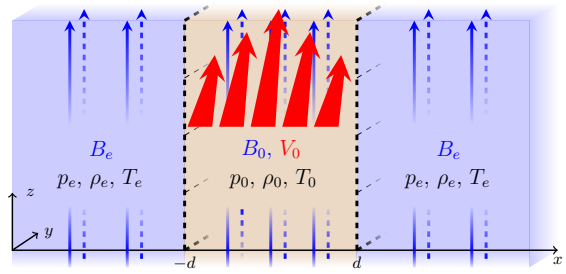

Figure 5.2: The equilibrium configuration for the magnetic slab system containing a jet with a triangular flow profile.

analytics more complicated, as also referenced in Zaqarashvili et al. (2021), but once a numerical study is completed based on the findings on wave dispersion here, it can serve as a basis of comparison against the non-magnetic case investigated by Zaqarashvili et al., and, in our hope, highlight how incorporating a magnetic field into the central region can shift instability limits.

For the sake of direct comparability, the new model kept as many of the characteristics of the one investigated by Zaqarashvili et al. (2021) as was possible. For clarity, the model is illustrated in Figure 5.2, and its background parameters can be described as follows:

$$\rho(x) = \begin{cases} \rho_e \\ \rho_0 \\ \rho_e \end{cases} \quad \mathbf{B}(x) = \begin{cases} (0,0,B_e) \\ (0,0,B_0) \\ (0,0,B_e) \end{cases} \quad \mathbf{V}(x) = \begin{cases} 0 & x < -d, \\ \mathbf{V}_0\left(1 - \alpha\frac{|x|}{d}\right) & |x| < d, \\ 0 & d < x. \end{cases} \tag{5.2}$$

This is, for now, a symmetric Cartesian model of a multi-layered waveguide. To proceed with the analysis, we suppose that it is filled with incompressible plasma, and it is under the effect of an antisymmetric (kink) oscillation. The interactions of the plasma and the magnetic fields permeating it are described by the ideal MHD equations (see Equations 2.1 - 2.4) expressed in their single fluid incompressible linearised form within each region of the model as:

$$\begin{aligned} \rho\left[\frac{\partial}{\partial t} + \mathbf{V}\cdot\nabla\right]\mathbf{u} + \rho\left(\mathbf{u}\cdot\nabla\right)\mathbf{V} &= -\nabla p_T + \frac{1}{4\pi}\left(\mathbf{B}\cdot\nabla\right)\mathbf{b}, \\ \left[\frac{\partial}{\partial t} + \mathbf{V}\cdot\nabla\right]\mathbf{b} &= \left(\mathbf{B}\cdot\nabla\right)\mathbf{u} + \left(\mathbf{B}\cdot\nabla\right)\mathbf{V}, \\ \nabla\cdot\mathbf{u} = 0, &\nabla\cdot\mathbf{b} = 0. \end{aligned} \tag{5.3}$$

Here, again, the unperturbed background parameters for densities, magnetic fields and flows are denoted with ρ, $\mathbf{B}$, and $\mathbf{V}$, respectively; while the small perturbations of the magnetic field, velocity, and total pressure are $\mathbf{b}$, $\mathbf{u}$, and p_T. Similarly to the model described by Zaqarashvili et al. (2021), the unperturbed magnetic field in each region is directed along the z axis and assumed to be homogeneous. Furthermore, we do not consider

the effect of gravity in the current extension of the model, either. The velocity of the jet is considered homogeneous in the y and z directions.

Next, we look for the normal modes of this system by assuming the form $\Phi = \Phi(x)\exp\{(i[k_y y + k_z z - \omega t])\}$. Then the expressions in Equation (5.3) can be transformed to give

$$\begin{aligned} \rho\left(\mathbf{k}\cdot\mathbf{V}-\omega\right)\left[\frac{\partial^2}{\partial x^2}-k^2\right]u_x &= \frac{k_z B_z}{4\pi}\left[\frac{\partial^2}{\partial x^2}-k^2\right]b_x, \\ \left(\mathbf{k}\cdot\mathbf{V}-\omega\right)b_x &= k_z B_z u_x, \end{aligned} \tag{5.4}$$

where $k = \left(k_y^2 + k_z^2\right)^{1/2}$ describes the wavenumber of the oscillations. At this point, we require that the speed of the waves does not become equal to the speed of the background flow or the Alfvén speed of a region ($\omega \neq \mathbf{k}\cdot\mathbf{V}$ and $\omega \neq k_z v_A$) to avoid resonances. Then, from Equation (5.4), the plasma motions in the slab system are governed by the following differential equation:

$$\left[\frac{\partial^2}{\partial x^2}-k^2\right]u_x = 0. \tag{5.5}$$

As before, we require that the solutions should be evanescent outside the slab, and inside, we prescribe the same form of (antisymmetric) solution utilised by Zaqarashvili et al. (2021):

$$u(x) = \begin{cases} \exp\left(-k[|x|]-d\right) & |x| > d, \\ B\frac{\cosh(kx)}{\cosh(kd)} + D\frac{\sinh(k|x|)}{\sinh(kd)} & |x| < d. \end{cases} \tag{5.6}$$

Next, these solutions must be matched across the slab boundaries, therefore they need to fulfil the continuity of the Lagrangian transverse velocity and of the total pressure at both interfaces. Additionally, the total pressure also needs to remain continuous at the slab centre. These conditions can be summed up as

$$\begin{aligned} \frac{u_x}{\left(\mathbf{k}\cdot\mathbf{V}-\omega\right)} &= \text{const.} \qquad \text{at } x = \pm d, \\ \rho\left[\left(\mathbf{k}\cdot\mathbf{V}-\omega\right) - \frac{k_z^2 v_A^2}{\left(\mathbf{k}\cdot\mathbf{V}-\omega\right)}\right]\frac{\partial u_x}{\partial x} & \\ -\rho\mathbf{k}\cdot\mathbf{V}'\left[1-\frac{k_z^2 v_A^2}{\left(\mathbf{k}\cdot\mathbf{V}-\omega\right)^2}\right]u_x &= \text{const.} \qquad \text{at } x = -d, 0, d. \end{aligned} \tag{5.7}$$

Substituting in the appropriate forms of the variables for each region and rearranging the

equations allows us to summarise these requirements in the following matrix form:

$$\begin{bmatrix} M_{11} & M_{12} & M_{13} \\ M_{21} & M_{22} & M_{23} \\ M_{31} & M_{32} & M_{33} \end{bmatrix} \begin{pmatrix} A \\ B \\ D \end{pmatrix} = \begin{pmatrix} 0 \\ 0 \\ 0 \end{pmatrix}, \tag{5.8}$$

where

$$\begin{aligned}
M_{11} &= (\mathbf{k}\cdot\mathbf{V_0})(1-\alpha)-\omega,\\
M_{12} &= \omega,\\
M_{13} &= \omega,\\
M_{21} &= \rho_e\left(k_z^2 v_{Ae}^2-\omega^2\right)\left((\mathbf{k}\cdot\mathbf{V_0})(1-\alpha)-\omega\right)^2,\\
M_{22} &= \left(\rho_0\omega\left[1-\alpha\right](\mathbf{k}\cdot\mathbf{V_0})-\omega\right)\left(\left[\{1-\alpha\}(\mathbf{k}\cdot\mathbf{V_0})-\omega\right]^2-k+z^2v_{A0}^2\right)\tanh(kd)\\
&\quad+\rho_0\frac{\alpha}{kd}\omega(\mathbf{k}\cdot\mathbf{V_0})\left(\left[\{1-\alpha\}(\mathbf{k}\cdot\mathbf{V_0})-\omega\right]^2-k+z^2v_{A0}^2\right),\\
M_{23} &= \left(\rho_0\omega\left[1-\alpha\right](\mathbf{k}\cdot\mathbf{V_0})-\omega\right)\left(\left[\{1-\alpha\}(\mathbf{k}\cdot\mathbf{V_0})-\omega\right]^2-k+z^2v_{A0}^2\right)\coth(kd)\\
&\quad+\rho_0\frac{\alpha}{kd}\omega(\mathbf{k}\cdot\mathbf{V_0})\left(\left[\{1-\alpha\}(\mathbf{k}\cdot\mathbf{V_0})-\omega\right]^2-k+z^2v_{A0}^2\right),\\
M_{31} &= 0,\\
M_{32} &= \frac{\alpha}{kd}(\mathbf{k}\cdot\mathbf{V_0})\tanh(kd),\\
M_{33} &= (\mathbf{k}\cdot\mathbf{V_0})-\omega.
\end{aligned} \tag{5.9}$$

Looking for non-trivial solutions, we require that the determinant of the matrix in Equation (5.8) should be zero. After simplifying with a factor of $\omega \neq 0$ and $(\alpha-1)\mathbf{k}\cdot\mathbf{V_0}-\omega\neq 0$, this condition yields the following dispersion relation:

$$d_4\omega^4+d_3\omega^3+d_2\omega^2+d_1\omega+d_0=0, \tag{5.10}$$

where

$$
\begin{aligned}
d_4 &= \left(\tanh(kd)\, R + 1\right), \\
d_3 &= \left(\alpha + \frac{\tanh(kd)\,\alpha}{kd} - 2 + \tanh(kd)\,(3\alpha - 4)\, R\right)(\mathbf{k}\cdot\mathbf{V_0}), \\
d_2 &= \left(\left(-1 + \frac{\tanh(kd)\,\alpha}{kd}\right)(\alpha - 1)\right. \\
&\quad \left. + \left(\tanh(kd)\left(3\,(\alpha-1)\,(\alpha-2) - \frac{\alpha^2}{d^2k^2}\right) + \frac{\alpha^2}{kd}\right) R\right)(\mathbf{k}\cdot\mathbf{V_0})^2 \\
&\quad - \tanh(kd)\, k_z^2 R v_{A0}^2 - k_z^2 v_{Ae}^2 \\
d_1 &= \left((\mathbf{k}\cdot\mathbf{V_0})^3\left(\tanh(kd)\left((\alpha-4)\,(\alpha-1) - \frac{2\alpha^2}{d^2k^2}\right) + \frac{2\alpha^2}{kd}\right) R\,(\alpha-1)\right. \\
&\quad \left. + (\mathbf{k}\cdot\mathbf{V_0})\left(\left(-\alpha - \frac{\tanh(kd)\,\alpha}{kd} + 2\right) k_z^2 v_{Ae}^2 + (-\alpha+2)\tanh(kd)\, k_z^2 v_{A0}^2 R\right)\right) \\
d_0 &= (\mathbf{k}\cdot\mathbf{V_0})^4\left(\left(1 - \alpha - \frac{\alpha^2}{d^2k^2}\right)\tanh(kd) + \frac{\alpha^2}{kd}\right) R\,(\alpha-1)^2 \\
&\quad + (\mathbf{k}\cdot\mathbf{V_0})^2\left(\left(\alpha - 1 - \frac{\alpha\,(\alpha-1)\tanh(kd)}{kd}\right) k_z^2 v_{Ae}^2\right. \\
&\quad \left. + \left(\left(\alpha - 1 + \frac{\alpha^2}{d^2k^2}\right)\tanh(kd) - \frac{\alpha^2}{kd}\right) k_z^2 v_{A0}^2 R\right),
\end{aligned}
\tag{5.11}
$$

and the density ratio is denoted by $R = \frac{\rho_0}{\rho_e}$.

This is a fairly complicated expression, however, it can be shown that the previous cases it has been built on can be recovered from this dispersion relation. Firstly, if the determinant from Equation 5.8 is evaluated at $v_{A0} = 0$, after appropriate factoring and simplifications, the expression can be reduced to the dispersion relation given for the non-magnetic jet by Zaqarashvili et al. (2021), also shown here in Equation (5.1). Second, if Equation (5.11) is evaluated at $\alpha = 0$, that is, in the case of a homogeneous magnetised jet enclosed in a symmetric magnetic slab system, the following relation is obtained:

$$
(\mathbf{k}\cdot\mathbf{V_0} - \omega)^2\left(R(k_z^2 v_{A0}^2 - (\omega - \mathbf{k}\cdot\mathbf{V_0})^2) + (k_z^2 v_{Ae}^2 - \omega^2)\coth(kd)\right) = 0. \tag{5.12}
$$

Since we have required for deriving the dispersion relation that $\mathbf{k}\cdot\mathbf{V_0} - \omega \neq 0$, it must be the second term that is set to zero. To further simplify the problem and check that our solutions are in accordance with previous literature, if now the flow is removed ($\mathbf{k}\cdot\mathbf{V_0} = 0$), that leads us back to the incompressible case of the dispersion relation for waves propa-

gating in a symmetric magnetic slab described by Edwin and Roberts (1982).

Further analytical progress might be made in certain limiting cases of this problem, such as weak external or internal fields, different values of the α parameter, propagation mainly along or in the transverse direction to the magnetic field. For the general case, however, a detailed numerical investigation should be made, which can explore the full dispersion relation and shed light on how the presence of magnetic fields all throughout the kink-oscillating slab system will influence the instability limit. So far, this has been beyond the scope of our study.

A future endeavour to further generalise this type of investigation of kink instabilities of triangular jets by placing the slab containing the jet in an asymmetric environment will inevitably encounter new analytical difficulties. One of these is the fact that the eigenmodes of asymmetric slab systems are also asymmetric by nature, and, as discussed in previous Chapters, they possess mixed mathematical and physical characteristics of sausage and kink-type oscillations. Careful consideration will have to be made when introducing an asymmetric quasi-kink mode oscillation into the system, and, if it is possible to follow the same methodology employed by Zaqarashvili et al. (2021), it is expected that the dispersion relation will take the form of a high-degree expression in ω, requiring extensive numerical investigations of the solutions. Furthermore, this study should be extended to asymmetric quasi-sausage modes as well, since they do possess an unperturbed layer somewhere within the slab, but the slab/jet axis itself is not left unperturbed by them. Therefore, the possibility that they might also give rise to instabilities remains an open question for now.

5.5. Thin-Slab Approximation

As a reminder, in the thin-slab limit, when $kd << 1$, the $\tanh(kd)$ function may be approximated by its argument, and the dispersion relation simplifies to more easily solvable equations. The general dispersion relation then becomes

$$\begin{aligned}
&(Rdk+1)\,\omega^4 + \left(2\alpha - 2 + kd\,(3\alpha-4)\,R\right)\omega^3 + \Big((\alpha-1)\left(\alpha - 1 + 3kd\,(\alpha\right. \\
&\left.-2)\,R\right)(\mathbf{k}\cdot\mathbf{V_0})^2 - kdk_z^2 R v_{A0}^2 - k_z^2 v_{Ae}^2\Big)\omega^2 + \Big((\mathbf{k}\cdot\mathbf{V_0})^3 kd\,(\alpha-4)\,(\alpha-1)^2\,R \\
&+(\mathbf{k}\cdot\mathbf{V_0})\left((-2\alpha+2)\,k_z^2 v_{Ae}^2 + (-\alpha+2)\,kdk_z^2 v_{A0}^2 R\right)\Big)\omega - \mathbf{k}\cdot\mathbf{V_0}^4 kd\,(\alpha-1)^3\,R \\
&+\mathbf{k}\cdot\mathbf{V_0}^2\left(-(\alpha-1)\,k_z^2 v_{Ae}^2 + kdk_z^2 R v_{A0}^2\right)(\alpha-1) = 0
\end{aligned} \tag{5.13}$$

This quartic equation can be further simplified in several limiting cases, in which some parameters of the internal flow profile fulfil further restrictions.

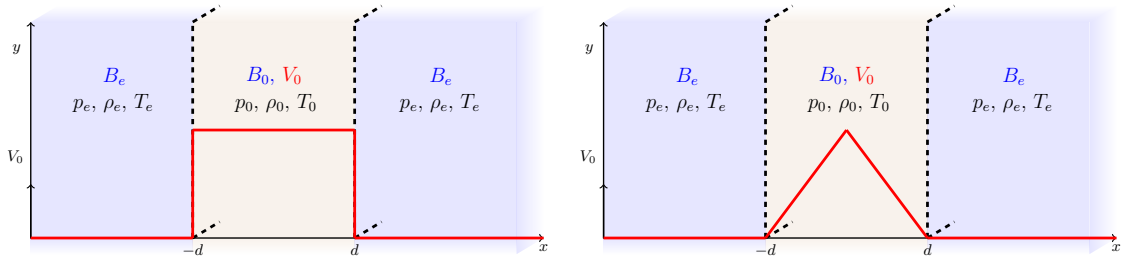

Figure 5.3: (a)Illustration of the slab system and the flow profile within for the case when the steepness parameter $\alpha = 0$. (b) Illustration of a slab system containing a triangular jet with steepness parameter $\alpha = 1$.

5.5.1. Homogeneous Jet ($\alpha = 0$)

Supposing that $\alpha = 0$, so that the flow speed across the slab is homogeneous, the dispersion relation (Equation 5.13) can be simplified to yield

$$\begin{aligned}&(Rdk+1)\,\omega^4 + (-4Rdk-2)\,\omega^3 + \Big(-(-6Rdk-1)\,(\mathbf{k}\cdot\mathbf{V_0})^2 - kdk_z^2Rv_{A0}^2 \\ &-k_z^2v_{Ae}^2\Big)\,\omega^2 + \Big(-4(\mathbf{k}\cdot\mathbf{V_0})^3kdR + (\mathbf{k}\cdot\mathbf{V_0})\left(2kdk_z^2Rv_{A0}^2 + 2k_z^2v_{Ae}^2\right)\Big)\,\omega \\ &+ (\mathbf{k}\cdot\mathbf{V_0})^4kdR - (\mathbf{k}\cdot\mathbf{V_0})^2\left(kdk_z^2Rv_{A0}^2 + k_z^2v_{Ae}^2\right) = 0. \end{aligned} \tag{5.14}$$

If we now suppose that the flow is parallel to the magnetic field, so that $\mathbf{k}\cdot\mathbf{V_0} = k_zV_z$, the quartic expression above further simplifies to

$$\begin{aligned}&(Rdk_z+1)\,\omega^4 + (-4Rdk_z-2)\,\omega^3 + \Big(-(-6Rdk_z-1)\,k_z^2V_z^2 - k_z^3dRv_{A0}^2 - k_z^2v_{Ae}^2\Big)\,\omega^2 \\ &+ \Big(-4k_z^4V_z^3dR + k_zV_z\left(2k_z^3dRv_{A0}^2 + 2k_z^2v_{Ae}^2\right)\Big)\,\omega \\ &+ k_z^5V_z^4dR - k_z^2V_z^2\left(k_z^3dRv_{A0}^2 + k_z^2v_{Ae}^2\right) = 0. \end{aligned} \tag{5.15}$$

If instead we suppose that the flow is incompressible, so that $\mathbf{k}\cdot\mathbf{V_0} = 0$, the dispersion relation simplifies to a quadratic equation:

$$(Rdk+1)\,\omega^2 + (-4Rdk-2)\,\omega - kdk_z^2Rv_{A0}^2 - k_z^2v_{Ae}^2 = 0. \tag{5.16}$$

Then the frequency solutions can be found as

$$\omega = \frac{1+2Rdk \pm \sqrt{R^2d^2k^2k_z^2v_{A0}^2 + kdk_z^2Rv_{A0}^2 + Rdkk_z^2v_{Ae}^2 + 4R^2d^2k^2 + k_z^2v_{Ae}^2 + 4Rdk + 1}}{Rdk+1}. \tag{5.17}$$

The frequency becomes imaginary (and thus the system becomes unstable) when the expression under the square root is negative, which provides us with a range of slab widths for which instability can occur:

$$kd_1 = \frac{-k_z^2 v_{A0}^2 - k_z^2 v_{Ae}^2 - 4 + \sqrt{k_z^4 v_{A0}^4 - 2k_z^4 v_{A0}^2 v_{Ae}^2 + k_z^4 v_{Ae}^4 + 4k_z^2 v_{A0}^2 - 8k_z^2 v_{Ae}^2}}{2\left(k_z^2 v_{A0}^2 + 4\right) R},$$
$$kd_2 = -\frac{k_z^2 v_{A0}^2 + k_z^2 v_{Ae}^2 + \sqrt{k_z^4 v_{A0}^4 - 2k_z^4 v_{A0}^2 v_{Ae}^2 + k_z^4 v_{Ae}^4 + 4k_z^2 v_{A0}^2 - 8k_z^2 v_{Ae}^2} + 4}{2\left(k_z^2 v_{A0}^2 + 4\right) R}, \quad (5.18)$$

and $kd_2 < kd < kd_1$.

5.5.2. Triangular Jet ($\alpha = 1$)

Supposing that $\alpha = 1$, so that the flow speed at the slab boundaries reaches zero, Equation (5.13) can be simplified to yield

$$\left(Rdk + 1\right)\omega^3 - Rdk\omega^2 + \left(-kdk_z^2 Rv_{A0}^2 - k_z^2 v_{Ae}^2\right)\omega + \mathbf{k}\cdot\mathbf{V_0} kdk_z^2 Rv_{A0}^2 = 0. \quad (5.19)$$

If we further suppose that the flow is parallel to the magnetic field, so that $\mathbf{k}\cdot\mathbf{V_0} = k_z V_z$, this further simplifies to a cubic equation:

$$\left(Rdk_z + 1\right)\omega^3 - Rdk_z\omega^2 + \left(-k_z^3 dRv_{A0}^2 - k_z^2 v_{Ae}^2\right)\omega + V_z k_z^4 dRv_{A0}^2 = 0. \quad (5.20)$$

Simpler analytical solutions can be obtained if instead we suppose that the flow is incompressible, so that $\mathbf{k}\cdot\mathbf{V_0} = 0$, we get a quadratic equation:

$$\left(Rdk + 1\right)\omega^2 - Rdk\omega - kdk_z^2 Rv_{A0}^2 - k_z^2 v_{Ae}^2 = 0. \quad (5.21)$$

From this, we can express the range of slab widths for which the system becomes unstable, namely, when $kd_2 < kd < kd_1$:

$$kd_1 = \frac{2\left(-k_z v_{A0}^2 - k_z v_{Ae}^2 + \sqrt{k_z^2 v_{A0}^4 - 2k_z^2 v_{A0}^2 v_{Ae}^2 + k_z^2 v_{Ae}^4 - v_{Ae}^2}\right) k_z}{\left(4k_z^2 v_{A0}^2 + 1\right) R},$$
$$kd_2 = -\frac{2\left(k_z v_{A0}^2 + k_z v_{Ae}^2 + \sqrt{k_z^2 v_{A0}^4 - 2k_z^2 v_{A0}^2 v_{Ae}^2 + k_z^2 v_{Ae}^4 - v_{Ae}^2}\right) k_z}{\left(4k_z^2 v_{A0}^2 + 1\right) R}. \quad (5.22)$$

A similar set of instability conditions can be found for the internal Alfvén speed as

$$v_{A0,1} = \frac{k_z v_{A0}^2 + \sqrt{k_z^2 v_{A0}^4 - k_z^2 v_{Ae}^4 + v_{Ae}^2}}{k_z},$$
$$v_{A0,2} = \frac{k_z v_{A0}^2 - \sqrt{k_z^2 v_{A0}^4 - k_z^2 v_{Ae}^4 + v_{Ae}^2}}{k_z}, \tag{5.23}$$

where $v_{A0,2} < v_{A0} < v_{A0,1}$.

5.6. Initial Numerical Results

In this Section, we present a few numerical solutions to the full dispersion relation (Equation 5.11) which were obtained using the Newton-Rhapson method implemented in a Python algorithm further developed from the one utilised in Barbulescu and Erdélyi (2018).

For this initial investigation, we prepared numerical solutions only for the case of vertical parallel propagation ($k_y V_{0y} = 0$) and began an exploration of how the key parameters of the slab system: the density ratio, $R = \rho_0/\rho_e$, the Alfvén speed ratio, v_{A0}/v_{Ae}, the steepness of the flow profile, α, and the flow speed in the z-direction, V_{0z}, influence the frequencies of the solutions as well as the instability limits.

First of all, in order to compare our results to similar problems already studied in the literature (Drazin, 2002; Zaqarashvili et al., 2021), in Figure 7 of the Appendix, we prepared the solutions to the simplified form of the dispersion relation (Equation 5.2) for the fully hydrodynamic case, where no external or internal magnetic fields are present. Without the stabilising effects of the magnetic field, all homogeneous jets ($\alpha = 0$) proved to be unstable regardless of slab width, while the instability of triangular jets ($\alpha = 1$) showed the same dependence on slab width as it did in the results of Zaqarashvili et al. (2021).

Returning to the magnetic problem, Figure 5.4 displays the solutions in a magnetic slab system under the effect of a kink oscillation. Figure 5.4a shows the case when the central region contains a homogeneous flow ($\alpha = 0$) moving through a medium much less dense than its environment. As it can easily be seen from the figure, instability occurs for a range of small values of the dimensionless slab width ($kd = k_z d$ due to the condition of parallel propagation we imposed). For wider slabs (approximately $k_z d > 0.5$), the system remains stable for the selected background parameters. In contrast, in 5.4b, we display the frequencies of solutions in the same slab system now containing a triangular flow ($\alpha = 1$). In this case, the unstable region encompasses a larger range of dimensionless slab widths, and only wide slabs with $k_z d > 2$ remain stable.

Keeping the requirement of parallel propagation and the triangular profile with a steepness of $\alpha = 1$, next we explored how changing the density and magnetic field ratios affects the instability limit. Figure 5.5a demonstrates that in a jet that is somewhat denser but

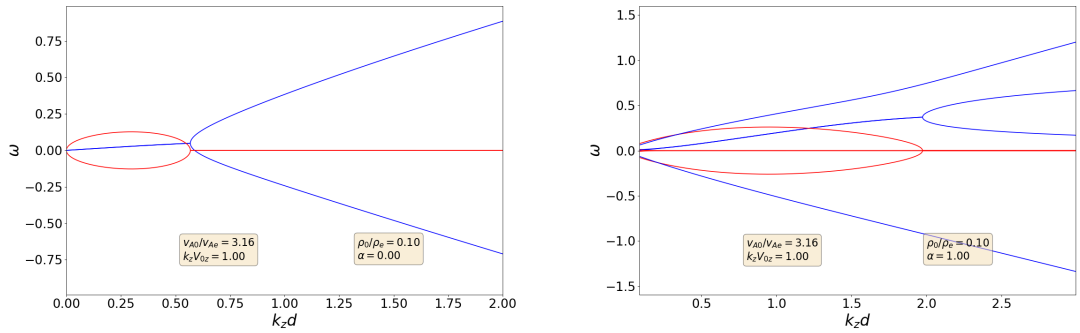

(a) (b)

Figure 5.4: The frequencies of the solutions to the dispersion relation of a magnetic slab embedded in a magnetic environment, where the slab contains a background flow and is subject to the kink oscillation, and the waves propagate parallel to the slab boundaries, in the vertical direction ($k_y V_{0y} = 0$).

still rarefied, permeated by a relatively weaker magnetic field compared to the one in Figure 5.4b, there is a small shift of the stable region towards narrower slabs, with the instability present only up to a slab width of around $k_z d = 1.9$. In Figure 5.5b, we get similar results to panel (a) by studying a dense but weakly magnetised jet, demonstrating that both the relative densities and magnetic field strengths within the slab and in its environment play a crucial role in allowing or preventing the onset of instability.

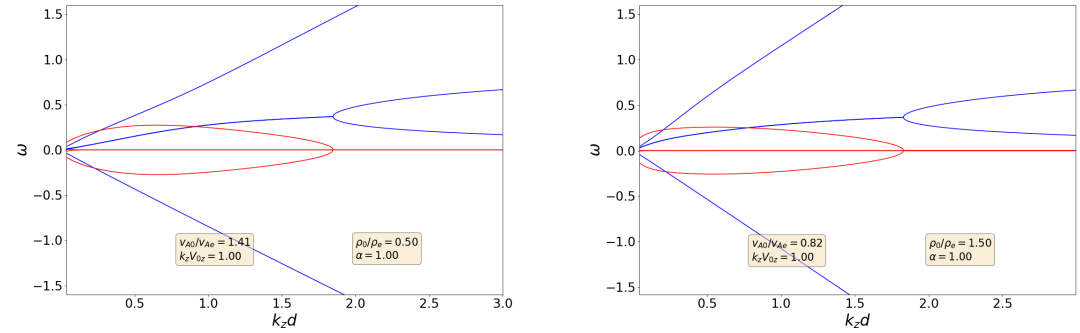

(a) (b)

Figure 5.5: The frequencies of the solutions to the dispersion relation of a magnetic slab embedded in a magnetic environment, where the slab contains a triangular background flow ($\alpha = 1$) and is subject to the kink oscillation, and the waves propagate parallel to the slab boundaries, in the vertical direction ($k_y V_{0y} = 0$).

Here, we have only presented a few examples of the solutions to this problem, which incorporates a wealth of changeable background parameters to explore. Future work will have to extend this numerical study, including, but not limited to the investigation of how

the solutions and instability limits depend on the relative strength of the flow (the Alfvén Mach number), which will bring with it the possibility of making further comparisons with the internally non-magnetic problem described by Zaqarashvili et al. (2021).

5.7. Conclusion

In this Chapter, we presented some early results on the stability of symmetric slab systems containing flows with different (homogeneous or triangular) profiles while they are guiding a kink oscillation. Building on the hydrodynamic (Drazin, 2002) and partially magnetic (Zaqarashvili et al., 2021) cases studied in the literature, here, the model was expanded with an internal magnetic field. The presence of such a field is also a possibility mentioned by Zaqarashvili et al. (2021) as one of the configurations that can give rise to solar jets. The slab description serves as a simple approximation of the quiet Sun magnetic field distribution, which is concentrated in thin regions at the photospheric level (which then proceed to widen in the higher layers of the atmosphere). Plasma flows corresponding to spicules may occur inside such magnetic concentrations (flux tubes or slabs), or between two neighbouring concentrations. Representing the system with three plasma regions, each of which are permeated by magnetic fields, allows for the presence of a weaker background field even between the strong concentrations, possibly widening the applicability of such a model, while keeping the previously studied configuration with a negligible background field as a special case.

The first results from the study of the fully magnetised, symmetric configuration presented here show that the equation governing the dispersion and stability of kink oscillations in triangular jets is, in the most general case, a transcendental equation containing the angular frequency of the modes up to the fourth power. Investigating the case when the slab is thin can reduce this to an algebraic quartic equation, which can then be studied in further limiting cases for analytical tractability and ease of understanding. In Section 5.5, we described the two extreme cases of a homogeneous jet (with a steepness of $\alpha = 0$) and a triangular flow profile which reaches zero flow speed at the slab boundaries ($\alpha = 1$). These approximations made it possible to find slab width or Alfvén speed values that determine the boundaries of the stable and unstable regions of the parameter space.

In Section 5.6, we complemented the first analytical insights with a handful of examples of numerical solutions to the dispersion relation. We made comparisons to the hydrodynamic cases in order to compare our results to previous studies and test their validity. Finally, we prepared solutions to the dispersion relation in the fully magnetised case, assuming that the flow and the propagation are parallel to the magnetic field ($k_y V_{0y} = 0$). These results led us to conclude that (at least for the parameter range examined), thin slabs with triangular jets are generally subject to instability, while wide slabs can remain stable. The critical dimensionless slab width for the onset of the instability is determined by an interaction between different background parameters, such as the density and Alfvén

speed ratios between the slab and its environment.

Overall, jets with triangular profiles provide a rich problem to be studied, and the illustrative cases presented above clearly confirm that the frequencies of the solutions and the instability limits are determined by several different parameters of the slab system. In the future, the initial numerical results presented here will be complemented with a study of instability limits encompassing a wider range of key background parameters. The continued study of this problem will have to include the detailed effects of the differences between the slab and its environment in density and Alfvén speed, as well as extend to different intermediate flow profiles ($0 < \alpha < 1$) and slanted directions of propagation ($k_y V_{0y} \neq 0$). In an effort to represent the lack of perfect environmental symmetry that may prevail in the solar atmosphere, a new analytical challenge could be to incorporate asymmetric (magnetic or non-magnetic) environments into this model, too.

A further extension to a wide range of Alfvén Mach numbers will allow us to make direct comparisons to the results of Zaqarashvili et al. (2021) obtained for the internally non-magnetic case and examine the magnitudes of magnetic fields needed to stabilise the fully magnetic system against slanted flows. Additionally, the imaginary parts of the complex frequencies in the unstable parameter ranges provide information about the growth time of the instability, which, for the internally non-magnetic case was found to be comparable to the lifetimes of spicules when substituting spicule-like density, magnetic field and flow parameters into the equations (Zaqarashvili et al., 2021). Tuning the extended, magnetised model to represent spicular regions and environments will further speak to the applicability of this simple representation of solar jets and the role that the kink instability may play in their behaviour and evolution.

Chapter 6.
Conclusion and Outlook

6.1. Overview of the Thesis

This Thesis summarises a series of investigations into the propagation and dispersion properties of magnetosonic waves in a collection of steady asymmetric magnetic slab configurations. Such waveguide models, utilising the complexity stemming from the various sources of asymmetry introduced, as well as the analytical tractability stemming from the Cartesian geometry, can serve as a versatile first approximation for investigating a number of solar atmospheric waveguides. Establishing a theoretical framework for slab-like solar features and then building on this to develop tools for solar magneto-seismology then allows us to utilise our theoretical understanding of wave dispersion as well as high-resolution observations to determine unknown physical parameters of solar atmospheric waveguides.

First, Chapter 1 summarised the fundamentals of the main topics recurring throughout this extended study of asymmetric solar jets and waveguides, such as the structure of our Sun, recent developments in solar atmospheric seismology, the magnetohydrodynamic description of magnetised plasmas, MHD waves first in a uniform medium, and then in a structured atmosphere. Finally, we described wave propagation in symmetric and asymmetric slab models of the solar atmosphere, and we provided a description of the asymmetric eigenmodes which would recur throughout the study of steady slab systems in later Chapters.

Next, in Chapter 2 we focused on waves propagating in an asymmetric steady slab system. After a summary of previous steady slab models, we proceeded to build new Cartesian waveguides containing bulk background flows upon their foundations. After deriving the dispersion relation for MHD waves in a static magnetic slab embedded in an asymmetric, non-magnetic environment containing asymmetric flows, we conducted an analytical as well as a numerical investigation of the effects of both sources of asymmetry (density and flows). We also described the consequences of the presence of asymmetric flows on the Kelvin-Helmholtz instability of the waveguide.

Chapter 3 was devoted to the study of MHD waves guided by a magnetic slab enclosed an asymmetric magnetic environment, in which the slab itself is under the effect of a bulk background flow. This served to provide a further extension to the scope and potential solar applications of asymmetric slab models. We derived the general dispersion relation

governing the propagation of MHD waves in this case, and we carried out a detailed analytical as well as numerical investigation of its solutions, including a study of the critical flow speed for the onset of the Kelvin-Helmholtz instability.

Next, in Chapter 4, we incorporated both external asymmetric magnetic fields and flows into the steady slab model again. We derived the full and decoupled dispersion relations of this system, and we looked at the high-β approximation in further analytical detail. This was followed by a study of applying various asymmetric magnetic slab systems to model magnetic bright points and their environment in the solar photosphere. To round out the expansion of asymmetric slab models, we proceeded to derive the dispersion relation for the most general case of an asymmetric, steady magnetic slab waveguide comprised of three layers.

Finally, in Chapter 5, we gave a summary of initial results on symmetric magnetic slabs under the effect of a triangular flow and an antisymmetric (kink) oscillation. We expanded the pre-existing hydrodynamic and internally non-magnetic studies by including magnetic fields in every region of the slab model. We obtained the general dispersion relation in an incompressible plasma filling this system, along with several analytical approximations in limiting cases of slab and flow parameters. We complemented these results by numerical solutions in illustrative HD and MHD cases, allowing a first insight into a larger parametric study to understand the behaviour of kink-oscillating slab systems permeated by various flow profiles.

6.2. Evaluation of Scope and Limitations

We have presented several, asymmetric and symmetric magnetic slab models applicable to different structures within the solar atmosphere and studied their eigenmodes as well as instabilities. It must be noted, however, that depending on the exact solar structure under investigation, we may want to use either flux tube or slab model. Furthermore, introducing additional elements into these models may in some cases also be worthwhile. These extensions may include non-linear effects, ignoring or incorporating dissipation, or choosing to set up either discontinuities or smooth gradients within the equilibrium configuration. These choices may sacrifice some of the simplicity of analytics, in order to better capture the physical characteristics of solar atmospheric phenomena.

The family of magnetic slab models (into which the configurations presented in this study can be grouped) takes the avenue of preserving simplicity in the interactions between the plasma and the magnetic fields, as well as in choosing the model geometry. Their method of introducing complexity into the distribution of plasma parameters within the model (compared to their classical, symmetric predecessors) is to include asymmetric environmental regions, extending the allowed parameter differences to from plasma parameters through magnetic field strengths to bulk background flows.

This is in line with several other recent studies, some of which we have described

in some detail in our Introduction. Figure 6.1 contains a collection of new results from the past few years in the investigation of MHD wave propagation and instabilities in asymmetric Cartesian waveguide models, as well as some suggestions as to the application of these models in solar and magnetospheric physics. This figure, of course, serves only as an illustrative collection of asymmetric slab models and their applications. Further details and full resolution images are available in the publications relevant to each specific model referenced below. The applications suggested here are not exclusive to any of these models, but they can each be viewed as an example of the corresponding models capturing a characteristic of a certain feature of the solar atmosphere (or even our own planet's magnetosphere).

In order of appearance, line (a) in Figure 6.1 shows the theoretical model of a static asymmetric slab system, where the central magnetised region is embedded in-between two non-magnetic asymmetric external regions. This was the configuration studied by Allcock and Erdélyi (2017), and Allcock and Erdélyi (2018) as well as Allcock et al. (2019) carried out a solar magneto-seismologic investigation using this model applied to fibrils of the solar chromosphere. This application immediately returns us to the issue of making a choice between flux tube and slab models. Namely, the same observations were first analysed as examples of oscillating flux tubes showing a superposition of sausage and kink modes (Morton et al., 2013). On one hand, considering the fibrils to be flux tubes of finite radial extent is a logical approach to take. On the other hand, a slab model might be able to capture any asymmetries in the fibril's environment in a mathematically and computationally more economical way and provide an alternate explanation for the observed wave properties.

Next, Figure 6.1(b) shows a similar asymmetric slab system, however, one which is closed in the z-direction, in order to facilitate the study of standing waves. A prime candidate for applying such a model is a prominence, that is, a thread of cooler, denser plasma embedded in-between regions where the plasma is under hot coronal conditions (Oxley et al., 2020a). The model was expanded in a different direction (remaining infinite in the z-direction) by dividing up the entire plasma volume into more segments around the magnetic slab (see Figure 6.1(c)). A detailed analytical description of this can be found in Shukhobodskaia and Erdélyi (2018), along with a suggested application to magnetic bright points and their surrounding intergranular lanes and granular cells.

A next step in studying the effects of asymmetries on magnetic slab systems and the waves they are able to guide was incorporating asymmetric external magnetic fields into the model. Figure 6.1(d) illustrates this configuration, which, along with its corresponding SMS tools, was investigated in a series of studies by Zsámberger et al. (2018); Zsámberger and Erdélyi (2020, 2021, 2022a). Among the several investigated possibilities of applications was that of coronal plumes or boundary regions of coronal holes and the quiet solar atmosphere, all of which can be subject to different magnetic fields and plasma parameters. When it comes to the study of standing waves, light bridges (light walls) separating

sunspots into two umbral cores provide a prominent opportunity to employ tools of SMS described in Oxley et al. (2020b) (illustrated in Figure 6.1(e). Lastly, propagating waves may also be studied in a slab system comprised of infinitely many magnetised plasma regions, all of which can even be characterised by different pressure, temperature, density and magnetic parameters (see Allcock et al. (2019)). Such a configuration, containing an arbitrary number of magnetised plasma domains, can also be tailored to applications to light bridges, as it can often happen that a big sunspot is divided up into not one but several umbral cores by more than one bridge (see Figure 6.1(f)).

At this point, we conclude the collection of static multi-layered asymmetric Cartesian waveguides and move into the territory of steady slab models. The first example of these configurations in Figure 6.1(g) is that of a magnetic slab containing a steady flow, enclosed in an asymmetric non-magnetic environment studied by Barbulescu and Erdélyi (2018), along with its application to CME flank regions. Incorporating multiple, asymmetric flows into this configuration instead, like we have done in Chapter 2 focuses on a different aspect of asymmetry, and, as Figure 6.1(h) illustrates, it allows us to look at applications such as the fibrillar structure in the penumbrae of sunspots, which is closely connected to the Evershed-flow (Tsiropoula, 2000; Borrero and Ichimoto, 2011).

Incorporating asymmetric external magnetic fields and keeping a steady flow inside the slab, like we explained in Chapter 3 and we show in Figure 6.1(i), we can offer a simple model of solar jets enclosed within a complex magnetic environment. A slab containing a homogeneous flow is also a limiting case of the kink-oscillating model we looked at in Chapter 5, which can be used to study instabilities in solar spicules.

Next, in Figure 6.1(j), we present the first model discussed in Chapter 4, one of a magnetic slab embedded in an asymmetric magnetic environment, where the environmental regions are also subject to background flows of different speeds. We demonstrate in Chapter 4.2.3 how this configuration can be used to model a magnetic bright point and its asymmetric intergranular environment, along with an explanation of what additional physical effects and conditions such a model captures compared with previous MBP-applications of slab geometries (such as the models presented in lines (d) and (h) of Figure 6.1).

Finally, the most general three-piece Cartesian slab model in this family is presented in Figure 6.1(k), where the slab and its environment are all subject to different equilibrium plasma, magnetic and flow parameters (see also Chapter 4). Such a generalisation of asymmetric slab models can offer another possibility to study penumbral waves, or, beyond the solar atmosphere, the triad of the Earth's magnetopause, magnetosheath, and bow shock region (Turkakin et al., 2013).

As this summary of the slab family also shows, a major advantage of slab models is their versatility of application (see e.g. Zsámberger and Erdélyi (2021) for a list of solar atmospheric configurations approximated as asymmetric magnetic slabs). However, there are also shortcomings tied to all infinite flux tube and slab models, whether they are symmetric (Edwin and Roberts (1982); Edwin and Roberts (1983)) or asymmetric (Zsámberger et al.

(2018); Barbulescu and Erdélyi (2018)). Namely, our Sun, and therefore its atmospheric structures, are all finite - as opposed to the infinite extent of the aforementioned models in multiple directions. This issue is partially resolved by "closing" the slab in one direction (Joarder and Roberts (1992);Oxley et al. (2020a); Oxley et al. (2020b)), which also allows us to focus on the study of standing waves.

Although many such improvements can be made to both flux tube and magnetic slab models, the choice between them eventually comes down to the influence of both the geometry of the solar feature under study, the information available, and the aim of the specific research project carried out. Some solar atmospheric features may be assumed to have a mostly cylindrical shape, but if there is only cross-sectional information available on them, or they exist wedged between strongly asymmetric areas of the solar atmosphere, a slab model sufficiently tailored to the actual research goal may deserve some consideration (see eg. the multiple studies carried out on observations of chromospheric fibrils (Morton et al., 2013; Allcock et al., 2019)). There are also elements of the rich structuring in our Sun's atmosphere that may assume a variety of shapes. For example, MBPs range from circular through elongated to highly irregularly shaped, and the forest of spicules might include both circular jet- and flat sheet-like structures. In general, if an atmospheric feature is sufficiently flat and elongated in at least one direction, a slab model can serve as a mathematically and computationally easy-to-use first approximation of said structure (see e.g. the cases of CME flanks, light bridges, or large-scale magnetospheric or solar atmospheric structuring).

There is a further caveat here, namely, that depending on the scales of solar atmospheric features serving as applications of slab models, it may also need to be examined whether gravitational stratification can be neglected, calling for the inclusion of a continuous change rather than a sharp jump in our models. These, in turn, can provide numerous opportunities to transform wave energy through processes such as resonant absorption or phase mixing (Priest (2014); Erdélyi and Nelson (2016)), and explain local contributions to the heating of the solar chromosphere and corona.

Furthermore, the complex problem of instabilities in a slab or flux tube may be approached from various directions, each of them focusing on a different consequence of the presence of flows in the system. With the work summarised in Chapters 2-4, we concentrated on one specific aspect of the problem, namely, the consequence of the presence of various sources of asymmetry in a steady magnetic slab system. We built up the generalised asymmetric model by exploring extensions of the steady slab model step by step (e.g. the externally non-magnetic slab system containing an external flow asymmetry in Chapter 2, and a jet-like slab model containing no external flows but placed in an asymmetric environment permeated by different magnetic fields in Chapter 3). This enabled us to cultivate a growing understanding of the consequences of each source of asymmetry compared to the classical symmetric slab models of Edwin and Roberts (1982) and Nakariakov and Roberts (1995).

A different type of extension of the slab models was provided by Chapter 5, building on the work of Zaqarashvili et al. (2021) and analysing the stability of triangular solar jets in slab geometries subject to a kink oscillation. This second line of investigation ties into the broader scope of another kind of approach to generalising slab models: introducing non-uniformities in (some or all of) the background parameters. As a different example from this heterogeneous group of studies, Tirry et al. (1998) expanded a single interface into a transitional region in the cold plasma approximation, in order to study the threshold for the onset of the Kelvin-Helmholtz instability, negative energy waves, and resonant absorption in a non-uniform system. Yet another approach is investigating the effects of different velocity profiles on the KHI-threshold, which has been carried out in both Cartesian and cylindrical geometries (see e.g. Michalke (1964), Blumen (1970), Ray (1982), Wu and Wang (1991)).

Beyond the piece-wise uniform nature of our models in Chapters 2 - 4, a further limiting assumption we made was that of purely parallel propagation, i.e. the choice of $k_y = 0$ and $v_y = 0$. This simplified the analytical work and helped us build solid foundations for understanding the rich problem of MHD waves in steady slabs. A future extension of this study to $k_y \neq 0$ (i.e., non-parallel propagation to the magnetic field but still parallel to the magnetic iso-surfaces) could allow us to investigate not only purely magnetosonic waves propagating along the slab, but also waves with mixed properties. This extended study could also account for further physical effects which influence the stability of the slab system, similarly e.g. to Andries et al. (2009), who studied the environment of coronal plumes by including a non-uniform transitional layer in a slab and a flux tube model (while allowing for the $k_y \neq 0$ case). There, it was found that the resonant flow instability can occur at a lower velocity threshold than the KHI, which is hugely important in determining whether a model with a certain parameter set will be stable or not.

Overall, it must be said that in future studies, several types of extensions can and should be added to the family of slab and jet models that we explored. However, proposing a near-exact theory of every solar atmospheric structure is a gargantuan task, and one which may only be achieved by carrying out thorough studies of its several building blocks. Exploring the family of asymmetric slab models, or, in the case of Chapter 5, symmetric triangular jets, helps us capture additional physical effects that had not been studied before in detail, and provide new contributions to our ever-expanding understanding of waves and instabilities in the solar atmosphere. We can find several possibilities of applications for all of these in the various features of our star, allowing us to gain valuable information as long as we keep both the strengths and limitations of these models in mind.

6.3. Future Aims

As described above, the collection of Cartesian multi-layered waveguide models may be expanded in numerous ways. We looked into the details of one of these possible directions

of generalisation through generalising the models of steady asymmetric slabs.

On the one hand, the wide variety of equilibrium parameters (background characteristic speeds and flows) that may be present in any given slab-like waveguide provides a very rich problem to investigate. In the static case, Zsámberger and Erdélyi (2021) provided a description of several solar waveguides which may be modeled as static asymmetric slabs, as well as providing analytical and numerical solutions for all of the different characteristic speed orderings that came with the applications. A simple but valuable extension of steady slab studies can be exploring numerical solutions for the phase speeds of guided waves as well as the KHI-thresholds of these various Cartesian models for a wider range of background parameters (high-, intermediate-, and low-β plasmas in each region, with different density, magnetic, and flow asymmetries between the regions). A study of increasing the density and flow asymmetries focused around a specific initial characteristic speed ordering was carried out for an externally non-magnetic steady slab system in Chapter 2. This could, however, be expanded to the more general models presented in Chapter 4, and to different starting equilibrium parameters (possibly corresponding to different solar waveguides).

Although the models described in Chapters 2-4 have all introduced various sources of asymmetry (kinetic, magnetic, flow) step-by-step, a new leap forward may come from the study of different flow profiles in one or more regions of the slab system. The study presented in Chapter 5 took a first step in this direction by studying triangular jets under the effect of a kink oscillation, based on the existing precursor cases in the literature, in order to link the lifetimes of solar spicules to the instabilities present in this system. In the future, different flow profiles may be examined, and, completing this initial study, the effects on non-parallel propagation can be explored in greater detail.

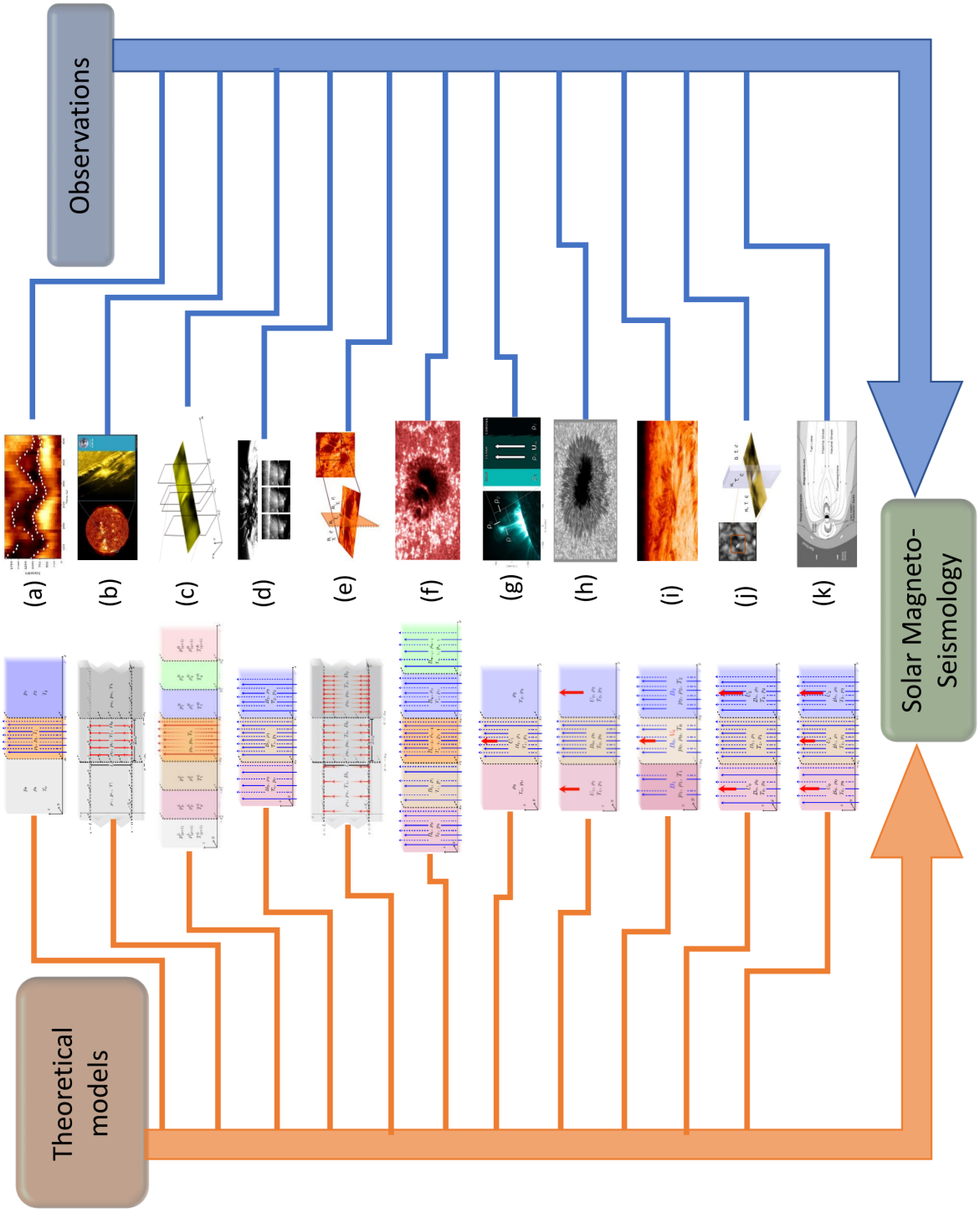

Figure 6.1: The family of recent asymmetric slab models and their potential applications to observable structures in solar magneto-seismology.

Chapter 7.
Summary

Overview of Magnetic Slab Models in Solar Physics

The solar atmosphere shows structuring on several different length scales from the global layers down to fine structuring in small-scale phenomena. It is a dynamic, coupled plasma environment permeated by ubiquitous magnetic fields and subject to flows of various speeds and profiles. Its elaborate structuring is a consequence of the interplay between the effects of gravity and the ubiquitous magnetic fields permeating the plasma. The presence of flows is one of several factors which may lead to the appearance of instabilities and turn this richly structured medium into an ever-changing, dynamic environment. From a theoretical point of view, several solar atmospheric features may be modelled as flux tube- or slab-like waveguides, supporting several types of magnetohydrodynamic (MHD) waves, which, in turn, can provide us with essential information about the waveguide media themselves. This principle is what the rapidly evolving field of solar magneto-seismology (SMS) is based upon: a combination of theoretical and observational information on MHD waves is utilised to learn about background parameters filling the structures guiding these waves which might be difficult to measure otherwise. Furthermore, MHD waves and instabilities can also contribute to the transport and transformation of energy within the solar atmosphere, and thus they are able to play a part in explaining one of the greatest enigmas in solar physics: the question of solar atmospheric heating.

One possible approach to take when constructing mathematical models of solar atmospheric waveguides is to rely on a slab geometry. Classical slab studies placed a layer of magnetised plasma between two other, symmetric plasma regions which could optionally contain symmetric magnetic fields as well (see e.g. Edwin and Roberts (1982)). There are several ways to expand these slab models and capture further physical processes which may take place in and around solar atmospheric slab waveguides, and one of these possibilities is to introduce asymmetry into the slab system. This line of investigation has recently been expanded to encompass plasma- and magnetic asymmetries (see Allcock and Erdélyi (2017) and Zsámberger et al. (2018)), as well as to start incorporating steady background flows into the system (Barbulescu and Erdélyi, 2018). Continuing this generalisation of slab models, in this Thesis, the effects of introducing and combining various sources of asymmetry (plasma, magnetic field and flow parameters), as well as including a triangular

flow profile in the central region were investigated.

7.1. Chapter 2 - Magnetohydrodynamic Waves and the Kelvin-Helmholtz Instability in a Magnetic Slab Enclosed by an Asymmetric Plasma- and Flow Environment

In Chapters 2 - 4, we investigated propagating magneto-acoustic waves in various steady asymmetric magnetic slab systems. We started by studying an externally non-magnetic asymmetric case in Chapter 2, and through multiple steps of introducing various sources of asymmetry, we finished this large segment by describing the most general case of a 3-layer piece-wise Cartesian model containing homogeneous steady flows in each region in Chapter 4.

In the first building block towards this generalised model in Chapter 2, we analysed a mathematical model of a magnetic slab placed in an asymmetric environment that contained asymmetric external flows. This served as a stepping stone towards more complex models and delineated the main properties of the slab systems that we were going to consistently keep throughout this series of studies. Namely, all the models we investigated contain sharp changes between plasma-, magnetic-, and flow properties in the form of two interfaces inserted into the volume, rather than continuous transitional regions being built into the models. Furthermore, all of our slab models are semi-infinite, as they contain structuring in the x-direction but remain unbounded in the y- and z-directions. The latter is an especially important restriction, since "closing" the slab in this additional direction could open up an avenue for studying standing waves (see for example Oxley et al. (2020a) and Oxley et al. (2020b)). Last but not least, we only study magneto-acoustic waves propagating in the z-direction, and we do not incorporate effects that rely on propagation in the perpendicular, y-direction. Section 6.2 provides further detail on alternative possibilities of expanding slab models and the physical processes they open up the studies for.

Overall, the slab model studied in Chapter 2 focused on the role that the asymmetry in environmental steady flows can play in determining the eigenmodes as well as their stability in a Cartesian system corresponding to the above-mentioned conditions. In order to place this line of investigation in its proper context, previous results for a single-flow asymmetric slab system published by Barbulescu and Erdélyi (2018) were summarised, and the symmetric counterpart of the problem was considered (see Nakariakov and Roberts (1995)).

We described the ideal MHD equations governing the interactions of magnetic fields and plasmas in a steady slab. These equations were then linearised and by seeking their plane-wave solutions propagating in the z-direction, a single ordinary differential equation to be solved was obtained for each region of the slab system in the place of the system of partial differential equations posed by the MHD framework. We restricted these solutions

to those corresponding to trapped modes of oscillation, which do not cause significant perturbations far away from the slab. Requiring the continuity of Lagrangian displacement and total pressure perturbations across the two interfaces delineating the slab allowed led us to a condition on the angular frequency, ω and the wavenumber, k ensuring that non-trivial solutions can be found to the system of equations thus obtained. This condition serves as the dispersion relation of the problem, which, in general, does not decouple into two separate equations governing sausage and kink-type modes (unlike its counterpart in the symmetric case). Such a decoupling was shown to be possible only in the weak asymmetry approximation, when the equilibrium plasma and flow parameters are similar but not identical on the two sides of the slab.

Using this decoupled dispersion relation, approximate solutions for the angular frequencies of the quasi-sausage and quasi-kink eigenmodes of this slab system were found in various limiting cases, such as in thin and wide slabs, or in zero- and infinite-β plasmas.

We devoted a section to investigating the dependence of the angular frequencies of surface modes on the two sources of asymmetry in the model. Through this process, both the density and the flow asymmetry were shown to have first-order effects on the frequencies and stability limits of waves propagating in the slab system.

While both the full and the approximate dispersion relations are transcendental equations which we could only provide analytical solutions for in approximate form (such as the limits listed above), we could obtain numerical solutions for them even in a more general case. We found that, as expected, the presence of bulk background flows broke the symmetry between the phase speeds of forward- and backward propagating modes. We demonstrated that the choice of external flow speeds and flow asymmetry has a significant effect on the phase speeds of eigenmodes, and it is able to influence both the exact frequencies, as well as the types of eigenmodes (e.g. surface or body modes) supported by the system. The choices of flow magnitudes and asymmetry further determined for which sets of equilibrium parameters certain waves remained stable. Through a series of figures and animations, we showed how the phase speeds, cut-offs, and the stability of modes changes compared to a symmetric system as density- or flow asymmetries (or both) are introduced.

7.2. Chapter 3 - Magnetohydrodynamic Wave Propagation and the Kelvin-Helmholtz Instability in a Magnetic Slab Enclosed in an Asymmetric Magnetic Environment

In this Chapter, we changed the studied model to one that provided a different kind of generalisation of the pioneering work on a steady asymmetric magnetic slab published by Barbulescu and Erdélyi (2018), focusing on the effects of external magnetic asymmetry introduced into the configuration of an asymmetric magnetic slab system containing a steady flow in the central region.

Starting from the ideal MHD equations and following a similar procedure to the one utilised in Chapter 2, in Chapter 3, too, we obtained the dispersion relation governing the parallel propagation of MHD waves in the asymmetric magnetic slab system studied in this section of our research. This transcendental equation connecting the angular frequencies and wavenumbers of eigenmode solutions is formally similar to the dispersion relations obtained in Barbulescu and Erdélyi (2018) and in Zsámberger et al. (2018) - in fact, it can be regarded as a combination of the two. Similarly to all asymmetric slab system studies of this kind, we showed that in the general case, the dispersion relation is one single equation, which governs the behaviour of both quasi-sausage and quasi-kink waves propagating along the slab, lending them a mixed character compared to their symmetric equivalents.

We described the approximation of weak asymmetry, too, in which case a decoupled dispersion relation for the problem could be obtained. This provided us with a more tractable expression to study further approximations and provide analytical solutions in.

Studying further limiting cases which we are likely to encounter in solar physics applications, i.e. as the thin slab and zero-β approximations, we found analytical solutions to the decoupled dispersion relation. These expressions were then used to determine the critical internal flow speed above which the Kelvin-Helmholtz instability can set in and make the initially small perturbations grow until they destabilise the entire slab system. We had to note that this threshold value depended heavily on the ordering of characteristic speeds, and therefore it could vary greatly with each solar application of the model.

A significant part of the analytical expressions of threshold speeds and wave frequencies we could provide was limited to the range of equilibrium parameters where one or more approximations (such as e.g. weak asymmetry and thin slab) were valid. To compensate for this limitation, we also employed numerical methods to provide solutions to the full dispersion relation for a wider parameter range. It was also shown that (at least for our choice of equilibrium parameters) the solutions to the full dispersion relation corresponded closely to the solutions of the weak asymmetry, as well as to the combined weak asymmetry and thin slab approximations, with the characteristic speeds being at least two orders of magnitude greater than the differences between the phase speeds of eigenmode solutions found in the exact vs. the approximate cases.

7.3. Chapter 4 - Further Generalisation of Slab Models Containing Asymmetric Flows

This Chapter was divided up between the introduction of two further Cartesian analytical models in order to further expand the validity of our results and an illustrative example of how the choice of model can affect the conclusions drawn from solar applications of the family of slab models.

First, we studied a two-flow asymmetric slab model, which incorporated bulk back-

ground flows into both external regions, which were also permeated by asymmetric magnetic fields. Following the method described in more detailed steps in Chapter 2, we derived the general dispersion relation governing the behaviour of magneto-acoustic eigenmodes of this slab system. This complex, transcendental equation still governs the behaviour of both quasi-kink and quasi-sausage waves guided by the slab system, but our understanding of it is helped by two previously studied problems. In fact, it may be regarded as a "combination" of the dispersion relations obtained for a static asymmetric magnetic slab (see Zsámberger et al. (2018)) and for a steady asymmetric externally non-magnetic slab (see Barbulescu and Erdélyi (2018)).

The decoupled dispersion relation of the problem was also obtained, which is valid in the case of weak asymmetry. Employing this approximation, we provided an example of analytical solutions in the limit of an infinite plasma-β describing every region of the system.

The configuration studied here, a.i. the asymmetric slab system incorporating plasma, magnetic and flow asymmetries in its external regions, is the ideal configuration to demonstrate the applicability of multi-layered Cartesian models to solar atmospheric features, as well as the influence of the exact configuration chosen on the phase speed and instability-related results obtained. Magnetic bright points, i.e. photospheric concentrations of magnetic fields corresponding to bright areas in observations, were chosen to demonstrate this effect. Using parameters corresponding to photospheric and MBP values of phase speeds, static slab studies found only surface modes propagating in the system (see also Zsámberger and Erdélyi (2021)). Incorporating steady flows in the external regions, even while zero external magnetic field strengths were assumed, demonstrated that the presence of any flow can markedly change these results through the appearance of instabilities and body modes (see Chapter 2). Applying the current model to a system composed of an MBP and its surrounding regions of an intergranular lane demonstrated that the flows expected to be present in this feature of the solar atmosphere result in the appearance of both body modes and unstable solutions, regardless of the presence or absence of external magnetic fields corresponding to conditions expected to be found around MBPs. However, it was also shown that the limiting speeds corresponding to the onset of the KHI can be different between the two cases, and the inclusion of asymmetric external magnetic fields results in the addition of cut-off frequencies for trapped oscillations in such a slab system.

Finally, we included a description of the most general case of an asymmetric steady slab system, where all three regions may have different pressures, temperatures, densities, magnetic fields and flow speeds characterising the equilibrium configuration. All of the previous cases investigated in Barbulescu and Erdélyi (2018) as well as in Chapters 2 - 4.2 can be obtained as specific, simplified cases of this system. It must be noted that while a two-flow system can be obtained from this configuration by changing the frame of reference to move with one of the prescribed flow speeds of the system, a one-flow system is not achievable in the generic asymmetric case (unless one of the three possible flow speeds

of the system is zero or the exact same as one of the other two).

7.4. Chapter 5 - On Instabilities in Dynamic Magnetic Slabs Driven by Kink Waves

Chapter 5 looked at wave propagation in jet-like solar slab systems utilising a different approach. Instead of focusing on the effects of asymmetry, here we investigated wave speeds and instabilities in the incompressible plasma limit of a symmetric slab system containing a triangular jet, which was under the effect of a kink oscillation. First, we provided further background information on the hydrodynamic and simpler, internally non-magnetic MHD cases of the problem, as well as on solar spicules, which serve as the main motivation for studying the instabilities of this model.

We showed that, in the most general case of a symmetric slab system, a transcendental equation containing the angular frequency of the guided waves up to the fourth power governs the behaviour of oscillations in the system. We provided simplified equations and - where they could concisely be expressed - solutions in several limiting cases of slab width and flow profile (going from a homogeneous to a triangular profile).

We also presented the results of our initial numerical study, including a comparison to the hydrodynamic case. In the fully magnetised system, we found that it was generally thin slabs where the instabilities appeared, while wide slabs can remain stable in the same parameter range. Our numerical results incorporated only waves that propagated parallel to the slab boundaries and the magnetic fields that permeated the configuration. In the future, an extension of these results to arbitrary propagation directions and further sets of equilibrium parameters can help us learn more about the stability of these slab systems and the spicules they may be used to model.

7.5. Further Improvements of Magnetic Slab Models

We have presented results on wave dispersion and instability limits in several, asymmetric and symmetric magnetic slab models, as well as their potential applications to solar atmospheric structures. This serves as a further generalisation of Cartesian models of the solar atmosphere focused on two of many possible avenues: incorporating asymmetry into a sharply divided background configuration and investigating the effects of different flow profiles within an oscillating slab. While these studies have contributed to a more detailed understanding of the propagation and instability of MHD waves in these structures, there are still several more steps to be taken in the future in order to capture a fuller picture of solar atmospheric phenomena. For example, the structuring can be expanded to encompass an infinite number of steady slabs, similarly to the static models included in Shukhobodskaia and Erdélyi (2018) and Allcock et al. (2019). Furthermore, gravitational

effects or gradually changing, continuous structuring could also be taken into account. Our jet studies in Chapter 5 took a step in this direction, but propagation in both the z- and y-directions (parallel and perpendicular to the magnetic field) could be allowed in these expanded models. Which effects to include in future studies will require careful considerations to be made about the properties of solar waveguides in focus, weighing up the trade-off between an ever more exact physical description and the analytical complexity as well as numerical capacity required to build our models. One thing is certain: while our Sun is only one of incredibly many stars in the Universe, it provides us with an incredibly diverse plasma environment to study.

8. fejezet

Összefoglalás

8.1. A mágneses rétegződések áttekintése a napfizikában

A naplégkör számos különböző méretskálán osztható kisebb szerkezeti elemekre, a globális légköri rétegektől kezdve egészen a kis skálájú jelenségek finomszerkezetéig. Napunk légköre egy dinamikus, csatolt plazmakörnyezet, amelyet mindenütt mágneses tér jár át és amelyben különféle sebességű és profilú áramlások találhatók. Ez a kifinomult szerkezet a gravitáció és a plazmában mindenütt jelenlévő mágneses terek összjátékának köszönhető. Az áramlások jelenléte továbbá egy a számos tényező közül, amelyek instabilitások megjelenéséhez vezethetnek, és ezt a gazdag szerkezetet mutató közeget folyamatosan változó, dinamikus környezetté teszik.

Elméleti szempontból vizsgálva a naplégkör számos eleme leírható fluxuscső- vagy mágneses rétegződés-jellegű hullámvezetőkkel, amelyek számos különféle magnetohidrodinamikai (MHD) hullámnak adnak otthont. E hullámok pedig lényeges információt képesek közvetíteni magukról a hullámvezető közegekről. Ezen az elven alapul a szoláris magnetoszeizmológia (SMS) sebesen fejlődő tudományága: az MHD hullámokra vonatkozó elméleti és észleléseken alapuló információk kombinálása által többet tudhatunk meg az e hullámokat vezető közegeket jellemző paraméterekről, amelyek más módon nehezen mérhetőnek bizonyulhatnak. Továbbá az MHD hullámok és instabilitások hozzájárulhatnak az energia szállításához és átalakításához is a naplégkörben, ezáltal pedig szerepet játszhatnak a napfizika egyik legnagyobb rejtélyének, a naplégkör fűtésének magyarázatában.

A naplégkör matematikai modellezése során az egyik lehetséges eljárás a rétegződéses geometria használata. A klasszikus réteg-modellek egy mágneses plazmaréteget két másik, szimmetrikus plazmatartomány közé helyeztek, amelyek szintén magukban foglalhattak mágneses tereket is (ld. például Edwin and Roberts (1982)). Ezek a rétegződéses modellek számos különböző módon bővíthetők annak érdekében, hogy képesek legyenek leírni további, a naplégkörbeli rétegződéses hullámvezetőkben és környezetükben végbemenő folyamatokat. E lehetőségek egyike pedig az aszimmetria beépítése a rendszerbe. Ebben a kutatási irányban a közelmúltban számos tanulmány készült melyek a klasszikus

modelleket plazma- és mágneses aszimmetriák beépítésével bővítették ki (ld. Allcock and Erdélyi (2017) és Zsámberger et al. (2018)), valamint megkezdték az egyensúlyi áramlások beépítését is a modellekbe (Barbulescu and Erdélyi, 2018). A rétegződéses modellek ezen típusát tovább általánosítva jelen értekezésben az aszimmetria különféle forrásainak (plazma, mágneses tér, áramlások) beépítését és kölcsönhatását, valamint a rétegződés központi régiójában található háromszög-profilú áramlás jelenlétének hatását vizsgáltuk.

8.2. 2. Fejezet - Magnetohidrodinamikai hullámok és a Kelvin-Helmholtz Instabilitás aszimmetrikus mágneses és áramlási környezetben foglalt mágneses rétegben

A 2 - 4. Fejezetekben a különféle aszimmetrikus mágneses rétegződéses rendszerek által vezetett magneto-akusztikus hullámokat vizsgáltuk. Kezdetben egy, kívülről nem mágneses aszimmetrikus esetet tanulmányoztunk a 2. Fejezetben, majd a különféle aszimmetriák bevezetésének számos lépését megtéve ezt a nagyobb részt átívelő vizsgálatot a homogén, stacionárius áramlásokat tartalmazó három rétegből álló descartes-i modellek legáltalánosabbikának leírásával fejeztük be a 4. Fejezetben.

Az első ilyen, az általános modell megszerkesztéséhez szükséges építőelemmel a 2. fejezetben foglalkoztunk, amelyben az aszimmetrikus áramlásokat tartalmazó, szintén aszimmetrikus, nem mágneses környezetbe helyezett mágneses réteg amtematikai modelljét elemeztük. Ez az összetettebb modellek irányába tett jelentős lépésként szolgált, ugyanakkor kijelölte a mágneses rétegződéses rendszerek azon alapvető tulajdonságait is, amelyeket végig következetesen megtartottunk e tanulmány-sorozatban. Így például minden, itt vizsgált modell éles határokat tartalmaz a plazma-, mágneses-, és áramlási tulajdonságok szempontjából, mégpedig két határfelület mentén, amelyeket a teljes vizsgált térfogatba illesztettünk (szemben a folytonos átmeneti régiók beépítésének alternatív ehetőségével). Továbbá az összes rétegződéses modellünk fél-végtelen konfiguráció, mivel a rétegződés csak az x irányan van jelen, miközben az y- és z irányokban nem jelöltünk ki határfelületeket. Ez utóbbi tulajdonság különösen fontos szereppel bír, mivel, ha függőlegesen „lezárjuk" a rétegeket, akkor új lehetőségeket nyitunk az állóhullámok tanulmányozására (ld. például Oxley et al. (2020a) és Oxley et al. (2020b)). Végül, de nem utolsósorban, csak a z irányban terjedő magneto-akusztikus hullámokat tanulmányozzuk, és nem foglalkozunk a merőleges (y irányú) terjedésen alapuló effektusokkal. A 6.2. szekció további részleteket tartalmaz a rétegződéses modellek kiterjesztésének alternatív lehetőségeivel, valamint az e kiterjesztések által tanulmányozható folyamatokkal kapcsolatban.

A 2. fejezetben tanulmányozott rétegződéses modell a környezet rétegeinek aszimmetrikus áramlásai által a fenti feltételeknek megfelelő descartes-i rendszer sajátmódusaira valamint instabilitására gyakorolt hatással foglalkozott. Annak érdekében, hogy megfelelő kontextusba helyezzük ezt a vizsgálatot, összefoglaltuk a Barbulescu and Erdélyi (2018)

által tanulmányozott, egyetlen áramlást tartalmazó aszimmetrikus rétegződéses rendszerre vonatkozó eredményeket, valamint figyelembe vettük a probléma szimmetrikus megfelelőjét (ld. Nakariakov and Roberts (1995)).

Megadtuk a stacionárius rétegződésben a plazma és a mágneses terek kölcsönhatásait meghatározó ideális MHD-egyenletek leírását. Ezen egyenletek linearizálása után a z irányban terjedő síkhullám megoldásokat kerestünk, miáltal minden régióra vonatkozóan kaptunk egy-egy közönséges differenciálegyenletet az MHD leírás keretében foglalt eredeti parciális differenciálegyenlet-rendszer helyett. A keresett megoldások körét tovább szűkítettük azáltal, hogy megköveteltük a módusok evaneszcens viselkedését a központi rétegen kívül, miáltal a rétegtől távol a vizsgált hullámok nem okoznak jelentős perturbációkat. Megkövetelve a Lagrange-féle elmozdulás és a teljes nyomás perturbációjának folytonosságát a központi réteg két határfelülete mentén, levezettünk egy, a körfrekvenciát (ω) és a hullámszámot (k) összekötő feltételt, amely biztosítja, hogy a kapott egyenletrendszernek nem triviális megoldását kapjuk. Ez a feltétel szolgál a modell diszperziós relációjaként, amely általános esetben nem csatolható szét két külön egyenletre, melyek a „hurka" (sausage) és „kihajlási" (kink) típusú módusokat külön-külön írnák le) ellentétben a rendszer szimmetrikus megfelelőjével). Amint bemutattuk, az egyenletek szétcsatolása csak a gyenge aszimmetria közelítésében lehetséges, amikor az egyensúlyi plazma- és áramlási paraméterek a központi réteg két oldalán hasonlóak (de nem feltétlen azonosak).

A szétcsatolt diszperziós reláció felhasználásával közelítő megoldásokat adtunk a „kvázi-hurka" és „kvázi-kihajlási" módusok körfrekvenciájára a rétegződéses rendszer leírásának különféle határeseteiben, így például a keskeny és vastag központi réteg, vagy a zéró- és végtelen-β plazmák esetében-

A következő szekciót annak szenteltük, hogy részletesebben megvizsgáljuk a felületi hullámok körfrekvenciájának függését a modellben jelen lévő kétféle aszimmetriától. E folyamat során demonstráltuk, hogy mint a sűrűség-, mind az áramlási aszimmetria első rendben gyakorol hatást a frekvenciákra és a rétegződésben terjedő hullámok stabilitását kifejező paraméterek határértékeire.

Bár mind a teljes, mind a közelítő diszperziós relációk transzcendens egyenletek, amelyekre csak közelítő analitikus megoldásokat tudtunk adni (például a fent említett határesetekben), numerikus módszerek segítségével általánosabb esetben is elő tudtunk állítani megoldásokat. Ennek során, elvárásainkkal összhangban, arra a megállapításra jutottunk, hogy az egyensúlyi áramlások jelenléte megtöri a mágneses erővonalak mentén előre illetve hátrafelé terjedő hullámok fázissebességei közötti szimmetriát. Szemléltettük, hogy a külső áramlási sebességek illetve a köztük fennálló aszimmetria megválasztása jelentős hatással bír a sajátmódusok fázissebességére, és mind magukat a pontos körfrekvenciákat, mind a rendszer által vezetett sajátmódusok típusát (pl. felületi vagy térfogati hullám módusok) képes befolyásolni. Az aszimmetria választott nagysága továbbá meghatározta azt is, hogy az adott típusú hullámok mely egyensúlyi paraméter-halmazokra maradtak stabilak. Ábrák és animációk sorozatának segítségével bemutattuk, hogy a módusok fázissebessége,

levágási sebessége, valamint stabilitása hogyan változik szimmetrikus rendszerbeli megfelelőikhez képest, amikor sűrűségbeli vagy áramlási (vagy mindkét típusú) aszimmetriát vezetünk be a modellbe.

8.3. 3. Fejezet - magnetohidrodinamikai hullámok terjedése és a Kelvin-Helmholtz instabilitás aszimmetrikus mágneses környezetbe helyezett mágneses rétegben

E fejezettel irányt váltottunk a Barbulescu and Erdélyi (2018) által a stacionárius aszimmetrikus mágneses rétegződések témájában publikált úttörő munka általánosításának folyamatában, és a központi rétegben stacionárius áramlást tartalmazó mágneses rétegződés modelljébe újonnan beépített külső mágneses aszimmetria hatásaira koncentráltunk.

Az ideálos MHD egyenletekből kiindulva, a 2. fejezetben követett lépésekhez hasonló levezetés által, a 3. fejezetben szintén levezettük az aktuális konfigurációban a párhuzamosan terjedő MHD hullámokra érvényes diszperziós relációt. A kapott transzcendens egyenlet, mely kapcsolatot teremt a sajátmódusok körfrekvenciái és a hullámszámai között, formálisan hasonlít a Barbulescu and Erdélyi (2018) és Zsámberger et al. (2018) által vizsgált problémákra érvényes diszperziós relációkra – tulajdonképp e kétféle diszperziós reláció kombinációjának tekinthető. Hasonlóan az ebbe a típusba tartozó többi aszimmetrikus mágneses rétegződéshez tanulmányhoz, demonstráltuk, hogy általános esetben a diszperziós reláció maga egyetlen egyenlet, amely egyszerre határozza meg a rétegződésben terjedő kvázi-hurka és kvázi-kihajlási módusok viselkedését, ezáltal (szimmetrikus megfelelőikhez képest) kevert tulajdonságokat kölcsönözve nekik.

Részleteztük a gyenge aszimmetria leírását is, mely esetben levezethető a probléma szétcsatolt diszperziós relációja. Ezáltal hozzájutottunk egy könnyebben kezelhető matematikai kifejezéshez, amelynek segítségével tanulmányozhattunk egyéb közelítéseket és analitikus megoldásokat adhattunk a diszperziós egyenletre.

További, a napfizikában előforduló határeseteket (így például a keskeny központi réteg és a zéró-β plazma esetét) tanulmányozva megadtuk a szétcsatolt diszperziós reláció analitikus megoldásait. E kifejezések segítésével ezután meghatároztuk a központi rétegbeli belső áramlás sebességének kritikus értékét, amelyet átlépve megjelenik a Kelvin-Helmholtz instabilitás, és az eredetileg kis perturbációkat addig erősíti, amíg a teljes rétegződést destabilizálja. Meg kellett állapítanunk, hogy ez a küszöbérték erősen függ a karakterisztikus sebességek rendezésétől, ezáltal pedig erősen változhat a modell különböző napfizikai alkalmazásai során.

A sebességküszöbök és hullámfrekvenciák vizsgálata során közölt analitikus közelítések jelentős részének érvényessége az egyensúlyi paraméterek azon tartományára korlátozódik, amelyben egy vagy akár több közelítés (pl. a gyenge aszimmetria és a keskeny központi réteg közelítése) érvényes. E korlátok ellensúlyozása érdekében numerikus módszerek segít-

ségével további megoldásokat kerestünk a teljes diszperziós relációra az egyensúlyi paraméterek szélesebb tartományában. Eközben illusztráltuk azt is, hogy (legalábbis az általunk választott egyensúlyi paraméterek mellett) a teljes diszperziós relációra adott megoldások igen jó közelítéssel megegyeznek a gyenge aszimmetria, valamint a gyenge aszimmetria és keskeny réteg közelítések esetében kapott megoldásokkal: a sajátmódusok teljes és közelítő fázissebesség megoldásai között kimutatható különbségek legalább két nagyságrenddel kisebbek voltak, mint maguk a modellezéshez használt karakterisztikus sebességek.

8.4. 4. Fejezet az aszimmetrikus áramlásokat tartalmazó rétegződéses modellek további általánosítása

E fejezetet további szekciókra osztottuk annak érdekében, hogy bemutassunk két hasonló, általánosabb descartes-i analitikus modellt eredményeink érvényességének kiterjesztéséhez, valamint hogy alaposabb leírását adjuk egy példaértékű estnek, amely illusztrálja, milyen befolyással bír a modell megválasztása a rétegződéses modellcsalád napfizikai alkalmazásai során levont következtetésekre.

Elsőként egy két áramlást tartalmazó aszimmetrikus modellt tanulmányoztunk, amelyben mindkét külső tartomány tartalmazott aszimmetrikus áramlásokat és mágneses tereket is. A 2. fejezetben részletesebben leírt módszert követve levezettük az ebben a rétegződéses rendszerben a magneto-akusztikus hullámok viselkedését meghatározó diszperziós relációt. Ez a komplex, transzcendens egyenlet mint a kvázi-kihajlási, mind a kvázi-hurka módusok viselkedését együttesen határozza meg, azonban a két, korábban már vizsgált rétegződéses probléma segít minket e viselkedés megértésében. Tulajdonképpen e rendszer diszperziós relációjára úgy is tekinthetünk, mint a statikus aszimmetrikus mágneses rétegződésre (ld. Zsámberger et al. (2018)) és a stacionárius, kívül nem mágneses aszimmetrikus rétegződésre (ld. Barbulescu and Erdélyi (2018)) érvényes diszperziós relációk „kombinációjára”.

A modellre érvényes szétcsatolt diszperziós relációt is levezettük, amely a gyenge aszimmetria esetére érvényes. E közelítést felhasználva bemutattuk az analitikus megoldások egy lehetséges típusát abban a határesetben, amikor a végtelen plazma-β közelítés írja le a rendszer mindegyik régióját.

Az itt tanulmányozott konfiguráció, azaz a külső régiókban plazma-, mágneses-, és áramlási aszimmetriákat egyaránt magában foglaló mágneses rétegződés modellje ideális lehetőséget kínál a többrétegű descartes-i modellek napfizikai alkalmazásaiban felfedezhető jellegzetességek bemutatására, valamint kifejezetten a választott modellnek a hullámok fázissebességére illetve az instabilitással kapcsolatos eredményekre gyakorolt hatásának szemléltetésére. E szemléltetés céljából a fényes mágnese pontokat (magnetic bright points, MBPs) választottuk ki, amelyek a megfigyeléseken a fotoszférában található, erős mágneses tér koncentrációkkal egybeeső fényes területek. A fotoszférikus körülményeknek valamint MBP-knek megfelelő karakterisztikus sebességekkel dolgozó, statikus rétegződésekre vo-

natkozó tanulmányok csak felületi hullámokat találtak a rendszerben (ld. Zsámberger and Erdélyi (2021)). A külső tartományokban megjelenő stacionárius áramlásokat beépítve a modellbe, még nulla külső mágneses térerősségek feltételezése mellett is, bemutatható, hogy bármilyen áramlás jelenléte jelentősen megváltoztathatja ezen eredményeket, nevezetesen az instabilitások és a térfogati hullámok megjelenése által (ld. 2. fejezet). A jelenlegi modellt alkalmazva egy fényes mágneses pontra, valamint ennek intergranuláris környezetére szemléltettük, hogy a naplégkör ezen jelenségének környezetében valószínűleg jelenlévő áramlások figyelembe vétele mind térfogati hullámok, mind instabil megoldások megjelenéséhez képes hozzájárulni, akár jelen vannak a rendszerben az MBP-k környezetére jellemző külső mágneses terek, akár nincsenek. Azonban arra is fény derült, hogy a Kelvin-Helmholtz instabilitás megjelenéséhez szükséges határsebességek különbözhetnek e két eset között. Továbbá az aszimmetrikus külső mágneses terek hozzáadása a modellhez a rétegződés egyes hullámaihoz tartozó levágási frekvenciák megjelenéséhez is vezet.

Végül belefoglaltuk a fejezetbe az aszimmetrikus stacionárius mágneses rétegződéses rendszerek legáltalánosabb esetének leírását is, amelynek egyensúlyi állapotában mindhárom régió eltérő nyomás, hőmérséklet, sűrűség, mágneses térerősség és áramlási sebesség értékekkel jellemezhető. Minden különleges eset, melyek leírását Barbulescu and Erdélyi (2018) és a 2 - 4.2. Fejezetek adják meg, előállítható e rendszer speciális, egyszerűsített eseteiként. Meg kell jegyeznünk, hogy a bár az általános, két áramlást tartalmazó rendszer előállítható ebből a konfigurációból a vonatkoztatási rendszer megváltoztatása segítségével („átülve” egy olyan vonatkoztatási rendszerbe, amely az egyik régió áramlási sebességével mozog), egy pusztán egyetlen áramlást tartalmazó rendszer nem állítható elő az általános három áramlásos rendszerből (kivéve ha a három lehetséges áramlási sebesség valamelyike zéró vagy egyenlő a rendszer egy másik régiójának áramlási sebességével).

8.5. 5. Fejezet A kihajlási módusú rezgésben lévő dinamikus mágneses rétegződések instabilitásáról

Az 5. fejezetben a jet-szerű naplégkörbeli mágneses rétegződésekben tapasztalható hullámterjedést vizsgáltuk egy némileg különböző megközelítés segítségével. Ahelyett, hogy az aszimmetria bevezetésének hatásaira koncentráltunk volna, e fejezetben egy kihajlási rezgés hatása alatt álló, háromszög-profilú jetet tartalmazó szimmetrikus rétegződés inkompresszibilis plazma határesetében megjelenő hullámsebességeket és instabilitásokat vizsgáltunk. Először is összefoglaltuk a probléma jobb megértéséhez szükséges háttérinformációkat a hidrodinamikai és az egyszerűbb, a központi rétegben nem mágneses MHD esetre vonatkozóan, valamint rövid leírását adtuk a naplégkör szpikuláinak. E rövid életű jetek szolgálnak a jelen modellben fellépő instabilitások vizsgálatának fő motivációjaként.

Levezetésünk során megmutattuk, hogy általános esetben e szimmetrikus rétegződéses rendszerben a hullámok viselkedését egy, a körfrekvenciát negyedfokú kifejezésben tartal-

mazó transzcendens egyenlet határozza meg. A központi rétegvastagság és az áramlási profil különböző (a homogén áramlástól a háromszögprofilig terjedő) határeseteiben egyszerűsített diszperziós egyenleteket vezettünk le, és, ahol lehetséges volt tömör kifejezésekre jutni, megadtuk ezek megoldásait is.

Bemutattuk továbbá megkezdett numerikus tanulmányunk kezdeti eredményeit is, beleértve a jelenlegi modell és a hidrodinamikai probléma megoldásinak összehasonlítását. Megállapítottuk, hogy a teljes egészében mágneses rendszerben általában a keskeny központi rétegek válnak instabillá, míg (a többi paraméter hasonló értékeinek megtartása mellett) a vastag központi réteggel jellemezhető rendszerek stabilak maradnak. Numerikus eredményeinket csak a párhuzamos terjedés határesetére közöltük, azaz arra az esetre, amikor a hullámok a réteghatárokkal valamint a rendszert átjáró mágneses terek irányával párhuzamosan terjednek. A kutatás jövőbeli folytatása során tervezzük ezen eredmények kiterjesztését szabadon megválasztott terjedési irányokra, valamint további egyensúlyi paraméter-halmazokra, hogy többet tudhassunk meg a rétegződések valamint az általuk modellezett szpikulák stabilitásáról.

8.6. A mágneses rétegződéses modellek továbbfejlesztése

Számos, szimmetrikus illetve aszimmetrikus mágneses rétegződéses modell esetére vezettük le és mutattuk be hullámterjedésre és instabilitási küszöbökre vonatkozó eredményeinket, valamint ezek lehetséges naplégkörbeli alkalmazásait. Kutatásunk a naplégkör descartes-i modelljeinek további általánosításának célját szolgálják, a megannyi lehetőség közül két módszerre koncentrálva: egyrészt az éles határrétegeket tartalmazó konfiguráció aszimmetrikussá tételére, másrészt pedig az rezgésben lévő rétegben foglalt különböző áramlási profilok hatásainak vizsgálatára. E tanulmányok hozzájárultak a leírt modellekben terjedő MHD hullámok és a fellépő instabilitások részletesebb megértéséhez, azonban még mindig számos további lépést kell megtennünk a naplégkör jelenségeinek jövőbeli teljesebb leírásának irányában. Például a rétegződés kiterjeszthető olya módon, hogy végtelen sok stacionárius mágneses réteget foglaljon magába, hasonlóan a Shukhobodskaia and Erdélyi (2018) és Allcock et al. (2019) által leírt statikus modellekhez. Továbbá figyelembe vehetők gravitációs effektusok vagy a modell régiói közötti fokozatos, folytonos átmenetek lehetősége. Az 5. fejezetben bemutatott, jetekre vonatkozó tanulmányaink már megtettek egy lépést ebben az irányban, de a továbbiakban például mind z-, mind y irányú (a mágneses térrel párhuzamos vagy arra merőleges) hullámterjedés is megengedhető lehetne a kibővített modellekben. Alapos megfontolás tárgyává kell tenni az egyes tanulmányozni kívánt naplégkörbeli hullámvezető közegek tulajdonságait annak megválasztásakor, mely fenti lehetőségeket kívánjuk belefoglalni jövőbeli tanulmányainkba. Ennek során pedig fel kell mérni az egyre pontosabb fizikai leírások jelentette előnyök, illetve a modellek vizsgálatához szükséges analitikai komplexitás és a szükséges számítási kapacitás jelentette problémák közötti viszonyt. Egy dolog mindenesetre bizonyos: bár Napunk csupán egy

az Univerzum számtalan csillaga közül, mégis rendkívül változatos plazma környezettel szolgál tanulmányaink számára.

Bibliography

M. Allcock and R. Erdélyi. Magnetohydrodynamic Waves in an Asymmetric Magnetic Slab. *Solar Phys.*, 292:35, Feb. 2017. doi: 10.1007/s11207-017-1054-y.

M. Allcock and R. Erdélyi. Solar Magnetoseismology with Magnetoacoustic Surface Waves in Asymmetric Magnetic Slab Waveguides. *Astrophys. J.*, 855(2):90, Mar 2018. doi: 10.3847/1538-4357/aaad0c.

M. Allcock, D. Shukhobodskaia, N. K. Zsámberger, and R. Erdélyi. Magnetohydrodynamic waves in multi-layered asymmetric waveguides: solar magneto-seismology theory and application. *Frontiers in Astronomy and Space Sciences*, 6:48, July 2019. doi: 10.3389/fspas.2019.00048.

J. Andries, T. van Doorsselaere, B. Roberts, G. Verth, E. Verwichte, and R. Erdélyi. Coronal Seismology by Means of Kink Oscillation Overtones. *Space Sci. Rev.*, 149:3–29, Dec. 2009. doi: 10.1007/s11214-009-9561-2.

I. Arregui. Wave heating of the solar atmosphere. *Philosophical Transactions of the Royal Society of London Series A*, 373:20140261–20140261, Apr. 2015. doi: 10.1098/rsta.2014.0261.

I. Arregui and M. Goossens. No unique solution to the seismological problem of standing kink magnetohydrodynamic waves. *Astron. Astrophys.*, 622:A44, Feb. 2019. doi: 10.1051/0004-6361/201833813.

I. Arregui, J. L. Ballester, R. Oliver, R. Soler, and J. Terradas. Prominence Seismology. In L. Bellot Rubio, F. Reale, and M. Carlsson, editors, *4th Hinode Science Meeting: Unsolved Problems and Recent Insights*, volume 455 of *Astronomical Society of the Pacific Conference Series*, page 211, May 2012a.

I. Arregui, R. Oliver, and J. L. Ballester. Prominence Oscillations. *Living Reviews in Solar Physics*, 9:2, Apr. 2012b. doi: 10.12942/lrsp-2012-2.

M. Aschwanden. *Physics of the Solar Corona.* Springer-Verlag, Berlin Heidelberg, 2005.

M. J. Aschwanden, L. Fletcher, C. J. Schrijver, and D. Alexander. Coronal Loop Oscillations Observed with the Transition Region and Coronal Explorer. *Astrophys. J.*, 520(2):880–894, Aug 1999. doi: 10.1086/307502.

E. H. Avrett and R. Loeser. Models of the Solar Chromosphere and Transition Region from SUMER and HRTS Observations: Formation of the Extreme-Ultraviolet Spectrum of Hydrogen, Carbon, and Oxygen. *The Astrophysical Journal Supplement Series*, 175(1):229–276, Mar. 2008. doi: 10.1086/523671.

D. Banerjee, R. Erdélyi, R. Oliver, and E. O'Shea. Present and Future Observing Trends in Atmospheric Magnetoseismology. *Solar Phys.*, 246:3–29, Nov. 2007. doi: 10.1007/s11207-007-9029-z.

M. Barbulescu and R. Erdélyi. Magnetoacoustic Waves and the Kelvin-Helmholtz Instability in a Steady Asymmetric Slab. I: The Effects of Varying Density Ratios. *Solar Phys.*, 293(6):86, Jun 2018. doi: 10.1007/s11207-018-1305-6.

J. M. Beckers. Solar Spicules. *Annual Review of Astronomy and Astrophysics*, 10:73, Jan. 1972. doi: 10.1146/annurev.aa.10.090172.000445.

T. E. Berger, C. J. Schrijver, R. A. Shine, T. D. Tarbell, A. M. Title, and G. Scharmer. New Observations of Subarcsecond Photospheric Bright Points. *Astrophys. J.*, 454:531, Nov. 1995. doi: 10.1086/176504.

T. E. Berger, G. Slater, N. Hurlburt, R. Shine, T. Tarbell, A. Title, B. W. Lites, T. J. Okamoto, K. Ichimoto, Y. Katsukawa, T. Magara, Y. Suematsu, and T. Shimizu. Quiescent Prominence Dynamics Observed with the Hinode Solar Optical Telescope. I. Turbulent Upflow Plumes. *Astrophys. J.*, 716(2): 1288–1307, June 2010. doi: 10.1088/0004-637X/716/2/1288.

W. Blumen. Shear layer instability of an inviscid compressible fluid. *Journal of Fluid Mechanics*, 40: 769–781, Jan. 1970. doi: 10.1017/S0022112070000435.

M. Bogdanova, I. Zhelyazkov, R. Joshi, and R. Chandra. Solar jet on 2014 April 16 modeled by Kelvin-Helmholtz instability. *New Astronomy*, 63:75–87, Aug. 2018. doi: 10.1016/j.newast.2018.03.001.

J. M. Borrero and K. Ichimoto. Magnetic Structure of Sunspots. *Living Reviews in Solar Physics*, 8(1):4, Sept. 2011. doi: 10.12942/lrsp-2011-4.

B. Bovelet and E. Wiehr. Dynamics of the solar active region finestructure. *Astron. Astrophys.*, 412: 249–255, Dec. 2003. doi: 10.1051/0004-6361:20031305.

R. J. Bray and R. E. Loughhead. Review of 'The Solar Chromosphere'. *The Observatory*, 95:148–148, Aug. 1975.

C. Briand and S. K. Solanki. Velocity fields below the magnetic canopy of solar flux tubes: evidence for high-speed downflows? *Astron. Astrophys.*, 330:1160–1168, Feb. 1998.

M. Carlsson, V. H. Hansteen, B. de Pontieu, S. McIntosh, T. D. Tarbell, D. Shine, S. Tsuneta, Y. Katsukawa, K. Ichimoto, Y. Suematsu, T. Shimizu, and S. Nagata. Can High Frequency Acoustic Waves Heat the Quiet Sun Chromosphere? *Pub. Astron. Soc. Japan*, 59:S663–S668, Nov. 2007. doi: 10.1093/pasj/59.sp3.S663.

S. Chandrasekhar. *Hydrodynamic and hydromagnetic stability*. 1961.

P. J. Crockett, M. Mathioudakis, D. B. Jess, S. Shelyag, F. P. Keenan, and D. J. Christian. The Area Distribution of Solar Magnetic Bright Points. *Astrophys. J. Lett.*, 722:L188–L193, Oct. 2010. doi: 10.1088/2041-8205/722/2/L188.

M. Cuntz, W. Rammacher, and Z. E. Musielak. Acoustic Heating of the Solar Chromosphere: Present Indeed and Locally Dominant. *Astrophys. J. Lett.*, 657:L57–L60, Mar. 2007. doi: 10.1086/512973.

S. Danilovic, M. Schüssler, and S. K. Solanki. Magnetic field intensification: comparison of 3D MHD simulations with Hinode/SP results. *Astron. Astrophys.*, 509:A76, Jan. 2010. doi: 10.1051/0004-6361/200912283.

I. De Moortel. An overview of coronal seismology. *Philosophical Transactions of the Royal Society of London Series A*, 363:2743–2760, Dec. 2005. doi: 10.1098/rsta.2005.1665.

I. de Moortel. Longitudinal Waves in Coronal Loops. *Space Sci. Rev.*, 149(1-4):65–81, Dec 2009. doi: 10.1007/s11214-009-9526-5.

I. De Moortel and V. M. Nakariakov. Magnetohydrodynamic waves and coronal seismology: an overview of recent results. *Philosophical Transactions of the Royal Society of London Series A*, 370:3193–3216, July 2012. doi: 10.1098/rsta.2011.0640.

B. De Pontieu, R. Erdélyi, and I. De Moortel. How to Channel Photospheric Oscillations into the Corona. *Astrophys. J. Lett.*, 624:L61–L64, May 2005. doi: 10.1086/430345.

B. De Pontieu, V. H. Hansteen, L. Rouppe van der Voort, M. van Noort, and M. Carlsson. High-Resolution Observations and Modeling of Dynamic Fibrils. *Astrophys. J.*, 655(1):624–641, Jan. 2007. doi: 10.1086/509070.

B. de Pontieu, S. McIntosh, V. H. Hansteen, M. Carlsson, C. J. Schrijver, T. D. Tarbell, A. M. Title, R. A. Shine, Y. Suematsu, S. Tsuneta, Y. Katsukawa, K. Ichimoto, T. Shimizu, and S. Nagata. A Tale of Two Spicules: The Impact of Spicules on the Magnetic Chromosphere. *Pub. Astron. Soc. Japan*, 59:S655, Nov. 2007. doi: 10.1093/pasj/59.sp3.S655.

C. E. DeForest and J. B. Gurman. Observation of Quasi-periodic Compressive Waves in Solar Polar Plumes. *Astrophys. J. Lett.*, 501:L217–L220, July 1998. doi: 10.1086/311460.

P. G. Drazin. *Introduction to Hydrodynamic Stability*. Cambridge Texts in Applied Mathematics. Cambridge University Press, 2002. doi: 10.1017/CBO9780511809064.

P. M. Edwin and B. Roberts. Wave propagation in a magnetically structured atmosphere. III - The slab in a magnetic environment. *Solar Phys.*, 76:239–259, Mar. 1982. doi: 10.1007/BF00170986.

P. M. Edwin and B. Roberts. Wave Propagation in a Magnetic Cylinder. *Solar Phys.*, 88:179–191, Oct. 1983. doi: 10.1007/BF00196186.

R. Erdélyi. Magnetic coupling of waves and oscillations in the lower solar atmosphere: can the tail wag the dog? *Philosophical Transactions of the Royal Society of London Series A*, 364:351–381, Feb. 2006a. doi: 10.1098/rsta.2005.1703.

R. Erdélyi. Magnetic seismology of the lower solar atmosphere. In *Proceedings of SOHO 18/GONG 2006/HELAS I, Beyond the spherical Sun*, volume 624 of *ESA Special Publication*, page 15.1, Oct. 2006b.

R. Erdélyi and C. J. Nelson. On The Role of MHD Waves in Heating Localised Magnetic Structures. In I. Dorotovic, C. E. Fischer, and M. Temmer, editors, *Coimbra Solar Physics Meeting: Ground-based Solar Observations in the Space Instrumentation Era*, volume 504 of *Astronomical Society of the Pacific Conference Series*, page 153, Apr. 2016.

R. Erdélyi and Y. Taroyan. Hinode EUV spectroscopic observations of coronal oscillations. *Astron. Astrophys.*, 489(3):L49–L52, Oct. 2008. doi: 10.1051/0004-6361:200810263.

ESA. Anatomy of our Sun, 2019. URL `https://www.esa.int/ESA_Multimedia/Images/2019/10/Anatomy_of_our_Sun`.

T. Felipe, M. Collados, E. Khomenko, C. Kuckein, A. Asensio Ramos, H. Balthasar, T. Berkefeld, C. Denker, A. Feller, M. Franz, A. Hofmann, J. Joshi, C. Kiess, A. Lagg, H. Nicklas, D. Orozco Suárez, A. Pastor Yabar, R. Rezaei, R. Schlichenmaier, D. Schmidt, W. Schmidt, M. Sigwarth, M. Sobotka, S. K. Solanki, D. Soltau, J. Staude, K. G. Strassmeier, R. Volkmer, O. von der Lühe, and T. Waldmann. Three-dimensional structure of a sunspot light bridge. *Astron. Astrophys.*, 596:A59, Nov. 2016. doi: 10.1051/0004-6361/201629586.

A. Fossum and M. Carlsson. Detectability of High Frequency Acoustic Waves with TRACE. In H. Lacoste, editor, *SOHO 13 Waves, Oscillations and Small-Scale Transients Events in the Solar Atmosphere: Joint View from SOHO and TRACE*, volume 547 of *ESA Special Publication*, page 125, Jan. 2004.

A. Fossum and M. Carlsson. Detectability of high frequency acoustic waves with TRACE. In A. Hanslmeier, A. Veronig, and M. Messerotti, editors, *Solar Magnetic Phenomena*, volume 320 of *Astrophysics and Space Science Library*, pages 239–242, 2005.

C. Foullon, E. Verwichte, V. M. Nakariakov, K. Nykyri, and C. J. Farrugia. Magnetic Kelvin-Helmholtz Instability at the Sun. *Astrophys. J. Lett.*, 729(1):L8, Mar. 2011. doi: 10.1088/2041-8205/729/1/L8.

C. Foullon, E. Verwichte, K. Nykyri, M. J. Aschwanden, and I. G. Hannah. Kelvin-Helmholtz Instability of the CME Reconnection Outflow Layer in the Low Corona. *Astrophys. J.*, 767(2):170, Apr. 2013. doi: 10.1088/0004-637X/767/2/170.

J. P. H. Goedbloed and S. Poedts. *Principles of Magnetohydrodynamics. With Applications to Laboratory and Astrophysical Plasmas*. Cambridge University Press, Cambridge, New York, 2004.

L. Golub and J. M. Pasachoff. *The Solar Corona*. 2009.

L. Golub, A. S. Krieger, J. K. Silk, A. F. Timothy, and G. S. Vaiana. Solar X-Ray Bright Points. *Astrophys. J. Lett.*, 189:L93, Apr. 1974. doi: 10.1086/181472.

H. Hasegawa, M. Fujimoto, T. D. Phan, H. Rème, A. Balogh, M. W. Dunlop, C. Hashimoto, and R. Tan-Dokoro. Transport of solar wind into Earth's magnetosphere through rolled-up Kelvin-Helmholtz vortices. *Nature*, 430(7001):755–758, Aug. 2004. doi: 10.1038/nature02799.

H. Helmholtz. Ueber discontinuirliche Fluessigkeitsbewegungen . *Monatsberichte der Koeniglichen Preussische Akademie der Wissenschaften zu Berlin*, 1868.

A. Hillier. The magnetic Rayleigh-Taylor instability in solar prominences. *Reviews of Modern Plasma Physics*, 2(1):1, Dec. 2018. doi: 10.1007/s41614-017-0013-2.

N. E. Hurlburt, D. Alexander, and A. M. Rucklidge. Complete Models of Axisymmetric Sunspots: Magnetoconvection with Coronal Heating. *Astrophys. J.*, 577(2):993–1005, Oct. 2002. doi: 10.1086/342154.

D. B. Jess, R. J. Morton, G. Verth, V. Fedun, S. D. T. Grant, and I. Giagkiozis. Multiwavelength Studies of MHD Waves in the Solar Chromosphere. An Overview of Recent Results. *Space Sci. Rev.*, 190(1-4): 103–161, July 2015. doi: 10.1007/s11214-015-0141-3.

R. L. Jiang, K. Shibata, H. Isobe, and C. Fang. Fan-shaped Jets in Three-dimensional Reconnection Simulation as a Model of Ubiquitous Solar Jets. *Astrophys. J. Lett.*, 726(2):L16, Jan 2011. doi: 10.1088/2041-8205/726/2/L16.

P. S. Joarder and B. Roberts. The modes of oscillation of a prominence. I - The slab with longitudinal magnetic field. *Astron. Astrophys.*, 256:264–272, Mar. 1992.

P. H. Keys, M. Mathioudakis, D. B. Jess, S. Shelyag, D. J. Christian, and F. P. Keenan. Tracking magnetic bright point motions through the solar atmosphere. *Mon. Not. Roy. Astron. Soc.*, 428:3220–3226, Feb. 2013. doi: 10.1093/mnras/sts268.

P. H. Keys, R. J. Morton, D. B. Jess, G. Verth, S. D. T. Grant, M. Mathioudakis, D. H. Mackay, J. G. Doyle, D. J. Christian, F. P. Keenan, and R. Erdélyi. Photospheric Observations of Surface and Body Modes in Solar Magnetic Pores. *Astrophys. J.*, 857(1):28, Apr 2018. doi: 10.3847/1538-4357/aab432.

E. Khomenko, A. Díaz, A. de Vicente, M. Collados, and M. Luna. Rayleigh-Taylor instability in prominences from numerical simulations including partial ionization effects. *Astron. Astrophys.*, 565:A45, May 2014. doi: 10.1051/0004-6361/201322918.

R. Komm, I. De Moortel, Y. Fan, S. Ilonidis, and O. Steiner. Sub-photosphere to Solar Atmosphere Connection. *Space Sci. Rev.*, 196:167–199, Dec. 2015. doi: 10.1007/s11214-013-0023-5.

D. Kuridze, T. V. Zaqarashvili, V. Henriques, M. Mathioudakis, F. P. Keenan, and A. Hanslmeier. Kelvin-Helmholtz Instability in Solar Chromospheric Jets: Theory and Observation. *Astrophys. J.*, 830(2): 133, Oct. 2016. doi: 10.3847/0004-637X/830/2/133.

X. Li, J. Zhang, S. Yang, and Y. Hou. Flow Instabilities in Solar Jets in Their Upstream and Downstream Regimes. *Astrophys. J.*, 875(1):52, Apr. 2019. doi: 10.3847/1538-4357/ab0f39.

S. L. Lippincott. Chromospheric Spicules. *Smithsonian Contributions to Astrophysics*, 2:15, Jan. 1957.

Y. Liu, Y. Xiang, R. Erdélyi, Z. Liu, D. Li, Z. Ning, Y. Bi, N. Wu, and J. Lin. Studies of Isolated and Non-isolated Photospheric Bright Points in an Active Region Observed by the New Vacuum Solar Telescope. *Astrophys. J.*, 856:17, Mar. 2018. doi: 10.3847/1538-4357/aab150.

M. Mak. *Atmospheric Dynamics*. Cambridge University Press, 2011. doi: 10.1017/CBO9780511762031.

M. Mathioudakis, D. B. Jess, and R. Erdélyi. Alfvén Waves in the Solar Atmosphere. From Theory to Observations. *Space Sci. Rev.*, 175:1–27, June 2013. doi: 10.1007/s11214-012-9944-7.

A. Michalke. On the inviscid instability of the hyperbolictangent velocity profile. *Journal of Fluid Mechanics*, 19:543–556, Jan. 1964. doi: 10.1017/S0022112064000908.

J. W. Miles. On the generation of surface waves by shear flows. *Journal of Fluid Mechanics*, 3:185–204, Jan. 1957. doi: 10.1017/S0022112057000567.

A. Miura. Anomalous transport by magnetohydrodynamic Kelvin-Helmholtz instabilities in the solar wind-magnetosphere interaction. *J. Geophys. Res.*, 89(A2):801–818, Feb. 1984. doi: 10.1029/JA089iA02p00801.

R. J. Morton, G. Verth, D. B. Jess, D. Kuridze, M. S. Ruderman, M. Mathioudakis, and R. Erdélyi. Observations of ubiquitous compressive waves in the Sun's chromosphere. *Nature Communications*, 3: 1315, Dec. 2012. doi: 10.1038/ncomms2324.

R. J. Morton, G. Verth, V. Fedun, S. Shelyag, and R. Erdélyi. Evidence for the Photospheric Excitation of Incompressible Chromospheric Waves. *Astrophys. J.*, 768:17, May 2013. doi: 10.1088/0004-637X/768/1/17.

U. V. Möstl, M. Temmer, and A. M. Veronig. The Kelvin-Helmholtz Instability at Coronal Mass Ejection Boundaries in the Solar Corona: Observations and 2.5D MHD Simulations. *Astrophys. J. Lett.*, 766 (1):L12, Mar. 2013. doi: 10.1088/2041-8205/766/1/L12.

V. M. Nakariakov and L. Ofman. Determination of the coronal magnetic field by coronal loop oscillations. *Astron. Astrophys.*, 372:L53–L56, June 2001. doi: 10.1051/0004-6361:20010607.

V. M. Nakariakov and B. Roberts. Magnetosonic Waves in Structured Atmospheres with Steady Flows, I. *Solar Phys.*, 159(2):213–228, Jul 1995. doi: 10.1007/BF00686530.

V. M. Nakariakov and E. Verwichte. Coronal Waves and Oscillations. *Living Reviews in Solar Physics*, 2: 3, May 2005. doi: 10.12942/lrsp-2005-3.

V. M. Nakariakov, L. Ofman, E. E. Deluca, B. Roberts, and J. M. Davila. TRACE observation of damped coronal loop oscillations: Implications for coronal heating. *Science*, 285:862–864, Aug. 1999. doi: 10.1126/science.285.5429.862.

L. Ofman and B. J. Thompson. SDO/AIA Observation of Kelvin-Helmholtz Instability in the Solar Corona. *Astrophys. J. Lett.*, 734(1):L11, June 2011. doi: 10.1088/2041-8205/734/1/L11.

W. Oxley, N. K. Zsámberger, and R. Erdélyi. Standing MHD Waves in a Magnetic Slab Embedded in an Asymmetric Plasma Environment: Slow Surface Waves. *Astrophys. J.*, 890(2):109, Feb. 2020a. doi: 10.3847/1538-4357/ab67b3.

W. Oxley, N. K. Zsámberger, and R. Erdélyi. Standing MHD Waves in a Magnetic Slab Embedded in an Asymmetric Magnetic Plasma Environment: Surface Waves. *Astrophys. J.*, 898(1):19, July 2020b. doi: 10.3847/1538-4357/ab9639.

C. D. Pike and H. E. Mason. Rotating Transition Region Features Observed with the SOHO Coronal Diagnostic Spectrometer. *Solar Phys.*, 182(2):333–348, Oct. 1998. doi: 10.1023/A:1005065704108.

E. Priest. *Magnetohydrodynamics of the Sun*. Cambridge University Press, Cambridge, 2014.

N. E. Raouafi, S. Patsourakos, E. Pariat, P. R. Young, A. C. Sterling, A. Savcheva, M. Shimojo, F. Moreno-Insertis, C. R. DeVore, V. Archontis, T. Török, H. Mason, W. Curdt, K. Meyer, K. Dalmasse, and Y. Matsui. Solar Coronal Jets: Observations, Theory, and Modeling. *Space Sci. Rev.*, 201(1-4):1–53, Nov. 2016. doi: 10.1007/s11214-016-0260-5.

T. P. Ray. The Effects of a Simple Shear Layer on the Growth of Kelvin-Helmholtz Instabilities. *Mon. Not. Roy. Astron. Soc.*, 198:617, Feb. 1982. doi: 10.1093/mnras/198.3.617.

B. Roberts. Wave propagation in a magnetically structured atmosphere. I - Surface waves at a magnetic interface. *Solar Phys.*, 69:27–38, Jan. 1981a. doi: 10.1007/BF00151253.

B. Roberts. Wave Propagation in a Magnetically Structured Atmosphere - Part Two - Waves in a Magnetic Slab. *Solar Phys.*, 69:39–56, Jan. 1981b. doi: 10.1007/BF00151254.

B. Roberts, P. M. Edwin, and A. O. Benz. On coronal oscillations. *Astrophys. J.*, 279:857–865, Apr. 1984. doi: 10.1086/161956.

W. O. Roberts. A Preliminary Report on Chromospheric Spicules of Extremely Short Lifetime. *Astrophys.*

J., 101:136, Mar. 1945. doi: 10.1086/144699.

H. Rosenberg. Evidence for MHD Pulsations in the Solar Corona. *Astron. Astrophys.*, 9:159, Nov. 1970.

L. H. M. Rouppe van der Voort, V. H. Hansteen, M. Carlsson, A. Fossum, E. Marthinussen, M. J. van Noort, and T. E. Berger. Solar magnetic elements at 0.1 arcsec resolution. II. Dynamical evolution. *Astron. Astrophys.*, 435:327–337, May 2005. doi: 10.1051/0004-6361:20042561.

M. S. Ruderman and R. Erdélyi. Transverse Oscillations of Coronal Loops. *Space Sci. Rev.*, 149:199–228, Dec. 2009. doi: 10.1007/s11214-009-9535-4.

M. Ryutova. The "Magnetosonic Streaming". *Astrophysical Letters and Communications*, 34:71, 1996.

M. Ryutova. *Physics of Magnetic Flux Tubes*, volume 417. Astrophysics and Space Science Library, Springer-Verlag, 2015. doi: 10.1007/978-3-662-45243-1.

M. Ryutova, T. Berger, Z. Frank, T. Tarbell, and A. Title. Observation of Plasma Instabilities in Quiescent Prominences. *Solar Phys.*, 267:75–94, Nov. 2010. doi: 10.1007/s11207-010-9638-9.

J. Sánchez Almeida, I. Márquez, J. A. Bonet, I. Domínguez Cerdeña, and R. Muller. Bright Points in the Internetwork Quiet Sun. *Astrophys. J. Lett.*, 609:L91–L94, July 2004. doi: 10.1086/422752.

R. Schlichenmaier, L. R. Bellot Rubio, M. Collados, R. Erdelyi, A. Feller, L. Fletcher, J. Jurcak, E. Khomenko, J. Leenaarts, S. Matthews, L. Belluzzi, M. Carlsson, K. Dalmasse, S. Danilovic, P. Gömöry, C. Kuckein, R. Manso Sainz, M. Martinez Gonzalez, M. Mathioudakis, A. Ortiz, T. L. Riethmüller, L. Rouppe van der Voort, P. J. A. Simoes, J. Trujillo Bueno, D. Utz, and F. Zuccarello. Science Requirement Document (SRD) for the European Solar Telescope (EST) (2nd edition, December 2019). *arXiv e-prints*, art. arXiv:1912.08650, Dec. 2019. doi: 10.48550/arXiv.1912.08650.

A. Secchi. *L'Astronomia in Roma nel pontificato di Pio IX: memoria.* Tipografia della Pace, 1877.

A. K. Sen. Effect of compressibility on kelvin-helmholtz instability in a plasma. *The Physics of Fluids*, 7 (8):1293–1298, 1964. doi: 10.1063/1.1711374. URL `https://aip.scitation.org/doi/abs/10.1063/1.1711374`.

Y. Shen. Observation and modelling of solar jets. *Proceedings of the Royal Society of London Series A*, 477(2246):217, Feb. 2021. doi: 10.1098/rspa.2020.0217.

K. Shibata, Y. Ishido, L. W. Acton, K. T. Strong, T. Hirayama, Y. Uchida, A. H. McAllister, R. Matsumoto, S. Tsuneta, T. Shimizu, H. Hara, T. Sakurai, K. Ichimoto, Y. Nishino, and Y. Ogawara. Observations of X-Ray Jets with the YOHKOH Soft X-Ray Telescope. *Pub. Astron. Soc. Japan*, 44:L173–L179, Oct. 1992.

D. Shukhobodskaia and R. Erdélyi. Propagation of Surface Magnetohydrodynamic Waves in Asymmetric Multilayered Plasma. *Astrophys. J.*, 868(2):128, Dec. 2018. doi: 10.3847/1538-4357/aae83c.

W. D. Smyth and J. N. Moum. Ocean mixing by kelvin-helmholtz instability. *Oceanography*, 25(2):140–149, 2012. ISSN 10428275, 2377617X. URL `http://www.jstor.org/stable/24861351`.

H. Socas-Navarro, V. Martínez Pillet, and B. W. Lites. Magnetic Properties of the Solar Internetwork. *Astrophys. J.*, 611(2):1139–1148, Aug. 2004. doi: 10.1086/422379.

S. K. Solanki, P. Barthol, S. Danilovic, A. Feller, A. Gandorfer, J. Hirzberger, T. L. Riethmüller, M. Schüssler, J. A. Bonet, V. Martínez Pillet, J. C. del Toro Iniesta, V. Domingo, J. Palacios, M. Knölker, N. Bello González, T. Berkefeld, M. Franz, W. Schmidt, and A. M. Title. SUNRISE: Instrument, Mission, Data, and First Results. *Astrophys. J. Lett.*, 723:L127–L133, Nov. 2010. doi: 10.1088/2041-8205/723/2/L127.

K. Somasundaram, S. Venkatraman, and M. P. Sengottuvel. Hydromagnetic surface waves along compressible cylindrical flux tubes with steady flows. *Plasma Physics and Controlled Fusion*, 41(11):1421–1428, Nov. 1999. doi: 10.1088/0741-3335/41/11/308.

Y. Taroyan and R. Erdélyi. Resonant and Kelvin-Helmholtz instabilities on the magnetopause. *Physics of Plasmas*, 9:3121–3129, July 2002. doi: 10.1063/1.1481746.

Y. Taroyan and M. S. Ruderman. MHD Waves and Instabilities in Space Plasma Flows. *Space Sci. Rev.*, 158(2-4):505–523, July 2011. doi: 10.1007/s11214-010-9737-9.

M. Terra-Homem, R. Erdélyi, and I. Ballai. Linear and non-linear MHD wave propagation in steady-state magnetic cylinders. *Solar Phys.*, 217(2):199–223, Nov. 2003. doi: 10.1023/B:SOLA.0000006901.22169.59.

W. Thomson. Hydrokinetic solutions and observations . *The London, Edinburgh, and Dublin Philosophical Magazine and Journal of Science*, 42(281):362–377, Nov. 1871.

W. J. Tirry, V. M. Cadez, R. Erdelyi, and M. Goossens. Resonant flow instability of MHD surface waves. *Astron. Astrophys.*, 332:786–794, Apr. 1998.

A. Tritschler, T. R. Rimmele, S. Berukoff, R. Casini, S. C. Craig, D. F. Elmore, R. P. Hubbard, J. R. Kuhn,

H. Lin, J. P. McMullin, K. P. Reardon, W. Schmidt, M. Warner, and F. Woger. DKIST: Observing the Sun at High Resolution. In G. T. van Belle and H. C. Harris, editors, *18th Cambridge Workshop on Cool Stars, Stellar Systems, and the Sun*, volume 18 of *Cambridge Workshop on Cool Stars, Stellar Systems, and the Sun*, pages 933–944, Jan. 2015.

G. Tsiropoula. Physical parameters and flows along chromospheric penumbral fibrils. *Astron. Astrophys.*, 357:735–742, May 2000.

G. Tsiropoula, K. Tziotziou, I. Kontogiannis, M. S. Madjarska, J. G. Doyle, and Y. Suematsu. Solar Fine-Scale Structures. I. Spicules and Other Small-Scale, Jet-Like Events at the Chromospheric Level: Observations and Physical Parameters. *Space Sci. Rev.*, 169(1-4):181–244, Sep 2012. doi: 10.1007/s11214-012-9920-2.

H. Turkakin, R. Rankin, and I. R. Mann. Primary and secondary compressible kelvin-helmholtz surface wave instabilities on the earth's magnetopause. *Journal of Geophysical Research: Space Physics*, 118 (7):4161–4175, 2013. doi: 10.1002/jgra.50394. URL `https://agupubs.onlinelibrary.wiley.com/doi/abs/10.1002/jgra.50394`.

P. Venkatakrishnan. Inhibition of convective collapse of solar magnetic flux tubes by radiative diffusion. *Nature*, 322:156, July 1986. doi: 10.1038/322156a0.

M. Vietri, A. Ferrara, and F. Miniati. The Survival of Interstellar Clouds against Kelvin-Helmholtz Instabilities. *Astrophys. J.*, 483(1):262–273, July 1997. doi: 10.1086/304202.

C.-Y. Wang and R. A. Chevalier. Instabilities and Clumping in Type IA Supernova Remnants. *Astrophys. J.*, 549(2):1119–1134, Mar. 2001. doi: 10.1086/319439.

T. Wang. Standing Slow-Mode Waves in Hot Coronal Loops: Observations, Modeling, and Coronal Seismology. *Space Sci. Rev.*, 158:397–419, July 2011. doi: 10.1007/s11214-010-9716-1.

S. Wedemeyer-Böhm, O. Steiner, J. Bruls, and W. Rammacher. What is Heating the Quiet-Sun Chromosphere? In P. Heinzel, I. Dorotovič, and R. J. Rutten, editors, *The Physics of Chromospheric Plasmas*, volume 368 of *Astronomical Society of the Pacific Conference Series*, page Heinzel, May 2007.

E. Wiehr, B. Bovelet, and J. Hirzberger. Brightness and size of small-scale solar magnetic flux concentrations. *Astron. Astrophys.*, 422:L63–L66, July 2004. doi: 10.1051/0004-6361:200400019.

D. Wu and D. Wang. The Kelvin-Helmholtz instability of a cylindrical flow with a shear layer. *Mon. Not. Roy. Astron. Soc.*, 250:760–768, June 1991. doi: 10.1093/mnras/250.4.760.

S. Yang, J. Zhang, and R. Erdélyi. Enhancement of a Sunspot Light Wall with External Disturbances. *Astrophys. J.*, 833(2):L18, Dec 2016. doi: 10.3847/2041-8213/833/2/L18.

S. Yang, J. Zhang, R. Erdélyi, Y. Hou, X. Li, and L. Yan. Sunspot Light Walls Suppressed by Nearby Brightenings. *Astrophys. J.*, 843(1):L15, Jul 2017. doi: 10.3847/2041-8213/aa7b2c.

D. Yuan, V. M. Nakariakov, Z. Huang, B. Li, J. Su, Y. Yan, and B. Tan. Oscillations in a Sunspot with Light Bridges. *Astrophys. J.*, 792(1):41, Sept. 2014. doi: 10.1088/0004-637X/792/1/41.

T. V. Zaqarashvili. Dynamic Kink Instability and Transverse Motions of Solar Spicules. *Astrophys. J. Lett.*, 893(2):L46, Apr. 2020. doi: 10.3847/2041-8213/ab881d.

T. V. Zaqarashvili and R. Erdélyi. Oscillations and Waves in Solar Spicules. *Space Sci. Rev.*, 149:355–388, Dec. 2009. doi: 10.1007/s11214-009-9549-y.

T. V. Zaqarashvili, S. Lomineishvili, P. Leitner, A. Hanslmeier, P. Gömöry, and M. Roth. Kink instability of triangular jets in the solar atmosphere. *Astron. Astrophys.*, 649:A179, May 2021. doi: 10.1051/0004-6361/202039381.

I. Zhelyazkov, T. V. Zaqarashvili, R. Chandra, A. K. Srivastava, and T. Mishonov. Kelvin-Helmholtz instability in solar cool surges. *Advances in Space Research*, 56(12):2727–2737, Dec. 2015. doi: 10.1016/j.asr.2015.05.003.

I. Zhelyazkov, T. V. Zaqarashvili, L. Ofman, and R. Chandra. Kelvin-Helmholtz instability in a twisting solar polar coronal hole jet observed by SDO/AIA. *Advances in Space Research*, 61(2):628–638, Jan. 2018. doi: 10.1016/j.asr.2017.06.003.

N. Zsamberger. Mathematical modelling of mhd waves in asymmetric waveguides with applications to solar physics. 2022. URL `https://etheses.whiterose.ac.uk/33022/`.

N. K. Zsámberger and R. Erdélyi. Magnetoacoustic Waves in a Magnetic Slab Embedded in an Asymmetric Magnetic Environment. II. Thin and Wide Slabs, Hot and Cold Plasmas. *Astrophys. J.*, 894(2):123, May 2020. doi: 10.3847/1538-4357/ab8791.

N. K. Zsámberger and R. Erdélyi. Magnetoacoustic Waves in a Magnetic Slab Embedded in an Asymmetric Magnetic Environment. III. Applications to the Solar Atmosphere. *Astrophys. J.*, 906(2):122, Jan. 2021. doi: 10.3847/1538-4357/abca9d.

N. K. Zsámberger and R. Erdélyi. Solar Magneto-seismology of a Magnetic Slab in an Asymmetric Magnetic Environment. *Astrophys. J.*, 2022a. [accepted].

N. K. Zsámberger and R. Erdélyi. Solar Magneto-seismology of a Magnetic Slab in an Asymmetric Magnetic Environment. *Astrophys. J.*, 934(2):155, Aug. 2022b. doi: 10.3847/1538-4357/ac7be3.

N. K. Zsámberger, M. Allcock, and R. Erdélyi. Magneto-acoustic Waves in a Magnetic Slab Embedded in an Asymmetric Magnetic Environment: The Effects of Asymmetry. *Astrophys. J.*, 853:136, Feb. 2018. doi: 10.3847/1538-4357/aa9ffe.

N. K. Zsámberger, C. M. Sánchez Montoya, and R. Erdélyi. Magnetohydrodynamic Waves in an Asymmetric Magnetic Slab with Different External Flows. *Astrophys. J.*, 937(1):23, Sept. 2022a. doi: 10.3847/1538-4357/ac8427.

N. K. Zsámberger, Y. Tong, B. Asztalos, and R. Erdélyi. MHD Wave Propagation and the Kelvin-Helmholtz Instability in an Asymmetric Magnetic Slab System. *Astrophys. J.*, 935(1):41, Aug. 2022b. doi: 10.3847/1538-4357/ac7ebf.

Appendix

A. The magnetic slab in an asymmetric non-magnetic environment with different flows

A.1. The dependence of the frequencies on the flow asymmetry

Here, we present the derivation of analytical results pertaining to the frequencies and instability thresholds of slow surface modes as functions of only the flow asymmetry parameter.

Quasi-sausage Modes

We start the investigation by expressing the angular frequency of the slow sausage surface mode from Equation (2.24) in terms of the flow asymmetry parameter, ε, in the thin-slab limit. Keeping terms to first order in ε, this process yields

$$\omega^2 = k^2 c_T^2 \left\{ 1 - \frac{2\left(c_0^2 - c_T^2\right) kx_0 \left(c_T - U_1\right)}{v_{A0}^2 c_0^2 E_s} \left(\left[c_T - U_1\right]^2 + \left[c_T - U_1\right] \left[\frac{F_s}{E_s} \{c_T - U_1\} - 2 \right] U_1 \varepsilon \right) \right\}, \tag{1}$$

where

$$\begin{aligned}
E_s &= (c_{T0} - U_1)^2 (D_{1s} + D_{2s}), \\
F_s &= (c_{T0} - U_1) \left(D_{2s} \frac{[c_{T0} - U_1]^2}{c_2^2 - \{c_{T0} - U_1\}} - 2D_{1s} \right), \\
G_s &= \frac{1}{2} D_{2s} (c_{T0} - U_1)^2 \frac{\left(\left[c_2^2 - \{c_{T0} - U_1\}^2 \right] + c_2^2 \left[c_{T0} - U_1\right]^2 \right)}{\left[c_2^2 - \{c_{T0} - U_1\}^2 \right]^2} + D_{1s}, \\
D_{1s} &= \frac{\rho_0}{\rho_1} \frac{\left(c_1^2 - \left[c_{T0} - U_1\right]^2 \right)^{1/2}}{c_1}, \\
D_{2s} &= \frac{\rho_0}{\rho_2} \frac{\left(c_2^2 - \left[c_{T0} - U_1\right]^2 \right)^{1/2}}{c_2}.
\end{aligned} \tag{2}$$

The threshold for the onset of the KHI is reached when the angular frequency has a

non-zero imaginary part: $\omega^2 < 0$. Rearranging the above equation to obtain an inequality for the critical value of flow asymmetry parameter, ε, yields:

$$\varepsilon > \left(\frac{v_{A0}^2 c_0^2 E_s}{2\left(c_0^2 - c_T^2\right) k x_0 (c_T - U_1)^2} - \left[c_{T0} - U_1\right]^2 \right) \left(U_1 \left[c_T - U_1\right] \left[\frac{F_s}{E_s} \left[c_T - U_1\right] - 2 \right] \right)^{-1}. \tag{3}$$

This means that for a fixed set of background parameters (characteristic speeds, densities, slab width, and left-hand-side flow), any such value of the right-hand side flow which takes ε above this critical value, will turn this quasi-sausage mode unstable to the KHI.

Quasi-kink Modes

Similarly, we can take the slow quasi-kink surface mode solutions from Equation (2.25) and express them in terms of a first-order approximation with respect to the flow asymmetry as

$$\omega^2 = k^2 v_{A0}^2 \left(1 - \frac{2}{v_{A0}^2 k x_0 U_1^3 E_k} \left[U_1^3 + \left\{ 2U_1^2 - \frac{F_k}{E_k} \right\} U_1 \varepsilon \right] \right), \tag{4}$$

where

$$\begin{aligned} E_k &= D_{1k} + D_{2k}, \\ F_k &= D_{1k} + D_{2k} \frac{U_1}{\left(c_2^2 - U_1^2\right)}, \\ D_{1k} &= \frac{\rho_0}{\rho_1} U_1^2 \frac{\sqrt{c_1^2 - U_1^2}}{c_1}, \\ D_{2k} &= \frac{\rho_0}{\rho_2} U_1^2 \frac{\sqrt{c_2^2 - U_1^2}}{c_2}. \end{aligned} \tag{5}$$

The Kelvin-Helmholtz instability sets in when $\omega^2 < 0$, which yields the following condition on the threshold flow asymmetry parameter for solar applications:

$$\varepsilon > \frac{U_1^2}{2} \frac{\left(v_{A0}^2 k x_0 E_k - 2\right)}{\left(2U_1^2 - F/E\right)} \tag{6}$$

is required for the quasi-kink oscillations of the asymmetric slab to become KHI-unstable.

If instead we have a fixed flow asymmetry in the system, then it is also possible to use Equations (1) and (4) to find the range of dimensionless slab width, kx_0, for which the slab becomes KHI-unstable. To illustrate this possibility using a simple example, we now suppose that $U_2 = 0$ and therefore $\varepsilon = -1$ is fixed. Then the critical slab width becomes

$$kx_0 > \frac{v_A^2 c_0^2 E_s}{2\left(c_T^2 - c_0^2\right)\left(c_T - U_1\right)^2 \left(\left[c_T - U_1\right] - \left[\frac{F_s}{E_s}\{c_T - U_1\} - 2\right] U_1 \right)} \tag{7}$$

for the quasi-sausage mode, and

$$kx_0 > \frac{2\left(\left[2U_1^2 - F_k/E_k\right] - U_1^2\right)}{v_{A0}^2 U_1^2 E_k} \tag{8}$$

for the quasi-kink mode. (We must note here that setting both external flow speeds to zero is not possible due to the way we defined the small parameter ε, as it contains U_1 in its denominator. Using a simple flow difference parameter instead of the relative magnitude of the flow difference we defined could keep the mathematical possibility of removing both steady flows open.)

A.2. The influence of the slab width and the flow asymmetry on the existence and instability of eigenmodes

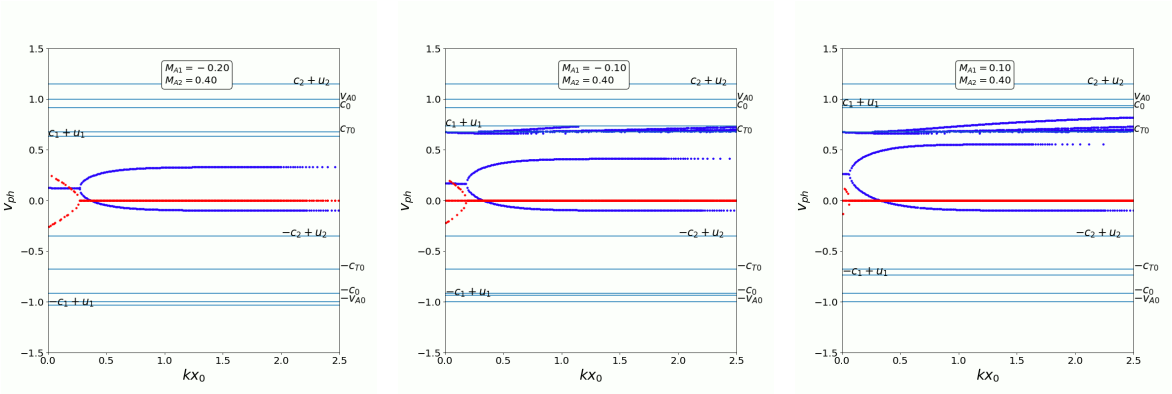

(a) (b) (c)

Figure 1: Trapped oscillation in a steady asymmetric magnetic slab for different magnitudes of flow asymmetry. Source: Zsámberger et al. (2022a).

A.3. Exploring the sources of asymmetry

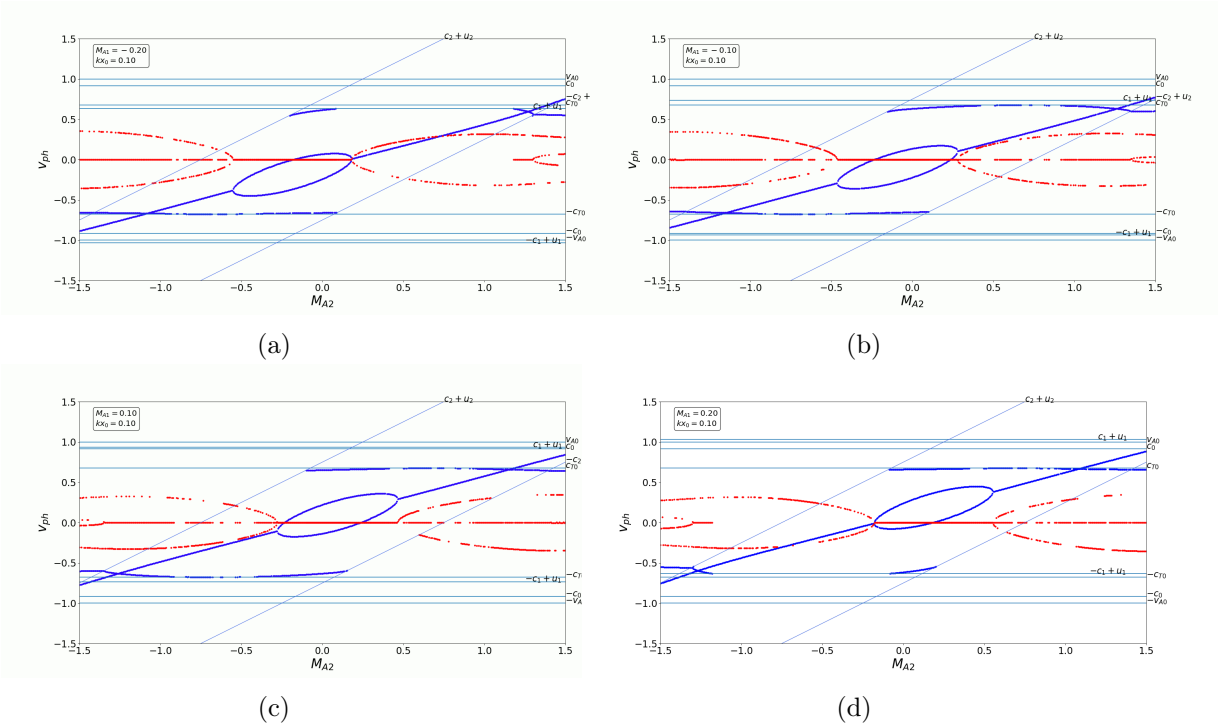

Figure 2: The phase speeds as a function of the external Alfvén Mach number on the right-hand side, for different fixed slab widths, kx_0 and left-hand-side Alfvén Mach numbers (M_{A1}). Source: Zsámberger et al. (2022a).

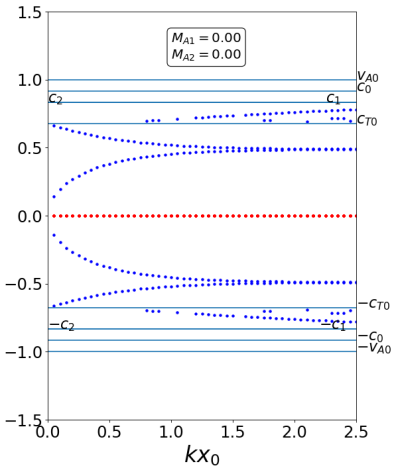

Figure 3: The phase speed of waves in a symmetric, static magnetic slab. Source: Zsámberger et al. (2022a).

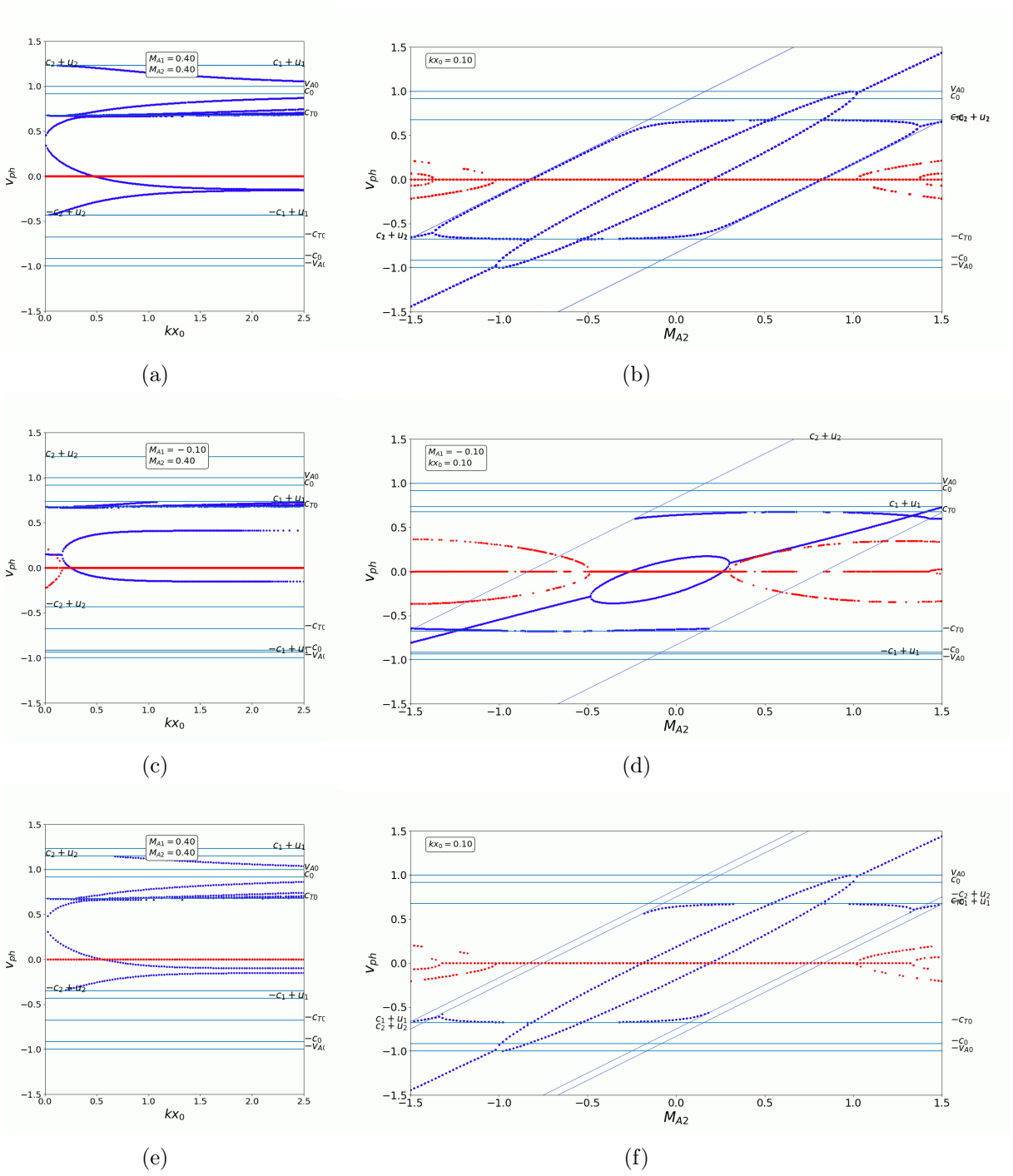

Figure 4: The phase speeds of trapped oscillations as a function of slab width (panels a, c, e) and right-hand-side flow speed (panels b, d, f). Source: Zsámberger et al. (2022a).

B. The steady magnetic slab in an asymmetric magnetic environment

B.1. The case of strong asymmetry

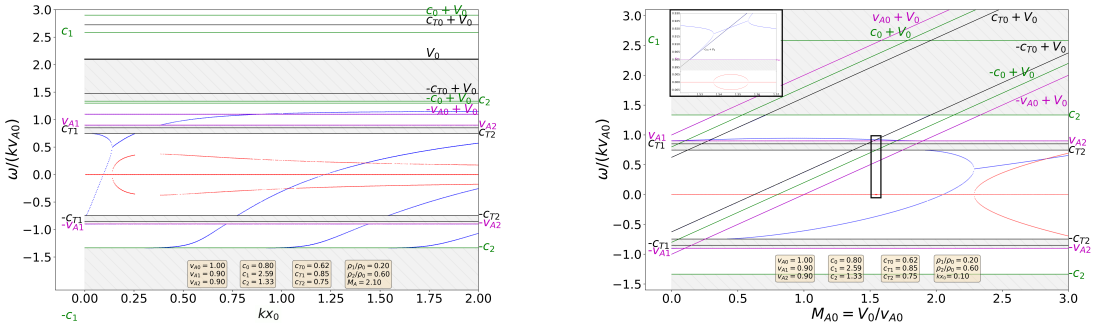

(a) (b)

Figure 5: The (a) slab width-dependence and (b) Alfvén Mach number-dependence of solutions of the full dispersion relation in a strongly asymmetric magnetic slab system. Source: Zsámberger et al. (2022b).

B.2. Comparison of solutions to the full and decoupled dispersion relations

This Figure provides a comparison of numerical results obtained using different approximations of the full dispersion relation. Panel (a) shows quasi-sausage modes, while panel (b) shows quasi-kink modes described by Equation (3.11). Panel (c) displays the quasi-sausage mode solutions obtained from Equation (3.12), and panel (d) shows the quasi-kink mode solutions described by Equation (3.17). All of these results were obtained using the same set of equilibrium parameters as for Figure 3.2b, namely: $c_0 = 0.8v_{A0}$, $c_1 = 1.51v_{A0}$, $c_2 = 1.33v_{A0}$, $v_{A1} = 0.9v_{A0}$, $v_{A2} = 0.9v_{A0}$, $\rho_1/\rho_0 = 0.5$, and $\rho_2/\rho_0 = 0.6$.

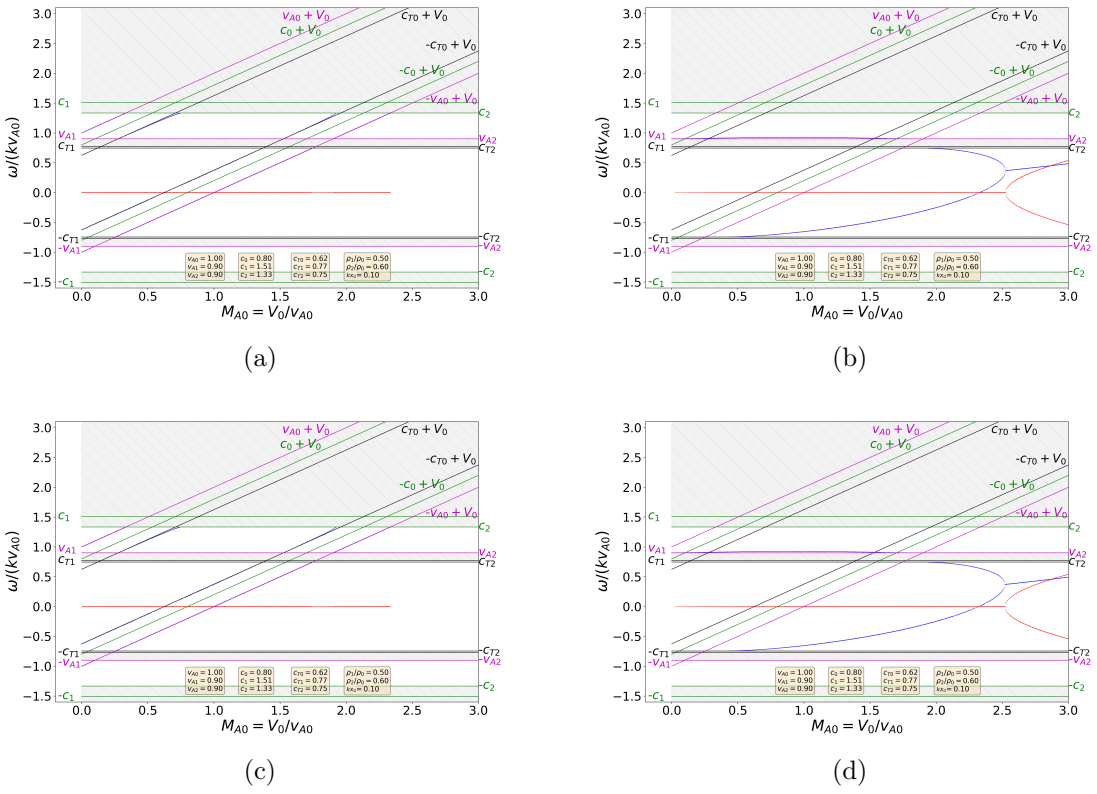

Figure 6: Solutions of various approximations of the full dispersion relation. Source: Zsámberger et al. (2022b).

C. Kink-oscillating jets with triangular flow profiles

C.1. Numerical solutions for a non-magnetic slab system

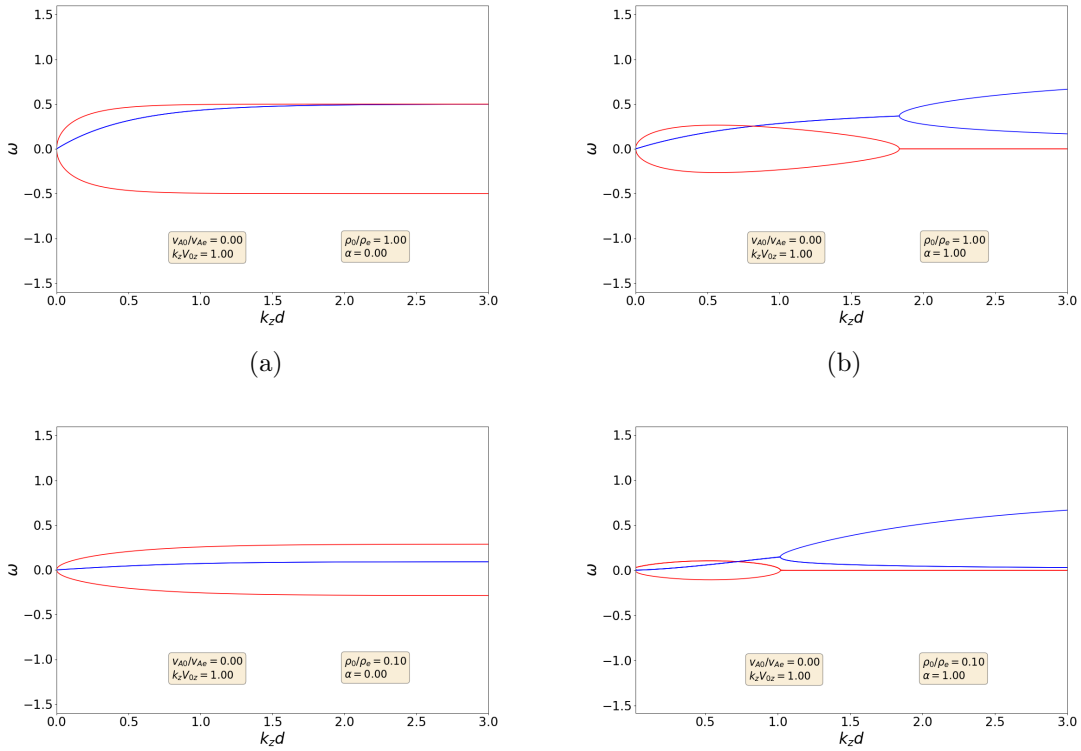

(a) (b)

(c) (d)

Figure 7: The frequencies of the solutions to the dispersion relation of a non-magnetic slab system under the effect of a kink oscillation, with a background flow in the central region.